

Electromagnetic Wave Chaos in Photonic Crystals

Thesis submitted to the University of Nottingham
for the degree of Doctor of Philosophy

by Andrew John Henning, MSci

September 2008

Abstract

Similarities in the form of the Schrödinger equation that governs the behaviour of electronic wavefunctions, and Maxwell's equations which govern the behaviour of electromagnetic waves, allow ideas that originated in solid state physics to be easily applied to electromagnetic waves in photonic structures. While electrons moving through a semiconductor experience a periodic variation in charge, in a photonic crystal electromagnetic waves experience a periodic variation in refractive index. This leads to ideas such as bandstructure being applicable to the one and two dimensional photonic crystals used in this work.

The following work will contain theoretical and experimental studies of the transmission through, and electric fields within, one dimensional photonic crystals. A slow variation in the structure of these crystals will lead to the bandstructure shifting, with an photonic analogy of electronic Bloch oscillations and Wannier-Stark ladders being seen in these structures.

The two dimensional photonic crystals will be shown, through Hamiltonian ray tracing, to support both stable and chaotic ray paths. Examination of the phase space reveals the existence of 'Dynamical Barriers', regions in phase space supporting stable ray trajectories that divide separate regions in which the ray trajectories are chaotic. Various manners in which the bandstructure may be varied will be presented, along with a proposed switch that may be made using these structures.

While the ray tracing will be carried out in photonic crystals in the limit of infinitesimally thin dielectric sheets, the model will then be developed to show the bandstructure of a photonic crystal made from finite width dielectric sheets, with examples of dispersion surfaces for these structures being presented.

Acknowledgements

Many thanks to:-

My supervisor Professor Mark Fromhold for all of his help over the last few years.

Professor Hans-Jurgen Stöckmann and his group in Germany for accommodating me and allowing me to carry out the microwave experiments I needed.

Dr Paul Wilkinson whose work on photonics I was continuing, and whose notes and ray tracing programs form the base that this thesis builds on.

To my parents, my brothers and sisters, Catherine, Sarah, Mark and Luke, and my brothers in-law, Marcus and Ian, for their encouragement and support over the years.

To the people from the physics department, including Adam Freeman, Giles Allison and Doug Ashton, who allowed me to drag them down the pub and moan at them, and who near the end of the PhD bought me drinks when money was tight.

List of Symbols

| symbol | definition |
|--------------|--|
| c | $2.9979 \times 10^8 \text{ m/s}$ |
| ϵ_0 | $8.854 \times 10^{-12} \text{ F m}^{-1}$ |
| μ_0 | $4\pi \times 10^{-7} \text{ H m}^{-1}$ |
| λ | A wavelength |
| \hbar | $1.055 \times 10^{-34} \text{ J s}$ |
| ω | Angular frequency |
| π | 3.141592654 |
| k | A wavevector |
| T | Kinetic Energy |
| V | Potential Energy |
| ϵ_r | Relative permittivity |
| Tr | A Transfer Matrix |
| H | A Hamiltonian |
| L | A Lagrangian |
| t | Time |
| ∞ | Infinity |

List of Publications

“Chaotic Transport in Semiconductor, Optical, and Cold-Atom Systems”
T.E. Judd, **A. Henning**, D.P.A. Hardwick, R.G. Scott, A.G. Balanov, P.B. Wilkinson, D. Fowler, A.M. Martin, T.M. Fromhold.
Progress of Theoretical Physics Supplement **166**, 169-178 (2007)

“Using Electromagnetic Wave Chaos to Control the Transmission of Light Through Modulated Photonic Crystal”
A. Henning, P.B. Wilkinson, T.M. Fromhold, T.M. Benson, P.D. Sewell.
2006 International Conference on Transparent Optical Networks **4**, 112 (2006)

Contents

| | | |
|----------|---|-----------|
| 1 | Bandstructures | 1 |
| 1.1 | Electronic wavefunctions and Electromagnetic waves | 2 |
| 1.1.1 | Dispersion relations | 3 |
| 1.2 | Defining the crystal | 5 |
| 1.3 | Floquet-Bloch theorem | 7 |
| 1.3.1 | Application to Electromagnetic waves | 7 |
| 1.4 | Single sheet guided modes | 14 |
| 1.5 | The Kronig-Penney model | 18 |
| 1.6 | Variation in cell size | 25 |
| 1.7 | Non-infinite lattices | 26 |
| 2 | Hamiltonian ray tracing | 27 |
| 2.1 | Lagrangian Mechanics | 31 |
| 2.1.1 | Hamilton's equations | 37 |
| 2.2 | Runge-Kutta methods | 40 |
| 2.2.1 | Higher order Runge-Kutta methods | 43 |
| 2.2.2 | The adaptive step size Runge-Kutta method using Cash-Karp parameters | 44 |
| 2.2.3 | Ray tracing | 45 |
| 3 | Chaos | 48 |
| 3.1 | Phase space | 49 |
| 3.1.1 | Integrable and non-Integrable systems | 49 |
| 3.1.2 | Dissipative and Non-Dissipative systems | 50 |
| 3.1.3 | Volumes in phase space | 51 |
| 3.2 | Lyapunov exponents | 52 |
| 3.3 | Poincaré sections | 53 |
| 4 | One dimensional Photonic crystals | 58 |
| 4.1 | Bloch oscillations | 59 |
| 4.2 | Arrangement of the dielectric sheets | 60 |
| 4.3 | Transmission through, and electric fields inside, short photonic crystals | 61 |

| | | |
|----------|---|------------|
| 4.3.1 | Constant cell length | 63 |
| 4.3.2 | Varying cell length | 66 |
| 4.4 | The form of the Bandstructure | 71 |
| 4.5 | Experimental measurements in the microwave regime | 74 |
| 4.5.1 | The experimental setup | 75 |
| 4.5.2 | Transmission experiments | 79 |
| 4.5.3 | Fields inside the crystal | 82 |
| 4.6 | Varying the sheet width | 86 |
| 5 | Two dimensional photonic crystals | 90 |
| 5.1 | Defining the crystal | 91 |
| 5.2 | The square-celled crystal | 94 |
| 5.3 | The band of interest | 96 |
| 5.4 | Dynamic Barriers | 101 |
| 5.5 | Switching | 104 |
| 5.6 | Separate values of m | 107 |
| 5.7 | Shifting the region of interest | 112 |
| 6 | Two dimensional photonic crystals, finite width sheets | 114 |
| 6.1 | Finite width sheets | 115 |
| 6.2 | One dimensional photonic crystals | 124 |
| 6.3 | Two dimensional photonic crystals | 125 |
| 7 | Appendix A | 128 |

Chapter 1

Bandstructures

Similarities in the form of the Schrödinger equation that governs the behaviour of electronic wavefunctions, and Maxwell's equations which govern the behaviour of electromagnetic waves, allow ideas that originated in solid state physics to be easily applied to electromagnetic waves in photonic structures [1, 2, 3, 4]. Calculations of the motion of electrons in materials may be carried out using dispersion relations, the relation between a particle's energy and its momentum. The energy of the photon is related to its frequency and its momentum is related to its wavenumber [5], and hence an analogous dispersion relation may be constructed for electromagnetic waves. We will see later from the form of the dispersion relation that there exist in materials either forbidden energies, in the case of electrons, or forbidden frequencies for photons. These forbidden regions are termed *Bandgaps*, with the groups of allowed energies/frequencies termed *Bands*.

This chapter will show the origins of the Floquet-Bloch theorem, and a statement of this theorem will then be used to model the bands and bandgaps in a photonic crystal. It may be noted that the statement of the Bloch theorem

used later in the chapter is not of the form derived on earlier pages, however the plane wave expansion gives a far fuller understanding of the theorem and so it is this that is used to illustrate the theory.

1.1 Electronic wavefunctions and Electromagnetic waves

The Schrödinger equation and Maxwell's equations are both linear eigenvalue problems. The Schrödinger equation has a dependence upon V , the potential, which plays a similar role to $\frac{1}{\epsilon(\vec{r})}$ in Maxwell's equation. While the Schrödinger equation deals with massive particles such as electrons, fermions, and a complex scalar field, Maxwell's equations deal with photons, bosons, and a real vector field. This leads to differences in the manner in which energy levels are populated; fermions being subject to Pauli's exclusion principle [6, 7, 8] meaning that only one particle may occupy each state, while bosons are not. Thus the population of states for fermions is given by Fermi-Dirac statistics, while for bosons it is given by Bose-Einstein statistics. Despite these differences, similarities in the form of the two equations can be seen by writing them in the following form. Schrödinger's equation

$$\left\{ -\frac{\hbar^2}{2m} \vec{\nabla}^2 + V(\vec{r}) \right\} \psi(\vec{r}) = E\psi(\vec{r}) \quad (1.1)$$

Maxwell's Equations

$$\left\{ \vec{\nabla} \times \frac{1}{\epsilon(\vec{r})} \vec{\nabla} \times \right\} \vec{H}(\vec{r}) = \frac{\omega^2}{c^2} \vec{H}(\vec{r}) \quad (1.2)$$

$$\left\{ \frac{1}{\epsilon(\vec{r})} \vec{\nabla} \times \vec{\nabla} \times \right\} \vec{E}(\vec{r}) = \frac{\omega^2}{c^2} \vec{E}(\vec{r}) \quad (1.3)$$

where $c = \frac{1}{\sqrt{\epsilon_0 \mu_0}}$ is the speed of light in a vacuum, and with the assumption that the field pattern used in Maxwells equations may be made from an appropriate combination of plane waves.

Both equation (1.1) and equation (1.2) can be rewritten in the form of a simple eigenvalue problem $OF = aF$, where O , if considering an infinite lattice, is a Hermitian operator acting on the wavefunction/electromagnetic wave. This operator has real eigenvalues corresponding to eigenvectors that, excluding degenerate cases, are orthogonal. It should be noted that the operator in (1.3) is not Hermitian due to the placement of the $\frac{1}{\epsilon(\vec{r})}$ term. Neither is (1.2) Hermitian if a non-infinite crystal is considered. It is possible to write (1.3) as a generalised eigenvalue problem of the form $O_1F = aO_2F$ however solving this is far more complicated.

As stated above, the role that V takes in the Schrödinger equation is mirrored to some extent by the $\frac{1}{\epsilon(\vec{r})}$ term in Maxwell's equations. Hence a periodic variation in refractive index should induce the same qualitative effects on electromagnetic waves as a periodic potential has on electrons, and useful effects known for electrons in solids should be transferable to light in a periodic dielectric medium.

1.1.1 Dispersion relations

If a wave travelling in free space is considered to have the form $\vec{E}(x, t) = \vec{E}_0 \exp^{i(kx - \omega t)}$, the dispersion relation [shown in figure 1.1(b)] is

$$\vec{\omega} = c\vec{k} \tag{1.4}$$

Where $\vec{\omega}$ is the angular frequency of the electromagnetic wave, c is the speed of light, and k is its wavevector defined as $\vec{k} = 2\pi/\lambda$. The use of the wavevector, a quantity that is inversely related to the wavelength, becomes more useful when

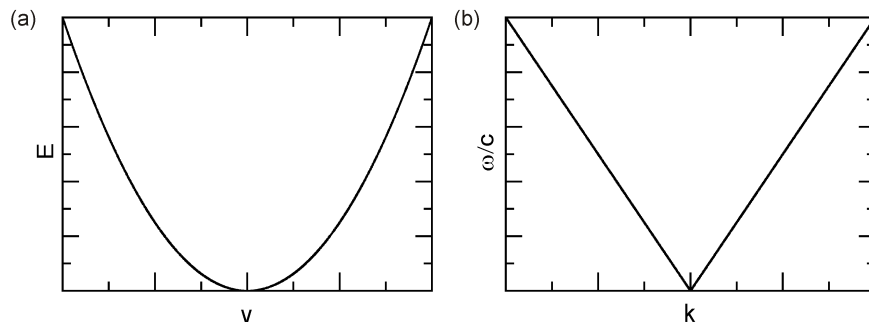


Figure 1.1: Dispersion relations for, (a) a particle in free space, (b) a photon in free space

potentials are written in the form of Fourier transforms [9] as these also involve terms whose units are $[length^{-1}]$.

For a particle in zero potential the dispersion relation [figure 1.1(a)] is

$$E = \frac{1}{2}mv^2 \quad (1.5)$$

Where E is the particle's kinetic energy, which is equal to its total energy in zero potential, m is the mass of the particle, and v is its velocity.

The dispersion relation is linear for an electromagnetic wave, but quadratic for a massive particle as can be seen in figure (1.1). While it can be seen from equations (1.4) and (1.5) that both dispersion relations are continuous functions in free space, it is the emergence of gaps in the allowed energies/frequencies in periodic potentials that is of interest in this thesis. It is this property that is exploited in materials such as semiconductors to control the behavior of electrons, and in photonic crystals to control the behavior of electromagnetic (E.M.) waves [10, 11, 12].

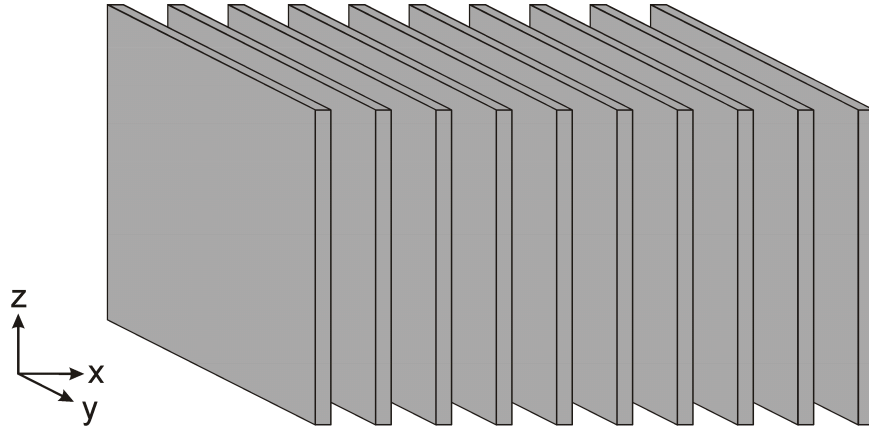


Figure 1.2: One dimensional photonic crystal, comprising dielectric sheets (grey) which are infinite in extent in the y and z directions

1.2 Defining the crystal

The photonic crystals that are being considered consist of infinite sets of parallel dielectric sheets, such as those shown in figure (1.2), with the crystal extending to infinity in every direction. This forms an infinite set of repeating identical cells each of which consists of a dielectric sheet and adjacent air gap. From this it may be seen that the structure has *discrete translational symmetry*, whereby a translation from any point by an integer number of cell lengths in the x direction gives a point whose environment is identical to the initial point.

So far the crystals described have been one dimensional crystals, that is, having variation only in one dimension. These structures may be extended into two or three dimensions by including a second (figure (1.3)) or third set of sheets that are perpendicular to the other sets. The structure of the crystal may be defined using any single complete set of points that exhibit discrete translational symmetry [14]. This set is known as the Bravais lattice [15]. In N dimensions (where $N = 1, 2, 3$) this lattice is defined by N translation vectors \vec{a}_i (where

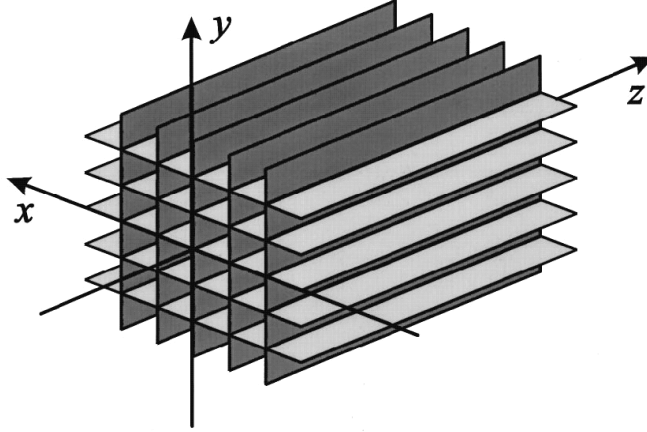


Figure 1.3: Two dimensional photonic crystal. Dielectric sheets (grey) are infinite in extent in the z direction (picture taken from [13])

$i = 1, 2, 3$). Thus in 3 dimensions the lattice may be defined by

$$\vec{r}_1 = u_1 \vec{a}_1 + u_2 \vec{a}_2 + u_3 \vec{a}_3 \quad (1.6)$$

where u_i ($i = 1, 2, 3$) are integers. For a crystal with $N < 3$ dimensions only the terms $a_{(i \leq N)}$ are included, with the crystal being invariant in the other $3 - N$ dimensions.

Thus for the one dimensional crystal, translation from one lattice point to any other may be given by

$$\vec{r}_1 = u_1 \vec{a}_1 \quad (1.7)$$

where $\vec{a}_1 = \hat{x}L$, where \hat{x} is a unit vector along the x direction, and L is the width of a single cell, that is the width of a single dielectric sheet and adjacent air gap.

1.3 Floquet-Bloch theorem

While the problem of the conduction of electrons through crystalline solids was solved by Felix Bloch, the solution that he arrived at had been independently arrived at by others when considering different problems. Floquet theory, while presenting the same results, was arrived at earlier through considerations of the properties of linear differential equations.

The following section will introduce Floquet-Bloch theory, and will show that a solution to Maxwell's equations will consist of the product of a plane wave and a periodic function. It may be seen from this solution that, in periodic potentials, there are frequencies at which no solution exists, the bandgaps associated with the crystal.

1.3.1 Application to Electromagnetic waves

A solution of Maxwell's equations in a periodic potential must exhibit the same periodicity as the lattice. That is not to say that the exact structure of each cell must be mimicked, only that the solution must have the same translational symmetry of the lattice.

Instead of looking for a direct solution to Maxwell's equations, a set of translational operators related to the Bravais lattice is considered [1]. These translational operators are set up to have the same translational symmetry as the crystal and will commute with the operator in equation (1.2). It may be shown that these two operators have a common set of eigenfunctions [16]. Care must be taken however as the eigenvalues of Maxwell's equations turn out to be a subset of the solution given by the translation operators. That is, an eigenfunction of Maxwell's equations is also an eigenfunction of the translation operators, but conversely, an eigenfunction of the translation operators is not necessarily an eigenfunction of Maxwell's equations. The set of Translation

operators is defined in the following way

$$T [H(\vec{r})] = H(\vec{r} + \sum_{i=1,N} n_i \vec{a}_i) \quad (1.8)$$

where n_i are integers and H is either the electric or magnetic field vector.

Since H is invariant under translation through any linear combination of lattice vectors, the translation operators will commute with the operator defined for Maxwell's equations by equation (1.2), which means that there may be a common set of eigenvectors.

An eigenvector \vec{u} of the translation operator will satisfy

$$T [\vec{u}] = \rho \vec{u} \quad (1.9)$$

where the eigenvalue ρ may take complex values, but must have a modulus of 1 in order to remain bounded at infinity. If it takes some other value the field will continuously diverge in one direction. This will lead to no locally integrable electromagnetic energy, and hence an unphysical solution to Maxwell's equations [1]. However, if a finite crystal is considered then this restriction no longer holds, as the increase in the field is restricted by the crystal's edge. Removing this restriction allows evanescent fields for waves that are meeting a crystal whose bandgap forbids propagation at that frequency.

The value of ρ must lie on a unit circle in complex space, and as such it may be represented as follows.

$$\rho = e^{i\theta} \quad (1.10)$$

where θ is restricted to real values. The value of θ represents the phase shift after a translation along a vector \vec{r} , an integer multiple of the direct lattice vectors \vec{a}_i , corresponding to any of the translations given by (1.8). This translation may be broken down into N separate translations, corresponding to the translations

in the direction of each of the direct lattice vectors \vec{a}_i .

$$T = \sum_{i=1,N} n_i T_i \quad (1.11)$$

and, in a similar way, the corresponding value of θ may be broken down into phase shifts in the direction of each of the direct lattice vectors,

$$\theta = \sum_{i=1,N} n_i \theta_i \quad (1.12)$$

here θ is the phase shift along the translation corresponding to $n_i \vec{a}_i$, with θ_i being the phase shift corresponding to a translation along the direct lattice vector \vec{a}_i . The wavevector \vec{k} may now be defined as $\vec{k} \cdot \vec{a}_i = \theta_i$ allowing (1.10) to be rewritten in the form,

$$\rho = \exp \left(i \vec{k} \cdot \sum_{i=1,N} n_i \vec{a}_i \right) \quad (1.13)$$

Looking at the effect of the translation on the eigenvector \vec{u} allows a new function \vec{v} to be constructed that will remain invariant after a translation given by T . The function $\vec{v} = \vec{u} \exp(-i \vec{k} \cdot \vec{r})$ may be shown to be invariant after a translation, T ,

$$\begin{aligned} T[\vec{v}] &= T \left[\vec{u} \exp(-i \vec{k} \cdot \vec{r}) \right] = T[\vec{u}] \exp \left(-i \vec{k} \cdot \left(\vec{r} + \sum_{i=1,N} n_i \vec{a}_i \right) \right) \\ &= \rho \vec{u} \exp \left(i \vec{k} \cdot \sum_{i=1,N} n_i \vec{a}_i \right) \exp(-i \vec{k} \cdot \vec{r}) = \vec{u} \exp(i \vec{k} \cdot \vec{r}) = \vec{v} \end{aligned} \quad (1.14)$$

As \vec{v} is a periodic function, this opens up the possibility of looking at it as a Fourier series. To this end, the reciprocal lattice will be defined and will consist of a lattice of points that correspond to the allowed terms in the Fourier series.

The reciprocal lattice is a lattice made from the basis vectors \vec{b}_1 , \vec{b}_2 and \vec{b}_3 that are related to the direct lattice vectors \vec{a}_1 , \vec{a}_2 and \vec{a}_3 as follows

$$\vec{b}_1 = 2\pi \frac{\vec{a}_2 \times \vec{a}_3}{\vec{a}_1 \cdot (\vec{a}_2 \times \vec{a}_3)}$$

$$\vec{b}_2 = 2\pi \frac{\vec{a}_3 \times \vec{a}_1}{\vec{a}_1 \cdot (\vec{a}_2 \times \vec{a}_3)}$$

$$\vec{b}_3 = 2\pi \frac{\vec{a}_1 \times \vec{a}_2}{\vec{a}_1 \cdot (\vec{a}_2 \times \vec{a}_3)}$$

this leads to the property of the vectors that

$$\vec{b}_i \cdot \vec{a}_i = 2\pi \delta_{ij}.$$

Here, δ_{ij} is a Kronecker delta function, which has the property that $\delta_{ij} = 1$ if $i = j$ and $\delta_{ij} = 0$ if $i \neq j$. This gives the reciprocal lattice as a set of points that are mapped by the set of vectors

$$\vec{G} = v_1 \vec{b}_1 + v_2 \vec{b}_2 + v_3 \vec{b}_3 \quad (1.15)$$

Since \vec{v} is spatially periodic, it can be represented as a Fourier series

$$\vec{v} = \sum_{\vec{G}} V(\vec{G}) \exp(i\vec{G} \cdot \vec{r})$$

which then gives

$$\vec{u} = \exp(i\vec{k} \cdot \vec{r}) \sum_{\vec{G}} V(\vec{G}) \exp(i\vec{G} \cdot \vec{r}) \quad (1.16)$$

leaving \vec{u} expressed as a product of a plane wave and a Fourier series with the periodicity of the crystal.

Thus \vec{u} is a superposition of plane waves with wavevectors given by,

$$\vec{k}_G = \vec{k} + \vec{G} \quad (1.17)$$

for every value of \vec{G} in the reciprocal lattice. While the phase velocity of each of the plane waves may differ, the group velocity of the waves is common to them all. This arises as the group velocity, the velocity of the energy propagation, is given by

$$\vec{v}_g = \frac{\partial \vec{\omega}}{\partial (\vec{k}_G)} = \frac{\partial \vec{\omega}}{\partial (\vec{k} + \vec{G})} \equiv \frac{\partial \vec{\omega}}{\partial \vec{k}} \quad (1.18)$$

as G is independent of $\vec{\omega}$. This leads to the dispersion relation of $\vec{k}(\vec{\omega})$ being equivalent to the dispersion relation of the entire Bloch wave.

It has been stated previously that solutions to Maxwell's equations must exhibit the same periodicity of the lattice, and it is the interference of multiple plane waves that allows them to do this [17]. While a single plane wave is unable to image the static potential of the crystal, the reflections that arise in the crystal combine to give an interference pattern that will. As the Bloch wave involves the interference of many plane waves in this manner, its behaviour in a crystal is often counterintuitive.

The interference pattern may be broken down into a standing wave component and a travelling wave component. It is then possible to consider the Bloch wave, from a Hamiltonian Optics perspective, in a Newtonian manner [18, 19]. The standing wave component is equated with the potential energy, and the travelling wave the kinetic energy. The greater the amount of the energy stored in the standing wave, the slower the propagation of the Bloch wave. At the point at which all of the energy is stored in the standing wave the fringes of the interference pattern have 100% visibility, and the Bloch wave will be stationary. This occurs at points in the crystal where the light is *Bragg reflected* [20, 21].

Bragg reflection is most easily explained when considering a plane wave, such as an X-ray, incident upon a crystal. If the layers are not perfectly reflecting the wave will be reflected from several different layers of the material. If the path difference between rays reflected from different sheets differs by a whole number of wavelengths the rays will interfere constructively, and a reflection of the plane wave will be seen. Due to the multiple plane waves that create the Bloch wave their Bragg reflections are slightly more complicated, however the same premise applies.

The Brillouin zone

The first Brillouin zone is the region in reciprocal space [22] that lies closer to the reciprocal lattice point at the origin than to any other [23], a region that may be shown to contain the complete set of modes that are supported by the crystal [24, 25]. This arises as any point outside of this region may be translated onto a point inside the region through a translation by a reciprocal lattice vector.

It has been seen earlier that any particular Bloch mode (labelled by index 1) is of the form,

$$\vec{u}_1 = \exp(i\vec{k}\cdot\vec{r}) \sum_{\vec{G}} V(\vec{G}) \exp(i\vec{G}\cdot\vec{r})$$

This gives the mode as the summation of the plane wave $\exp(i\vec{k}\cdot\vec{r})$, and its reflections which are given by the set of reciprocal lattice points. The set of reflected waves thus has the form $\exp(i(\vec{k}+\vec{G})\cdot\vec{r})$ where \vec{G} is the set of reciprocal lattice vectors. If a second Bloch mode is considered with the form,

$$\vec{u}_2 = \exp(i\vec{k}'\cdot\vec{r}) \sum_{\vec{G}} V(\vec{G}) \exp(i\vec{G}\cdot\vec{r})$$

where $\vec{k}' = \vec{k} + \vec{G}_1$, and \vec{G}_1 is an arbitrary reciprocal lattice vector, it may easily

be shown that \vec{u}_1 and \vec{u}_2 are equivalent modes. This arises due to the infinite extent and periodic nature of the reciprocal lattice. For any vector, \vec{G}_1 , in the lattice there must also exist a vector, $-\vec{G}_1$, and hence a reflected wave with the form $\exp(i(\vec{k}' - \vec{G}_1) \cdot \vec{r}) = \exp(i\vec{k}' \cdot \vec{r})$. This wave will be scattered again, and as such, any wave that is given by \vec{u}_1 will be reproduced. In the same way, the plane wave $\exp(i\vec{k} \cdot \vec{r})$ is reflected to give $\exp(i(\vec{k} + G) \cdot \vec{r})$, which will be further scattered from the reciprocal lattice points. Thus any wave in the mode \vec{u}_1 must be present in mode \vec{u}_2 and vice versa. The only difference that will arise is due to the coefficients $V(\vec{G})$, which give the strength of the scattering from each lattice point. The values of these coefficients will change the amplitude of each wave but not the form of the Bloch mode.

Thus for any mode in the crystal with a value of \vec{k} outside the first Brillouin zone, an equivalent one will be found in it. Plotting dispersion curves outside this range only introduces redundant results. For this reason dispersion curves will be plotted using the *Reduced zone scheme*, whereby only the values of \vec{k} in the first Brillouin zone are plotted. In the case of the one dimensional crystal that has been considered so far, the first Brillouin zone limits the values of \vec{k} to the range $-\pi/a < \vec{k} < \pi/a$, where a is the cell length. The dispersion curve plotted in the reduced zone scheme is shown in figure (1.4). The solutions are periodic in \vec{k} over a range of $2\pi/a$, hence a solution for a value of $\vec{k} = \vec{k}_1$ inside this range is actually a solution for the set of points $|\vec{k}| = |\vec{k}_1| + 2n\pi/a$, where n is an integer.

In the case of the two dimensional photonic crystal that has been discussed so far the first Brillouin zone is square and covers the range

$$-\pi/a < k_x < \pi/a, \quad -\pi/b < k_y < \pi/b \quad (1.19)$$

where a and b are the cell lengths in the x and y directions respectively.

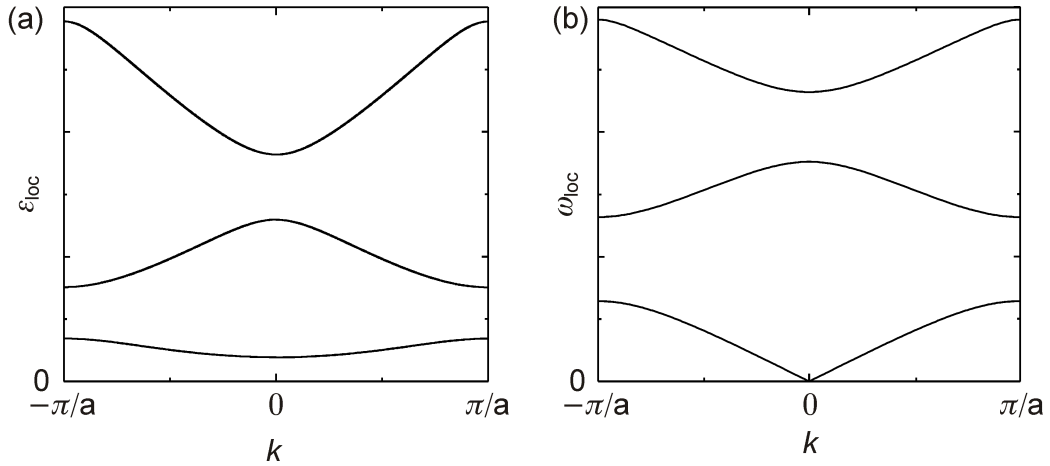


Figure 1.4: (a) shows the dispersion curves for electrons in a one dimensional semiconductor superlattice, while (b) shows the dispersion curves for a one dimensional photonic crystal [26]

1.4 Single sheet guided modes

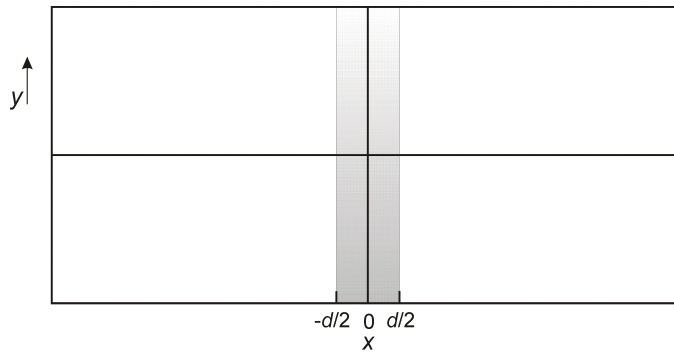


Figure 1.5: A single dielectric sheet (grey), infinite in extent in the y and z directions

While the photonic crystals that are being considered in this piece of work consist of infinite sets of parallel dielectric sheets, the behaviour of electromagnetic waves in a single sheet acts as an aid to the understanding of these larger sets.

The sheet that is being considered, as shown in figure (1.5), extends from $-\frac{d}{2}$ to $\frac{d}{2}$ in the x direction, and is infinite in extent in the y and z directions.

An electromagnetic wave that is confined to move in the x,y plane will take the form,

$$\vec{E} = \vec{E}(x) \exp^{i(k_y y - \omega t)} \quad (1.20)$$

The component of the electric field in the y direction, being tangential to the sheet, will be continuous across the boundary and thus will have a constant value across the three regions. However, the x component of the field must be considered in each of the three regions separately.

A wave originating in free space on the left hand side of the sheet leads to fields in the different regions of the form,

$$\begin{aligned} E_x(\vec{x}) = & A e^{ik_{1x}(x-d/2)} + B e^{-ik_x(x-d/2)} & (x < -d/2) \\ & C e^{ik_{2x}x} + D e^{-ik_{2x}x} & (-d/2 < x < d/2) \\ & F e^{ik_{1x}(x+d/2)} & (x > d/2) \end{aligned} \quad (1.21)$$

Where A, B, C, D and F are constants that are found by applying the correct boundary conditions [27]. There is only one term in the region $x > d/2$ which corresponds to a wave travelling to the right. As this wave will not be reflected, no left-travelling wave exists.

The polarisation of the light, i.e. the orientation of the field with respect to the sheet, is important when applying boundary conditions and hence finding values for the constants A, B, C, D , and F . The electromagnetic waves may take one of two polarisations, S or P , with the orientation of the fields for these two polarisations being shown in figure (1.6). In both cases, we set the z component of the wavevector to zero for simplicity. This confines the wave to propagate in the x, y plane, with the x and y components of the wavevector being related by $\vec{k}^2 = \vec{k}_x^2 + \vec{k}_y^2$. For P polarisation the electric field oscillates in the plane of the page as shown in fig 1.6(b), while for S polarisation the electric field oscillates out of the page [fig 1.6(a)]. The solutions to these two different orientations

are completely different, and so can be treated separately. As it is the S polarisation that will primarily be used in the later work, unless stated explicitly, from this point on any electromagnetic wave will be considered to be S polarised.

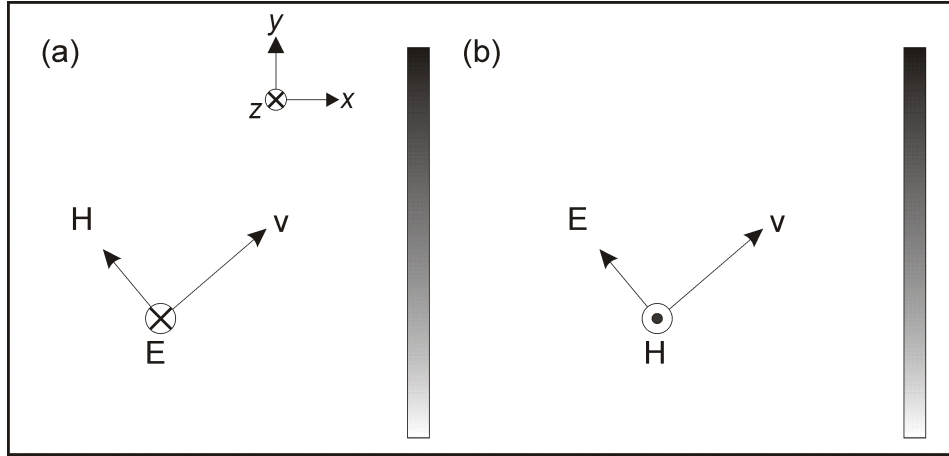


Figure 1.6: Schematic of an E.M. wave incident on a dielectric sheet (shaded) showing electric field (E), magnetic field (H) and the direction of propagation (v) (a) S -polarisation (b) P -polarisation

Guided waves

A second case that should be considered is that of a wave that is already present in the sheet. If the wavevector in the y direction is greater than the free space wavevector, after applying the correct boundary conditions, it may be seen that in air the x component of the wavevector is imaginary, thus the field decays exponentially outside of the sheet. This solution confines the ray inside the sheet, as upon meeting a boundary the ray will be totally internally reflected. However, if the component of the wavevector in the y direction is less than the free-space wavevector the wave will not be confined, and the fields will take the form given in the last section.

For S polarisation, the fields for electromagnetic waves that originate in the

sheet and that are confined to the sheet under the condition of total internal reflection, are given by

$$\begin{aligned}
 E(x) = & \begin{aligned} & A_1 e^{q_x(x-d/2)} && (x < -d/2) \\ & B_1 e^{ik_{2x}x} + C_1 e^{-ik_{2x}x} && (-d/2 < x < d/2) \\ & D_1 e^{q_x(x+d/2)} && (x > d/2) \end{aligned} \end{aligned} \quad (1.22)$$

Where A_1 , B_1 , C_1 , and D_1 are again constants that may be obtained by applying the boundary conditions at the interfaces between the dielectric sheet and the air [27]. In equation (1.22), k_{2x} is the x component of the wavevector in the material and $q_x = ik_{1x}$ is the x component of the wavevector in the air multiplied by $i = \sqrt{-1}$. This form is chosen purely as a convenience to distinguish between the guided and unguided waves. If q_x is not positive the electromagnetic wave is no longer guided, and the fields will take the same form as in equation (1.21) with $A = 0$ as there will be no wave incident upon the sheet from the left.

The exponential decay of the field in the air means that it decays to virtually zero within a distance of a few wavelengths from the sheets. However, if a second sheet is placed sufficiently close to the original sheet, the field will couple to the second sheet and excite a mode in it.

The two dimensional photonic crystals considered later in this work will initially be formed from a set of infinitesimally thin sheets. In order to consider this limit, the sheets are defined by the single parameter m where $m = \epsilon_r d$. Here d is the effective width of the sheet and ϵ_r is its effective relative permittivity, chosen so that $\epsilon_r \rightarrow \infty$ as $d \rightarrow 0$. In this limit, guided modes survive for S polarisation, but not for P polarisation [13].

1.5 The Kronig-Penney model

The Kronig-Penney model describes the effect that the potential created by a lattice of atoms has on an electron by considering the potential to be an array of square potential wells. Although this yields a system that is easy to solve, and that shows some important effects, the approximation is generally too great for quantitative calculations of other effects. However, the photonic crystals already considered create just this ‘potential’ landscape, and hence are an ideal systems to be modelled in this manner. The boundary conditions for the electric and magnetic fields at the interface between two materials allow the reflection and transmission coefficients to be calculated. These may be used to determine the relation between the amplitude of the left and right travelling components of the wave on either side of the interface [28]. As it is easy to relate the left and right travelling components of the wave at any two points in a homogeneous material, the additional ability to relate the components across a boundary allows the relationship between components in one cell and the next to be calculated. This may be combined with a statement of Bloch’s theorem to find the dispersion relation for these structures.

Initially, an infinite one dimensional photonic crystal is considered. A cross section of three cells of this crystal is shown in figure (1.7). Each of the cells is identical, consisting of a single dielectric sheet and an air gap. Once again the electromagnetic wave takes the form

$$\vec{E}_n = \vec{E}(x) \exp^{i(k_y y - \omega t)} \quad (1.23)$$

with $\vec{E}(x)$ taking the form

$$\vec{E}(x) = \vec{A}_n e^{i\vec{k}_n x} + \vec{B}_n e^{-i\vec{k}_n x} \quad (1.24)$$

where n represents the cell number, \vec{k}_n is the wavevector in the corresponding medium and \vec{A}_n and \vec{B}_n give the amplitudes (and orientation) of the left and right travelling components.

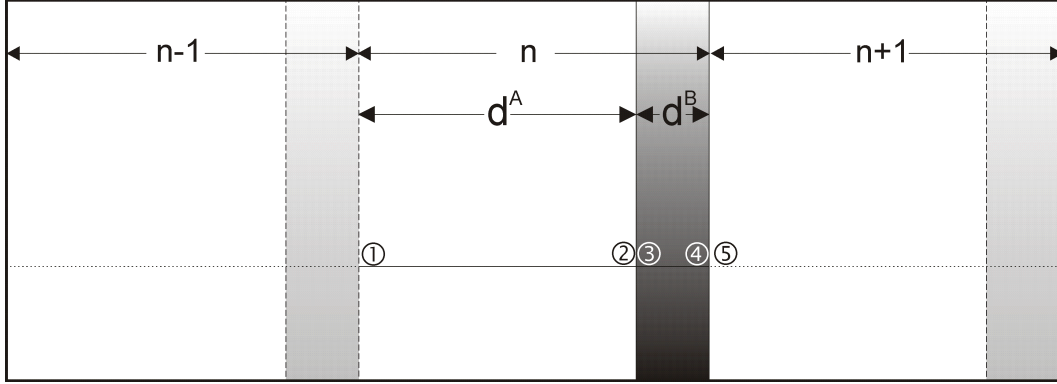


Figure 1.7: A cross section of three cells of a one-dimensional photonic crystal. Transmission is calculated across the cell that is shown darker than its neighbors. The width of the air gap is d^A , and the sheet d^B .

It is useful to write the electric field distribution $\vec{E}(x)$ at a point in the crystal as a column vector of the following form

$$\begin{bmatrix} \vec{E}_{x=\alpha}^+ \\ \vec{E}_{x=\alpha}^- \end{bmatrix} = \begin{bmatrix} \vec{A}_{x=\alpha} \exp^{i\vec{k}_{x=\alpha}x} \\ \vec{B}_{x=\alpha} \exp^{-i\vec{k}_{x=\alpha}x} \end{bmatrix}$$

where $\vec{E}_{x=\alpha}^+$ and $\vec{E}_{x=\alpha}^-$ are the components travelling to the right and left respectively at the point $x = \alpha$. The total electric field at any point in the crystal is gained by summing the different components of the wave at that point. If the wave is travelling through a homogeneous material, the relationship between the field at $x = \alpha$ and $x = \beta$ is given by,

$$\begin{bmatrix} \vec{E}_{x=\alpha}^+ \\ \vec{E}_{x=\alpha}^- \end{bmatrix} = \begin{bmatrix} e^{i\vec{k}_\alpha(\beta-\alpha)} & 0 \\ 0 & e^{-i\vec{k}_\alpha(\beta-\alpha)} \end{bmatrix} \begin{bmatrix} \vec{E}_{x=\beta}^+ \\ \vec{E}_{x=\beta}^- \end{bmatrix} \quad (1.25)$$

The matrix multiplication just advances the phase of each wave by the correct

amount through this translation in space. This is only true for homogeneous regions of space, that is, where the refractive index is constant. Thus while the wavevector has been labelled \vec{k}_α , it could equally have been labelled \vec{k}_β , or the wavevector at any point between.

The second situation of interest is the relation between left and right travelling waves either side of a boundary between materials with different refractive index. This is obtained through the application of the correct boundary conditions to the electric and magnetic fields [27]. As mentioned previously, the solutions for S and P polarised waves incident on the boundary are different, with the solutions only being equivalent for a ray that is travelling perpendicular to the surface. For S polarisation, the relation between the fields of waves on either side of the interface is given by,

$$\begin{bmatrix} \vec{E}_1^+ \\ \vec{E}_1^- \end{bmatrix} = \begin{bmatrix} \left(\frac{1}{2} + \frac{\vec{k}_2}{2k_1}\right) & \left(\frac{1}{2} - \frac{\vec{k}_2}{2k_1}\right) \\ \left(\frac{1}{2} - \frac{\vec{k}_2}{2k_1}\right) & \left(\frac{1}{2} + \frac{\vec{k}_2}{2k_1}\right) \end{bmatrix} \begin{bmatrix} \vec{E}_2^+ \\ \vec{E}_2^- \end{bmatrix} \quad (1.26)$$

where \vec{k}_1 is the wavevector in material 1, and \vec{k}_2 is the wavevector in material 2. It is at this point that the advantage of writing the fields in the form of column vectors becomes apparent. If $x = \beta$ was a point on a boundary between two different materials, then \vec{E}_1^+ and \vec{E}_1^- are equivalent to $\vec{E}_{x=\beta}^+$ and $\vec{E}_{x=\beta}^-$ respectively. Substituting (1.26) into (1.25) then gives the relation between waves at the point in material 1, $x = \alpha$, and the point inside material 2, $x = \beta$,

$$\begin{bmatrix} \vec{E}_{x=\alpha}^+ \\ \vec{E}_{x=\alpha}^- \end{bmatrix} = \begin{bmatrix} e^{i\vec{k}_\alpha(\beta-\alpha)} & 0 \\ 0 & e^{-i\vec{k}_\alpha(\beta-\alpha)} \end{bmatrix} \begin{bmatrix} \left(\frac{1}{2} + \frac{\vec{k}_2}{2k_1}\right) & \left(\frac{1}{2} - \frac{\vec{k}_2}{2k_1}\right) \\ \left(\frac{1}{2} - \frac{\vec{k}_2}{2k_1}\right) & \left(\frac{1}{2} + \frac{\vec{k}_2}{2k_1}\right) \end{bmatrix} \begin{bmatrix} \vec{E}_{2,x=\beta}^+ \\ \vec{E}_{2,x=\beta}^- \end{bmatrix}$$

Multiplying out the first and second matrices on the right hand side leaves a 2x2 matrix that describes the relation between the waves at $x = \alpha$ and those inside the second material at $x = \beta$. The waves at $x = \beta$ may be related to waves

at any other point inside the second material in the same manner as shown in (1.25), and waves inside the material at the boundary may be related to waves outside the material at the boundary in the same manner as (1.26). By using a series of steps of the form shown in (1.25) and (1.26) the relation between waves at any two points in the crystal may be obtained in the form of a single 2x2 matrix.

Figure (1.7) shows the steps needed to calculate the relation between waves at the beginning of cell n and the beginning of cell $n+1$. The propagation of the wave from point 1 to point 2, and from point 3 to point 4 need to be included, as does the relation of the waves at the boundary between the materials, points 2 to 3 and points 4 to 5. If the wavevector in the air gap is labelled \vec{k}_a , and in the dielectric sheet it is \vec{k}_b , this the relation,

$$\begin{aligned}
\begin{bmatrix} \vec{E}_1^+ \\ \vec{E}_1^- \end{bmatrix} &= \begin{bmatrix} e^{i\vec{k}_a A} & 0 \\ 0 & e^{-i\vec{k}_a A} \end{bmatrix} \begin{bmatrix} \left(\frac{1}{2} + \frac{\vec{k}_b}{2\vec{k}_a}\right) & \left(\frac{1}{2} - \frac{\vec{k}_b}{2\vec{k}_a}\right) \\ \left(\frac{1}{2} - \frac{\vec{k}_b}{2\vec{k}_a}\right) & \left(\frac{1}{2} + \frac{\vec{k}_b}{2\vec{k}_a}\right) \end{bmatrix} \begin{bmatrix} e^{i\vec{k}_b B} & 0 \\ 0 & e^{-i\vec{k}_b B} \end{bmatrix} \\
&\quad \times \begin{bmatrix} \left(\frac{1}{2} + \frac{\vec{k}_a}{2\vec{k}_b}\right) & \left(\frac{1}{2} - \frac{\vec{k}_a}{2\vec{k}_b}\right) \\ \left(\frac{1}{2} - \frac{\vec{k}_a}{2\vec{k}_b}\right) & \left(\frac{1}{2} + \frac{\vec{k}_a}{2\vec{k}_b}\right) \end{bmatrix} \begin{bmatrix} \vec{E}_5^+ \\ \vec{E}_5^- \end{bmatrix} \\
&= \begin{bmatrix} A & B \\ C & D \end{bmatrix} \begin{bmatrix} \vec{E}_5^+ \\ \vec{E}_5^- \end{bmatrix}
\end{aligned} \tag{1.27}$$

This is a far superior method than just considering waves created by reflection and transmission at each boundary. In such calculations, if the system includes two or more partially reflecting surfaces, the multiple reflections will need to be truncated at some point, or dealt with in some other way to sum the infinite series that will be generated.

Bloch's theorem relates the field at any point in a single cell to the equivalent

point in the next cell in the following manner,

$$\vec{E}_{n+1}(\vec{r} + \hat{x}(A+B)) = \exp^{-i\mu_x(A+B)} \vec{E}_n(r) \quad (1.28)$$

where $(A+B)$ is the length of a single cell and $\vec{\mu}_x$ is the Bloch wavevector. The set of solutions are restricted to those where the Bloch wavevector is real. Writing equation (1.28) as a column vector relating the left and right travelling components of the field gives,

$$\begin{bmatrix} \vec{E}_{n+1}^+ \\ \vec{E}_{n+1}^- \end{bmatrix} = e^{-i\mu_x(A+B)} \begin{bmatrix} \vec{E}_n^+ \\ \vec{E}_n^- \end{bmatrix} \quad (1.29)$$

Thus we have two statements, (1.27) and (1.29), relating the field at one point to the equivalent point in the next cell. Identifying \vec{E}_n with \vec{E}_1 , and \vec{E}_{n+1} with \vec{E}_5 , allows the use of (1.29) to eliminate the \vec{E}_{n+1} terms in (1.27),

$$\begin{bmatrix} A & B \\ C & D \end{bmatrix}^{-1} \begin{bmatrix} \vec{E}_n^+ \\ \vec{E}_n^- \end{bmatrix} = e^{-i\mu_x a} \begin{bmatrix} \vec{E}_n^+ \\ \vec{E}_n^- \end{bmatrix} \quad (1.30)$$

Thus $e^{-i\mu_x a}$ may be identified as an eigenvalue of the matrix on the left hand side. The solution of this for photonic crystals with finite width sheets may be seen in Appendix A, and is used chapter 6. However reference [13] solves this in the limit of infinitesimally thin sheets that have been described previously, giving a rearranged version of (1.30) as,

$$\begin{bmatrix} [1 + i(\frac{m\vec{k}^2}{2k_x})]e^{i\vec{k}_x a} - e^{i\vec{\mu}_x a} & i(\frac{m\vec{k}^2}{2k_x})e^{-i(2n-1)\vec{k}_x a} \\ -i(\frac{m\vec{k}^2}{2k_x})e^{i(2n-1)\vec{k}_x a} & [1 - i(\frac{m\vec{k}^2}{2k_x})]e^{-i\vec{k}_x a} - e^{i\vec{\mu}_x a} \end{bmatrix} \begin{bmatrix} \vec{E}_n^+ \\ \vec{E}_n^- \end{bmatrix} = 0$$

Where $m = \epsilon_r d$, the width of the sheet, d , multiplied by its relative permittivity,

ϵ_r .

Writing this as two simultaneous equations, and substituting to eliminate either \vec{E}_n^+ or \vec{E}_n^- gives,

$$\cos(\vec{\mu}_x a) = \cos(\vec{k}_x a) - \frac{m_x \vec{k}^2}{2\vec{k}_x} \sin(\vec{k}_x a) \quad (1.31)$$

As the relation between ω and \vec{k}_x is known equation (1.31) gives the dispersion relation for the crystal, the relation between $\vec{\mu}_x$ and ω .

This, however, is not the only solution that may be found in these crystals. As has been shown earlier, waves may propagate through a sheet under the conditions of total internal reflection. If a second sheet is placed sufficiently close to the first, the wave will couple to it through the evanescent fields found outside the sheet. The dispersion curve for waves guided in this manner is gained by replacing k_x by iq_x , and leads to the second dispersion relationship.

$$\cos(\vec{\mu}_x a) = \cosh(\vec{q}_x a) - \frac{m_x \omega^2}{2c^2 \vec{q}_x} \sinh(\vec{q}_x a) \quad (1.32)$$

Two dimensional crystals

Extending these ideas to two dimensions is trivial as the above method may be applied in each direction separately, leading to the dispersion relations

$$\cos(\vec{\mu}_x a) = \cos(\vec{k}_x a) - \frac{m_x \vec{k}^2}{2\vec{k}_x} \sin(\vec{k}_x a) \quad (1.33a)$$

$$\cos(\vec{\mu}_y a) = \cos(\vec{k}_y a) - \frac{m_y \vec{k}^2}{2\vec{k}_y} \sin(\vec{k}_y a) \quad (1.33b)$$

and, for waves with evanescent fields,

$$\cos(\vec{\mu}_x a) = \cosh(\vec{q}_x a) - \frac{m_x \omega^2}{2c^2 \vec{q}_x} \sin(\vec{q}_x a) \quad (1.34a)$$

$$\cos(\vec{\mu}_y a) = \cosh(\vec{q}_y a) - \frac{m_y \omega^2}{2c^2 \vec{q}_y} \sin(\vec{q}_y a) \quad (1.34b)$$

Thus a Bloch wave that is made from waves with a locally propagating character in the x direction, and a locally evanescent character in the y , would be described using equations (1.33a) and (1.34b).

An example of the dispersion surface for a two dimensional photonic crystal is shown in figure (1.8). Although the first Brillouin zone covers the region $-\pi < \vec{\mu}_x l_x < \pi, -\pi < \vec{\mu}_y l_y < \pi$, it is symmetric about $\vec{\mu}_x l_x = 0$ and $\vec{\mu}_y l_y = 0$. Thus every solution lies in the range shown, which is known as the *reduced Brillouin Zone*.

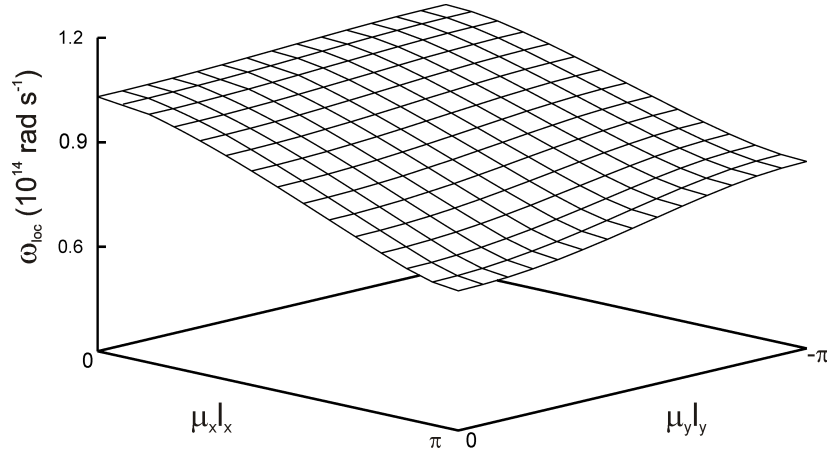


Figure 1.8: An example of a dispersion surface of a two dimensional photonic crystal

The solutions for P polarisation may be obtained in a similar manner, leading

to the dispersion relations for locally propagating waves,

$$\cos(\vec{\mu}_x a) = \cos(\vec{k}_x a) - \frac{m_x \vec{k}^2}{2\vec{k}_x} \sin(\vec{k}_x a) \quad (1.35a)$$

$$\cos(\vec{\mu}_y a) = \cos(\vec{k}_y a) - \frac{m_y \vec{k}^2}{2\vec{k}_y} \sin(\vec{k}_y a) \quad (1.35b)$$

while for locally evanescent waves they are changed to,

$$\cos(\vec{\mu}_x a) = \cosh(\vec{q}_x a) - \frac{m_x \omega^2}{2c^2 \vec{q}_x} \sinh(\vec{q}_x a) \quad (1.36a)$$

$$\cos(\vec{\mu}_y a) = \cosh(\vec{q}_y a) - \frac{m_y \omega^2}{2c^2 \vec{q}_y} \sinh(\vec{q}_y a) \quad (1.36b)$$

1.6 Variation in cell size

The photonic crystals that have been considered so far have been defined as having a constant cell size. Although this makes the dispersion relation far easier to determine, the crystals that it creates are quite limited. It is, however, possible to slowly vary the cell size in the crystal and, provided the variation is sufficiently slow, consider the bandstructure at any point to be equivalent to that of an infinite crystal with a cell length equivalent to the local cell size. The bandstructure will then slowly vary throughout the crystal, scaling up or down depending upon the local cell size [26]. This leads to the possibility of a Bloch wave propagating through the crystal encountering the top or bottom of the band that it is in, and hence meeting a region for which there is no solution at that frequency. Upon meeting the edge of the band, the light is *Bragg reflected*. If, in a one dimensional photonic crystal, the cell size constantly increases/decreases, the Bloch wave, upon meeting a point where it is reflected from the top/bottom of the band, travels through the crystal until it meets the bottom/top of the band and is reflected once again. Thus the Bloch wave is

confined to a region of the crystal for which the range of local cell sizes allow the propagation of a Bloch wave of that frequency, which is separated by two adjacent spatial regions for which there are no propagating solutions. In this manner, a situation analogous to an electronic Bloch Oscillation may be set up [26]. It should be noted that there are several variations on this method that introduce photonic Bloch oscillations that are analogous to electronic Bloch Oscillations, which reveal different aspects of the electronic Bloch Oscillations [29, 30, 31].

1.7 Non-infinite lattices

As has been mentioned previously, there exists a solution to Maxwells equations for electromagnetic waves that are incident upon a crystal even if their frequency falls within a bandgap. This occurs as, in order for a wave to be incident upon the surface, the crystal may not infinite. Thus the restriction that ρ must have a value that lies on a unit circle in complex space no longer holds, and a solution for an exponentially decaying wave may be found. If the crystal is sufficiently thin, or if a region of the crystal where the wave may propagate is sufficiently close to the surface, the wave will still have an appreciable magnitude having passed through the forbidden region. Thus the wave incident upon the surface will couple to the allowed region, and will excite a wave with appreciable magnitude in it. Thus, in a similar manner to the tunneling of particles through a barrier where motion is classically forbidden, E.M. waves may tunnel through analogous ‘forbidden’ regions.

Chapter 2

Hamiltonian ray tracing

Hamiltonian mechanics is a branch of classical mechanics that arose out of *Lagrangian mechanics* in the 1830's [32]. It is built upon the principle of least action, that is, for any problem to be solved a function may be found whose integral is minimized along the path the system takes. In the case of concern here, that of light, the quantity to be minimized is the *optical path length* [33, 34, 35]. This is a quantity obtained by multiplying the distance travelled by the refractive index of the material the light is travelling through.

While arising out of Lagrangian mechanics, Hamiltonian mechanics may be formulated without reference to it, and offers a different perspective on problems to Newtonian mechanics. Although conditions such as the absence of work against friction are generally needed, when a solution is obtainable it may prove easier to find, and may yield an answer that gives more insight into the problem, than a solution obtained using Newtonian mechanics.

This chapter will start with a brief introduction of several ideas such as generalised coordinates and phase space. These will subsequently be used in a derivation of the Lagrangian which will lead on to Hamilton's equations, a set

of first order equations that will describe the evolution of the system. Finally the chapter will use these ideas, combined with those from the previous chapter, to describe the ray tracing process that has been used in the later work.

Phase space

The evolution of a system depends upon not only the current positions of the elements that make it up, but other variables such as the momenta of these elements [36, 37, 32].

If the positions and momenta are each defined in N dimensions then the system is said to have N degrees of freedom. The *Phase space* is a $2N$ dimensional space with an axis for each dimension in which the position and momentum defined. The state of the system may then be completely specified by a point in this $2N$ dimensional space [38].

While the extra dimensions make the path difficult to visualise, plots of slices of the phase space help give insight to the behaviour of system that is not apparent from the paths in real space. These slices, known as *Poincaré sections*, will be explained more fully in the next chapter.

The systems considered here are said to have a *degree of freedom* for each pair of position and momentum coordinates. Thus the particle moving in the six dimensional phase space is said to have three degrees of freedom.

Holonomic constraints

In virtually all systems of interest there will be some constraints that need to be taken into account; a surface the particle is moving on, an impassible wall etc. These may be classified in two ways, *holonomic* and *non-holonomic*. A holonomic constraint is one that may be written in the form,

$$f(r_1, r_2, r_3 \dots r_n, t) = 0 \tag{2.1}$$

where r_i ($i = 1, 2, \dots, n$) are the coordinates that define the system and t is time.

An example of a holonomic constraint is that of an object whose position is restricted to lie on a ring of radius R in the x, y plane. This constraint may be written in the form $x^2 + y^2 - R^2 = 0$. The consequence of this constraint is that, as this condition restricts the solution to a one dimensional curve in this two dimensional plane, the number coordinates needed to specify the state of the system is reduced by one. Any holonomic constraint that is specified with α dimensions explicitly restricts the solution to a $\alpha - 1$ dimensional surface. Thus in the case of the particle being restricted to move on the surface of a sphere, the holonomic constraint will have the form $x^2 + y^2 + z^2 - R^2 = 0$, a two dimensional solution for a holonomic constraint involving three dimensions explicitly. As such, if a system with N degrees of freedom has A holonomic constraints applied to it the state of the system is completely specified in phase space by $n = 2N - A$ coordinates.

By contrast, a non-holonomic constraint is one that restricts the accessible volume of phase space, while leaving the number of dimensions needed to define the system unchanged. An example of this is an impassable wall on the x axis at $x = 10$. While an object constrained to move in the region $x - 10 > 0$, that is x is restricted to values greater than 10, is forbidden from moving in a region of phase space, within that region it is allowed to move in the same number of dimensions as it would without the constraint.

Generalised co-ordinates

The state of the system may be totally specified by a number of coordinates equal to twice the number of degrees of freedom that the system has. Up to this point the systems have been considered using Cartesian coordinates, however this is rarely the most useful set of coordinates, and the holonomic constraints that are applied to the system may mean that the coordinates are no longer

independent. This is demonstrated by returning to the example of a particle confined to lie on a ring of radius R in the x, y plane. Any displacement in the x or y direction must be associated with a translation in the other in order to satisfy $x^2 + y^2 - R^2 = 0$. In this case, a transformation of the coordinate system from Cartesian coordinates to polar coordinates simplifies the problem greatly. Figure (2.1) illustrates the problem with both coordinate sets; The particle's position being specified by x and y in the Cartesian system, and by R and θ in polar coordinates. While both systems use two coordinates to specify

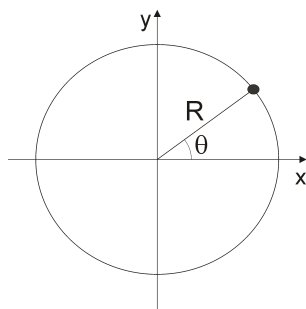


Figure 2.1: A particle confined to lie on a ring radius R in the x, y plane

the position of the particle, as R is always constant, a value of θ is enough to specify the state of the system. Thus R defines the one dimensional surface that the solution must lie on and θ the position on this surface. The coordinates are independent as θ may change independently of R , and should we wish to consider a second ring with a radius R_1 , the change in R may be made independently of θ .

In the same manner, the position of the system on the n dimensional surface in the $2N$ dimensional phase space may be specified completely by n coordinates, if a system of independent coordinates is found. It should be noted that the set of coordinates may not be related to the Cartesian coordinates in a simple manner. The holonomic constraints may, for instance, give a relation between a momentum coordinate and a spatial coordinate, or a non-linear relation between

several variables. Thus the system of independent coordinates, the generalised coordinates, may also need to be specified in terms of unobvious quantities.

2.1 Lagrangian Mechanics

The n generalised coordinates define a surface in phase space that contains all possible states of the system, and each coordinate may take any value that is not forbidden by non-holonomic constraints. As these n coordinates specify points on this surface and no other, that is only solutions that satisfy the constraints, it becomes possible to consider the evolution of a system without explicit reference to forces that arise due to the constraints applied to the system.

To solve a problem with Newtonian mechanics, all the forces on a system must be specified at all times, including those that arise from the constraints. For problems such as a bead that is constrained to move on a curved wire, the forces of constraint become very difficult to specify. As such, problems may become very difficult or impossible to solve. For such problems, a Lagrangian/Hamiltonian mechanics approach may prove more successful; Having found the set of generalised coordinates, and the kinetic and potential energy in terms of them, a solution to Lagrange's equations of motion may be found.

The following section will introduce the Lagrangian, L , a quantity that involves V , the potential energy, and T , the kinetic energy of the system. Having found the Lagrangian, which may also be related to the Hamiltonian, the dynamics of the system may be determined from Lagrange's equations of motion.

It should be noted that while, previously, systems consisting of only a single particle have been considered, systems of numerous particles will be considered from this point on, with constraints relating the dynamics of the particles.

D'Alembert's principle

D'Alembert used a device thought up by James Bernoulli to examine the system under a virtual displacement, an infinitesimal displacement that complies with the forces and constraints on to system at a fixed time t [32]. The equation of motion,

$$\vec{F}_i = \dot{\vec{p}}_i$$

may be rearranged to give,

$$\vec{F}_i - \dot{\vec{p}}_i = 0$$

which shows that the system will be in equilibrium if the force applied to it is equivalent to the actual force on it combined with a force equal to $-\dot{\vec{p}}$. Thus, if, instead of making an infinitesimal displacement to the system under the force \vec{F} , the force is replaced by $\vec{F} - \dot{\vec{p}}$, the work done on a system of i particles may be written as,

$$\sum_i \left(\vec{F}_i - \dot{\vec{p}}_i \right) \cdot \delta \vec{r}_i = 0$$

where \vec{F}_i is the total force on the system, both the force applied to the system and the force of constraint. These two contributions to the total force may be considered separately and hence the above equation may be written as,

$$\sum_i \left(\vec{F}_{(applied,i)} - \dot{\vec{p}}_i \right) \cdot \delta \vec{r}_i + \sum_i \left(\vec{F}_{(constraint,i)} \right) \cdot \delta \vec{r}_i = 0$$

If the second term may be set to zero, then the only forces that are considered are those that are applied to the system; No consideration of the forces that are needed to satisfy the conditions of constraint need be made.

In order to set the second term to zero, systems that involve friction must be excluded. If a particle is moving on a surface in the absence of friction, the

force that constrains the particle is perpendicular to the surface. This allows a virtual displacement to be made tangential to the surface without introducing any virtual work. However, in the same situation in the presence of friction, any displacement will involve virtual work being done.

The elimination of the second term leaves D'Alembert's principle (2.2),

$$\sum_i \left(\vec{F}_{(applied,i)} - \dot{\vec{p}}_i \right) \cdot \delta \vec{r}_i = 0 \quad (2.2)$$

While the sum in equation (2.2) may be set to zero, the independent ($\vec{F}_{applied,i} - \dot{\vec{p}}_i$) terms in general may not. This arises as the δr_i have not been specified as independent, and, as such, constraints on the system may couple the $\delta \vec{r}_i$.

A simple example of this coupling of coordinates involves considering an object rolling down hill where friction is present. As mentioned previously, Hamiltonian mechanics is not easily applicable to systems where work is being done against friction, however as the object is rolling the point of contact does not slide across the surface and hence no work is done. If an arbitrary displacement of $\delta \vec{r}$ down the slope is made to the object, both the change in the position of the object and the corresponding rotation must be made. This may be considered as two separate changes, corresponding to two different coordinates. Alternatively, as is the case for independent coordinates, both of these changes may be related to a single coordinate. In the first case, where this shift is defined by changes in two coordinates, a change in one coordinate determines the change in the other. In the second case both changes are accounted for by one coordinate, so a change in this coordinate may be considered without affecting the systems state with respect to any of the other coordinates.

The relation of the displacement in the generalised coordinates q_j to the

coordinate \vec{r}_i is given by,

$$\delta\vec{r}_i = \sum_j \frac{\partial\vec{r}_i}{\partial q_j} \delta q_j$$

The work due to $\vec{F}_{(applied,i)}$ in terms of the generalised coordinates is then,

$$\sum_i \vec{F}_{(applied,i)} \cdot \delta\vec{r}_i = \sum_{i,j} \vec{F}_{(applied,i)} \cdot \frac{\partial\vec{r}_i}{\partial q_j} \delta q_j = \sum_j Q_j \delta q_j \quad (2.3)$$

where Q_j is the generalised force. As has been mentioned previously, the generalised coordinates may be unobvious quantities that relate to the system, and may not have the dimensions of length. In the same manner, the generalised force does not necessarily have the dimensions of force, but $Q_j \delta q_j$ must have the dimensions of work.

In a similar way, the \dot{p}_i term in equation (2.2) may be related to the generalised coordinates by,

$$\sum_i \dot{p}_i \cdot \delta\vec{r}_i = \sum_{i,j} \dot{p}_i \cdot \frac{\partial\vec{r}_i}{\partial q_j} \delta q_j = \sum_{i,j} m_i \ddot{\vec{r}}_i \cdot \frac{\partial\vec{r}_i}{\partial q_j} \delta q_j \quad (2.4)$$

If the term $\sum_{i,j} m_i \ddot{\vec{r}}_i \cdot \frac{\partial\vec{r}_i}{\partial q_j}$ is expanded in the following manner,

$$\sum_i m_i \ddot{\vec{r}}_i \cdot \frac{\partial\vec{r}_i}{\partial q_j} = \sum_i \left\{ \frac{d}{dt} \left(m_i \dot{\vec{r}}_i \cdot \frac{\partial\vec{r}_i}{\partial q_j} \right) - m_i \dot{\vec{r}}_i \cdot \frac{d}{dt} \left(\frac{\partial\vec{r}_i}{\partial q_j} \right) \right\} \quad (2.5)$$

and the following relationship is found [32],

$$\frac{\partial\vec{v}_i}{\partial \dot{q}_j} = \frac{\partial\vec{r}_i}{\partial q_j} \quad (2.6)$$

these two equations (2.5) and (2.6) may be substituted into equation (2.4), and, after it is rearranged, the following is obtained,

$$\sum_i m_i \ddot{\vec{r}}_i \cdot \frac{\partial \vec{r}_i}{\partial q_j} \cdot \delta q_j = \sum_j \left\{ \frac{d}{dt} \left(\frac{\partial}{\partial \dot{q}_j} \left(\sum_i \frac{1}{2} m_i \vec{v}_i^2 \right) \right) - \frac{\partial}{\partial q_j} \left(\sum_i \frac{1}{2} m_i \vec{v}_i^2 \right) \right\} \delta q_j \quad (2.7)$$

D'Alembert's principle can then be rewritten as.

$$\sum_j \left[\left\{ \frac{d}{dt} \left(\frac{\partial}{\partial \dot{q}_j} \left(\sum_i \frac{1}{2} m_i v_i^2 \right) \right) - \frac{\partial}{\partial q_j} \left(\sum_i \frac{1}{2} m_i v_i^2 \right) \right\} - Q_j \right] \delta q_j = 0 \quad (2.8)$$

$\sum_i \frac{1}{2} m_i v_i^2$ is identified as the kinetic energy of the system, T . The evolution of the system is thus dependent upon the differential of the kinetic energy with respect to the generalised coordinates, time, the time differential of the generalised coordinates, and the generalised force. Substituting in T gives,

$$\sum_j \left[\left\{ \frac{d}{dt} \left(\frac{\partial T}{\partial \dot{q}_j} \right) - \frac{\partial T}{\partial q_j} \right\} - Q_j \right] \delta q_j = 0 \quad (2.9)$$

As q_j has been specified as the set of generalised coordinates, the displacement in each of these directions is independent of displacements in the others. In order for equation (2.2) to hold, each element of the sum, the equation for each value of j , must be equal to zero. Thus the equations of motion for the system separate out into j equations of the form,

$$\frac{d}{dt} \left(\frac{\partial T}{\partial \dot{q}_j} \right) - \frac{\partial T}{\partial q_j} = Q_j \quad (2.10)$$

If the forces are derivable from a scalar potential energy function, V , where the force is equal to the negative gradient of this function, $\vec{F}_i = -\nabla_i V$, then equation (2.3) gives the generalised force for each value of j as,

$$Q_j = \sum_i \vec{F}_i \cdot \frac{\partial \vec{r}_i}{\partial q_j} = - \sum_i \nabla_i V \cdot \frac{\partial \vec{r}_i}{\partial q_j} = - \frac{\partial V}{\partial q_j} \quad (2.11)$$

substituting this into equation (2.10) and rearranging gives,

$$\frac{d}{dt} \left(\frac{\partial T}{\partial \dot{q}_j} \right) - \frac{\partial(T - V)}{\partial q_j} = 0 \quad (2.12)$$

As V is not dependent upon \dot{q}_j , to simplify the maths it is possible to include V in the first term,

$$\frac{d}{dt} \left(\frac{\partial(T - V)}{\partial \dot{q}_j} \right) - \frac{\partial(T - V)}{\partial q_j} = 0 \quad (2.13)$$

Rewriting the equation of motion like this, while not changing the result of the equation, allows the Lagrangian to be defined as $T - V$, and Lagrange's equations may be written as,

$$\frac{d}{dt} \left(\frac{\partial L}{\partial \dot{q}_j} \right) - \frac{\partial L}{\partial q_j} = 0 \quad (2.14)$$

The dynamics of the system are now given by a set of j equations that depend only upon derivatives of the kinetic energy and the potential energy. While $T - V$ will always give a suitable Lagrangian for the system, it is possible to find other solutions for the Lagrangian.

If L does not depend upon t explicitly, the derivative of L with respect to t is as follows,

$$\frac{dL}{dt} = \sum_j \left(\frac{\partial L}{\partial q_j} \frac{dq_j}{dt} + \frac{\partial L}{\partial \dot{q}_j} \frac{d\dot{q}_j}{dt} \right) \quad (2.15)$$

Replacing the term $\frac{\partial L}{\partial q_j}$ by using Lagrange's equation, (2.14), gives,

$$\frac{dL}{dt} = \sum_j \left(\dot{q}_j \frac{d}{dt} \left(\frac{\partial L}{\partial \dot{q}_j} \right) + \frac{\partial L}{\partial \dot{q}_j} \ddot{q}_j \right) = \sum_j \frac{d}{dt} \left(\dot{q}_j \left(\frac{\partial L}{\partial \dot{q}_j} \right) \right) \quad (2.16)$$

rearranging this leads to,

$$\frac{d}{dt} \left[\left(\sum_j \dot{q}_j \left(\frac{\partial L}{\partial \dot{q}_j} \right) \right) - L \right] = 0 \quad (2.17)$$

By integrating this with respect to t it may be seen that the quantity in the square bracket is a constant which is equal to the total energy of the system, and is defined as the system's Hamiltonian.

$$\sum_j \dot{q}_j p_j - L = \text{constant} = H(q_j, p_j, t) \quad (2.18)$$

where p_j defined as the generalised momentum associated with the generalised coordinate, $p_j = \frac{\partial L}{\partial \dot{q}_j}$.

2.1.1 Hamilton's equations

The differential of $H(q_j, p_j, t)$ may be obtained using the chain rule to give,

$$dH = \sum_j \left\{ \frac{\partial H}{\partial q_j} dq_j + \frac{\partial H}{\partial p_j} dp_j \right\} + \frac{\partial H}{\partial t} dt \quad (2.19)$$

However, the differential of H may also be obtained using equation (2.18),

$$dH = \sum_j (\dot{q}_j dp_j - \dot{p}_j dq_j) - \frac{\partial L}{\partial t} dt \quad (2.20)$$

Comparing the coefficients of the dq_j, dp_j & dt terms in these two definitions of dH gives Hamilton's equations of motion,

$$\dot{q}_j = \frac{\partial H}{\partial p_j}, \quad \dot{p}_j = -\frac{\partial H}{\partial q_j} \quad (2.21)$$

Thus, the dynamics of the system are defined by $2n$ first order differential equations. If the Lagrangian of the system can be identified, a Hamiltonian can be obtained, and once the generalised coordinates and momentum have been identified, the evolution of the system can be given.

This is just one formalism of Hamilton's equations. An alternative method involves a variational principle. Here, the time integral of a quantity, known as the *action*, is minimised over the time interval. The action of the system needed to determine the path that a ray of light will take is given by Fermat's principle, *the principle of least time*. This states that the path that the light will take will minimise the optical path length, the refractive index of the material multiplied by the distance the the light travels through it [39, 34]. Thus the condition for the path that the light will take is,

$$\delta \int_{t_1}^{t_2} n(r) \dot{r} dt = 0 \quad (2.22)$$

This is the weak formulation of Fermat's principle. Lagranges equations may also be obtained in a variational form,

$$\int_{t_1}^{t_2} L(r, \dot{r}, t) dt = \text{extremum} \quad (2.23)$$

A comparison of equations (2.22) and (2.23) identifies the Lagrangian as [40, 41],

$$L(r, \dot{r}, t) = n(r) \dot{r} \quad (2.24)$$

This may then be used in equation (2.18) to gain the Hamiltonian for this system,

$$H = \sum_j \dot{q}_j p_j - L = \dot{r} \cdot p - n(r) \dot{r} \quad (2.25)$$

As the generalised momentum $p_j = \frac{\partial L}{\partial \dot{q}_j}$, and identifying q_j as \vec{r} , then

$$p = \frac{\partial L}{\partial \dot{\vec{r}}} = n(r) \hat{\dot{\vec{r}}} = \frac{n(r) \dot{\vec{r}}}{|\dot{\vec{r}}|} \quad (2.26)$$

rearranging this, and substituting in for $v = |\dot{\vec{r}}|$, gives

$$\dot{\vec{r}} = \frac{vp}{n(\vec{r})} \quad (2.27)$$

This may then be substituted into equation (2.25), and after rearranging,

$$H = c \left(\frac{p \cdot p}{n^2(\vec{r})} - 1 \right) \quad (2.28)$$

In an inhomogeneous medium $p = n \hat{k} = c \vec{k} / \omega$, and so,

$$H = c^2 k^2 / n(r)^2 - \omega^2 \Rightarrow \omega_{loc} - \omega \quad (2.29)$$

Where ω_{loc} corresponds to the local dispersion relation.

Now that H has been determined, if a point that lies in a band is chosen as the starting point for a ray, then its subsequent path may be found using the pair of Hamilton's equations corresponding to this system [42, 26]

$$\frac{d\vec{r}}{dt} = \frac{\partial H}{\partial \vec{\mu}}, \quad \frac{d\vec{\mu}}{dt} = -\frac{\partial H}{\partial \vec{r}} \quad (2.30)$$

The numerical process used in calculating the ray path will be explained more fully in the next section.

2.2 Runge-Kutta methods

Many functions may be represented by a Taylor [43] series expansion, an infinite series with terms that involve the derivatives of the function at a point $x = a$. The Taylor series expansion of a function $f(x)$ is given by,

$$f(x) = \sum_{n=0}^{\infty} \frac{f^{(n)}(a)}{n!} (x-a)^n = f(a) + \frac{f'(a)}{1!} (x-a) + \frac{f''(a)}{2!} (x-a)^2 + \frac{f'''(a)}{3!} (x-a)^3 + \dots \quad (2.31)$$

Where

$$f'(a) = \left. \frac{\partial f(x)}{\partial x} \right|_{x=a}, f''(a) = \left. \frac{\partial^2 f(x)}{\partial x^2} \right|_{x=a}, \text{ etc}$$

As this involves an infinite sum it is rarely possible to obtain an exact analytical expression for $f(x)$. However, an approximate solution may be found by truncating the series. The accuracy of the approximation is given in terms of the point that the series is truncated at. A first order solution involves terms up to those involving a , a second order solution involves terms up to a^2 and so on. It should be noted that while a second order solution is normally more accurate than a first order solution, this is not always the case.

The Runge-Kutta methods that will be introduced later use combinations of low accuracy steps in order to match a Taylor series up to the desired number of terms. A fourth order Runge-Kutta method will be introduced, and it is this that has been used to numerically calculate the ray paths in the photonic crystals. As with any numerical calculation that is carried out, a balance between accuracy and the time in which a solution is gained must be made, with fourth order being a common choice for Runge-Kutta methods.

Euler method

If the value of a function $f(x, y)$ is known at a point $x = x_n, y = y_n$, one of the simplest ways of making an approximation of the function at the point $x = x_n + h$ is through the use of the *Euler method* [44]. This involves calculating the first order derivative of the function with respect to x at the point $x = x_n$, and assuming this is the constant rate of change of y across the interval. Hence the value of y_{n+1} , the value of y at the point $x = x_{n+1}$ is related to the original point x_n, y_n by,

$$y_{n+1} = y_n + h \left. \frac{\partial f(x, y)}{\partial x} \right|_{x_n, y_n} \quad (2.32)$$

While this is a very simple method for advancing a function from $x = x_n$ to $x = x_n + h$, it only provides first order accuracy. That is, if the function $f(x, y)$ was expanded as a *Taylor series*, the series will only match up to the terms containing a , and any change in the value of y that is due to higher order terms is ignored.

The midpoint method

The midpoint method, a second order Runge-Kutta method, uses a series of Euler style steps in order to create a second order solution. Instead of calculating a value for y after a single step of length h in the x direction, its value after a step of length $h/2$ is calculated. From this new point a second order calculation of the derivative across the entire step may be obtained. The increased accuracy arises from the fact that the new derivative is symmetrical, that is, it uses information about the derivative from both a forward and backwards step. The fact that this changes the method to second order may be shown using Taylor expansions. Initially, the value of the function at $x + h/2$ may be related to its

value and derivatives at x by a Taylor series, shown here omitting terms $\geq h^3$,

$$f(x + h/2) = f(x) + \frac{h}{2}f'(x) + \frac{h^2}{8}f''(x) + O(h^3) \quad (2.33)$$

where $O(h^3)$ is the error introduced by ignoring the terms involving $h^{\geq 3}$.

A similar expansion may then be found relating the value of the function at $x - h/2$ to the value and derivatives at x ,

$$f(x - h/2) = f(x) - \frac{h}{2}f'(x) + \frac{h^2}{8}f''(x) + O(h^3) \quad (2.34)$$

The term $\frac{h^2}{8}f''(x)$ is common to both expansions and may be eliminated by subtracting (2.34) from (2.33) to leave,

$$f(x + h/2) - f(x - h/2) = hf'(x) + O(h^3) \quad (2.35)$$

If $f(x + h/2) = y_{n+1}$ and $f(x - h/2) = y_n$ then (2.35) may be written,

$$y_{n+1} = y_n + hf'(x)|_{x_{n+1/2}, y_{n+1/2}} + O(h^3) \quad (2.36)$$

This is of the same form as equation (2.32), however, as the second order terms have been eliminated instead of ignored, the first term that is missing is of order h^3 . It should, however, be noted that while equation (2.36) is second order, the derivative needs to be taken at the midpoint, $x_{n+1/2}, y_{n+1/2}$, the value of which is still obtained from a first order step. While this step is half the length of the second order steps, it is possible that it will introduce a significant source of error if the function varies quickly, or is not nicely behaved. However, if these are significant factors then it is likely that this entire process would fail, with second order accuracy not being sufficient to capture the rapid fluctuations.

2.2.1 Higher order Runge-Kutta methods

The previous section has shown how the Taylor expansions of two evaluations of the derivative may be combined in a manner that eliminates the second order terms. In a similar manner, numerous evaluations of the derivative at different points may lead to a set of Taylor series that may be combined in such a way to eliminate higher order terms. As such, a fourth order solution may be obtained through the use of the following evaluations [45],

$$\begin{aligned}k_1 &= hf'(x_n, y_n) \\k_2 &= hf'\left(x_n + \frac{h}{2}, y_n + \frac{k_1}{2}\right) \\k_3 &= hf'\left(x_n + \frac{h}{2}, y_n + \frac{k_2}{2}\right) \\k_4 &= hf'(x_n + h, y_n + k_3) \\y_{n+1} &= y_n + \frac{k_1}{6} + \frac{k_2}{3} + \frac{k_3}{3} + \frac{k_4}{6} + O(h^5)\end{aligned}\tag{2.37}$$

While this gives a higher order solution, the number of calculations that are needed are increased, and hence it will take longer to evaluate.

It is useful when running numerical calculations to be able to make an estimate of the error in the solution. If the error is then too large, as each of the terms depend on h , the accuracy of the calculation may be increased by repeating it using a smaller step size. As such, if a fourth order solution is desired, it is useful to make an additional calculation of a fifth order solution and use the difference between these two solutions as an estimate of the error. This process is made far faster to evaluate if the points at which the differentials are evaluated are common to both solutions, that is to say the same set of k_i are used in each calculation, with different combinations of them resulting in either a fourth or fifth order solution.

2.2.2 The adaptive step size Runge-Kutta method using Cash-Karp parameters

There are numerous ways in which to obtain an estimate of the error when using Runge-Kutta methods, one of the simplest being a comparison with a repetition of the calculation using a step size of half the length. The disadvantage of this method is that many more calculations are needed to carry out both of these evaluations than are needed for the initial calculation itself.

The 'Cash-Karp' parameters [45] are a set of constants that may be used to multiply a set of derivatives calculated at a common set of points across the step in such a manner as to obtain both a fourth and a fifth order solution. The difference in these solutions gives an estimate of error, and may be related to the step size h in such a way as to allow an estimate of the error for a step size, h_1 , to be made.

As these two calculations should give a common solution up to fourth order accuracy, the main source of error should arise from the fifth order term, and, as such, scale as h^5 . Thus if the error for a step of length h is too large, the step size that should restrict the error to the required amount may be estimated as,

$$h_1 = h \left| \frac{TOL}{\Delta} \right|^{0.2} \quad (2.38)$$

where h_1 is the estimated step length and TOL is the maximum allowed value of the estimated error.

If the values of y need to be calculated between two points $x = a$ and $x = b$, where $b - a > h$, then the calculation will need to progress in a series of steps, with the solution of one step being the point from which the next step is calculated. While each step will need to be repeated if the estimated error is too large, if the step size is too small the calculation will take longer than necessary.

As such, if the estimated error is far smaller than TOL , equation (2.38) may be used in order to calculate the maximum step size that may be used. In this case, however, the step that has been taken does not need to be repeated, as its solution already lies within the required tolerance. It should be noted that in practice a program written to carry out this calculation should actually use a value of h_1 that is slightly smaller than that given by equation (2.38). This is because the value of h_1 is only an estimate and, as such, may be slightly too large. If this happens, the program may never adjust to a step size that satisfies the tolerance, or, if it does, it may have carried out sufficient calculations that the use of a slightly smaller step would have allowed the program to have run faster.

Thus, a program should be written in a manner that allows it to adjust to a small step size in regions where the function is varying rapidly, and to save time by doing fewer calculations in regions where the function is only varying slowly. [45, 44]

2.2.3 Ray tracing

The bandstructure of a two dimensional photonic crystal of the form defined in the last chapter was given by pairs of equations of the form,

$$\cos(\vec{\mu}_x a) = \cos(\vec{k}_x a) - \frac{m_x \vec{k}^2}{2k_x} \sin(\vec{k}_x a) \quad (2.39a)$$

$$\cos(\vec{\mu}_y a) = \cos(\vec{k}_y a) - \frac{m_y \vec{k}^2}{2k_y} \sin(\vec{k}_y a) \quad (2.39b)$$

Hamilton's equations, which determine the trajectory of a ray passing through the system, have been shown to be,

$$\frac{d\vec{r}}{dt} = \frac{\partial H}{\partial \vec{\mu}}, \quad \frac{d\vec{\mu}}{dt} = -\frac{\partial H}{\partial \vec{r}} \quad (2.40)$$

With the Hamiltonian of the system being,

$$H(\vec{r}, \vec{\mu}, \omega) = \omega_{loc}(\vec{\mu}, l(x), l(y)) - \omega \quad (2.41)$$

where $\vec{\mu}$ is the bloch wavevector and $l(x)$ and $l(y)$ are the local cell length in the x and y directions respectively. As ω_{loc} is the local bandstructure of the system, these equations are all that are needed in order to calculate a ray's path through the crystal.

Initially, the value of ω for the ray needs to be set (labelled as ω_1), and a starting point found in such a way that allows equations (2.39a) and (2.39b) to be satisfied, alongside the condition that $k_x^2 + k_y^2 = \epsilon_r^2 \omega^2 / c^2$. To do this, equations (2.39a) and (2.39b) are solved numerically, using the *minpack* subroutine *hybrd1* to find values for \vec{k}_x and \vec{k}_y .

Having found a starting position for the ray, the path it takes may be found from a numerical solution of the equations (2.40). These are solved through the use of the fourth order Runge-Kutta method described earlier. As the value of ω_1 is constant, the variation of H with respect to $\vec{\mu}$ and \vec{r} is determined by the change in the bandstructure. As such,

$$\frac{\partial H}{\partial \vec{\mu}} = \frac{\partial \omega_{loc}}{\partial \vec{\mu}} \quad \text{and} \quad \frac{\partial H}{\partial \vec{r}} = \frac{\partial \omega_{loc}}{\partial \vec{r}} \quad (2.42)$$

The first order derivatives that are used in the solution of the Runge-Kutta method are obtained by calculating the change in ω_{loc} using a midpoint method. The value of ω_{loc} is calculated at the points $\vec{r} + d\vec{r}$ and $\vec{r} - d\vec{r}$, or $\vec{\mu} + d\vec{\mu}$ and $\vec{\mu} - d\vec{\mu}$, and the first order derivatives are then given as

$$\frac{\partial \omega_{loc}(\vec{r}, \vec{\mu})}{\partial \vec{r}} \approx \frac{\omega_{loc}(\vec{r} + \delta\vec{r}, \vec{\mu}) + \omega_{loc}(\vec{r} - \delta\vec{r}, \vec{\mu})}{2\delta\vec{r}} \quad (2.43)$$

and

$$\frac{\partial \omega_{loc}(\vec{r}, \vec{\mu})}{\partial \vec{\mu}} \approx \frac{\omega_{loc}(\vec{r}, \vec{\mu} + \delta \vec{\mu}) + \omega_{loc}(\vec{r}, \vec{\mu} - \delta \vec{\mu})}{2\delta \vec{\mu}} \quad (2.44)$$

where $d\vec{r}$ and $d\vec{\mu}$ take preset values for a uniform crystal, and preset values that are scaled by the local cell length in the slowly varying crystals.

Chapter 3

Chaos

Even in apparently simple *deterministic* systems, whose future state may be completely specified by a set of equations, highly complex and apparently random behaviour may be found. In these cases it is possible that the systems are exhibiting *Chaotic* behavior, which makes predictions of the long term future state of the system impossible to make. This arises not from a failure in the equations to describe the evolution of the system, but instead from the extremely high sensitivity of the system to the initial conditions [46]. As such, to know the state of the system at some point in the distant future the initial conditions would need to be known to an unattainable level of accuracy.

Chaos is a phenomena that has only been considered in any depth in recent times, aided greatly by the use of modern computers to carry out numerical solutions to equations that previously may have been deemed too laborious, or too unimportant. This was compounded by the belief that the maths that describes the universe would have a simple and beautiful solution. Mathematicians and Physicists tended to focus on problems they could solve, and these would be those for which the solutions often are periodic. This led experimentalists who

observed complex motion to ascribe it to ‘noise’ created by the effect of outside influences on the system. The assumption was that removing the effects would cause the system to revert to simple behaviour with an elegant mathematical solution.

3.1 Phase space

The previous chapter showed that the evolution of paths in a Hamiltonian system are completely defined by pairs of equations involving generalised position and momentum. Thus the state of a particle in N dimensional space is completely defined by $2N$ values, and the evolution of the state of the particle as time passes may be viewed as a path being traced through phase space. It is consideration of these paths in phase space that will give the definition of chaos that is used in this work. Along with this a slightly more general consideration of systems, including those for which work is done against friction, will be made.

3.1.1 Integrable and non-Integrable systems

It has been mentioned in the previous chapter that, if there are a independent constants for the system, the state of the system is restricted to lie on a $2N - a$ dimensional surface in the $2N$ dimensional phase space. In the special case for which the number of independent constants is equal to the number of degrees of freedom of the system, the system may be said to be integrable [47]. In this case all paths in the system must be either periodic or quasi-periodic, but not chaotic. It is not the case, however, that if one region of phase space is integrable then the entire system is. Many systems have phase spaces containing a mix of both integrable and non-integrable regions.

In Hamiltonian systems, for which the Hamiltonian is independent of time,

the Hamiltonian will be a constant of motion and is often identified as the system's total energy. Other constants of motion will depend on $p(t)$ and $q(t)$ but must remain constant as $p(t)$ and $q(t)$ change with time.

The variation of a function of p and q , $f(p, q)$, with respect to time may be expanded as follows,

$$\frac{df}{dt} = \frac{dp}{dt} \cdot \frac{\partial f}{\partial p} + \frac{dq}{dt} \cdot \frac{\partial f}{\partial q} \quad (3.1)$$

Using Hamilton's equations, as given in the previous chapter, the following relation may be gained,

$$\frac{df}{dt} = \frac{\partial H}{\partial p} \cdot \frac{\partial f}{\partial q} - \frac{\partial H}{\partial q} \cdot \frac{\partial f}{\partial p} \quad (3.2)$$

Following this, if the *Poisson bracket*, $\{a_1, a_2\}$, of two functions a_1 and a_2 is defined as,

$$\{a_1, a_2\} = \frac{\partial a_2}{\partial p} \cdot \frac{\partial a_1}{\partial q} - \frac{\partial a_2}{\partial q} \cdot \frac{\partial a_1}{\partial p} \quad (3.3)$$

Then the right hand side of equation (3.2) may be identified as the Poisson bracket of H and f . As such, the function $f(p, q)$ is a constant with respect to time if $\{H, f\} = 0$.

It should be noted that simply finding a function that is a constant of the motion is not sufficient to reduce the number of dimensions that a solution for the system may move in, these constants must also be independent. A new function that is a constant of motion is only independent if it may not be created out of combinations of the existing set of constants of motion.

3.1.2 Dissipative and Non-Dissipative systems

When considering the time evolution of systems, the distinction between dissipative and non-dissipative systems becomes important. In dissipative systems,

for example where friction plays a role, energy is not a constant and the paths that occur in the system converge toward a set of solutions known as an attractor [48, 47]. It is possible that more than one attractor will exist for a system. In such a case the region of phase space that converges upon an attractor is known as its basin of attraction. There may exist points between two basins of attraction that are drawn to neither. This, however, will be a saddle point, and as such the points that correspond to it will be both uncommon and unstable. The system will exhibit transient behaviour whilst a path dissipates its energy and closes onto the attractor. Thereafter the path will behave in a manner similar to other paths starting on that basin of attraction. Consequently the initial behaviour of the system may be quite different from the system's long term behaviour. The behaviour that is seen before the system settles into a steady state is known as transient behavior.

Hamiltonian systems generally do not exhibit this type of transient behaviour. These two different cases, dissipative and non-dissipative, will also have signatures in the nature of the paths in phase space; volumes in phase space being preserved for non-dissipative systems, but changing in dissipative systems.

3.1.3 Volumes in phase space

In Hamiltonian, non-dissipative, systems, Liouville's theory may be used in order to show that volumes of phase space are incompressible [32, 36]. As a consequence, as the system evolves the shape of the phase-space region occupied by a set of trajectories may change but its volume is conserved.

If the paths that lie on the surface of a volume in phase space are considered at time t , then at some later time, it may be seen that all the points that were initially inside the surface remain there. If this were not the case, the path of

a point that was inside the volume must have crossed a path that was on the surface. This is something that cannot happen, as, if the paths cross, then they simultaneously occupy the same point in phase space. As the evolution of each point in phase space is uniquely defined, then these two paths must evolve in the same manner. That is to say they must be the same path. By the same reasoning, no point that started outside of the volume that is being considered here may enter it. The shape of the region may distort as the system evolves but the volume occupied by that region may not change. As the volume remains constant, and the region contains a constant number of trajectories, then the density of states in the phase space must be constant.

3.2 Lyapunov exponents

The rate at which two paths, starting a distance dx apart in phase space, separate may be quantified through the use of *Lyapunov exponents*. The direction in which the displacement is made will affect the rate at which the two paths separate. As such, if an N dimensional system is considered then there will be $2N$ Lyapunov exponents, one associated with a displacement in each dimension of the phase space.

If the separation of two paths at a time t is given as $d_{t,i}(X)$, $i = 1, 2, 3 \dots 2N$ corresponding to the $2N$ dimensions in phase space, and X is the separation of the paths in dimension i , then the set of $2N$ Lyapunov exponents λ_i may be defined as [37],

$$\lambda_i = \lim_{t \rightarrow \infty} \frac{1}{t} \ln \left| \frac{d_{t,i}(X)}{d_{0,i}(X)} \right| \quad (3.4)$$

In Hamiltonian systems, the fact that volumes are preserved in phase space has the consequence that the Lyapunov exponents must sum to zero. The largest Lyapunov exponent is termed the ‘maximal Lyapunov exponent’. If the

value of this is both positive and real then the separation of the paths will be exponential, corresponding to chaotic behaviour [49, 50]. While there are many ways in which Chaos may be defined, in this work we will consider a path to be in a chaotic area of phase space if one of its associated Lyapunov exponents is real and positive. The separation of the paths may be rewritten as,

$$|d_{t,i}(X)| \approx \exp^{\lambda_i t} |d_{0,i}(X)| \quad (3.5)$$

This exponential separation of paths is what makes the long term behaviour of chaotic paths so impossible to predict. There will always be a limit to the accuracy that the starting point may be measured to and any slight error will result in a completely different path. It should be noted that it is these individual paths that need to be considered if chaos is to be found; considerations of volumes of phase space will not show this behaviour.

The paths in the system will not all suddenly change from being periodic to being chaotic, however. As the perturbation on the system increases, different regions will become chaotic.

3.3 Poincaré sections

For a system with 2 or more degrees of freedom, the phase space in which the state of the system is defined has too many dimensions to visualise simply. To visualise the dynamics, a representation of the system in a reduced number of dimensions is needed. A Poincaré section is such a representation. Poincaré sections may be taken in one of two manners, the first of which involves considering how a path crosses a two dimensional plane in phase space. Every time the path in phase space crosses this plane, the point at which it crosses is marked. This is shown in figure (3.1) for both an aperiodic [3.1(a)], and periodic path

[3.1(b)]. The spread of the points plotted on the section may indicate whether a path is stable or unstable, or be indicative of other properties of the system, such as dissipation.

If the path is periodic with a period t , then at a time t after crossing the plane in phase space it will cross it again at the same point. The path may not have crossed the plane at any other points during this interval, or it may have crossed the plane again once, or many times. If the path is aperiodic then it will never return to a point at which it has crossed the plane previously.

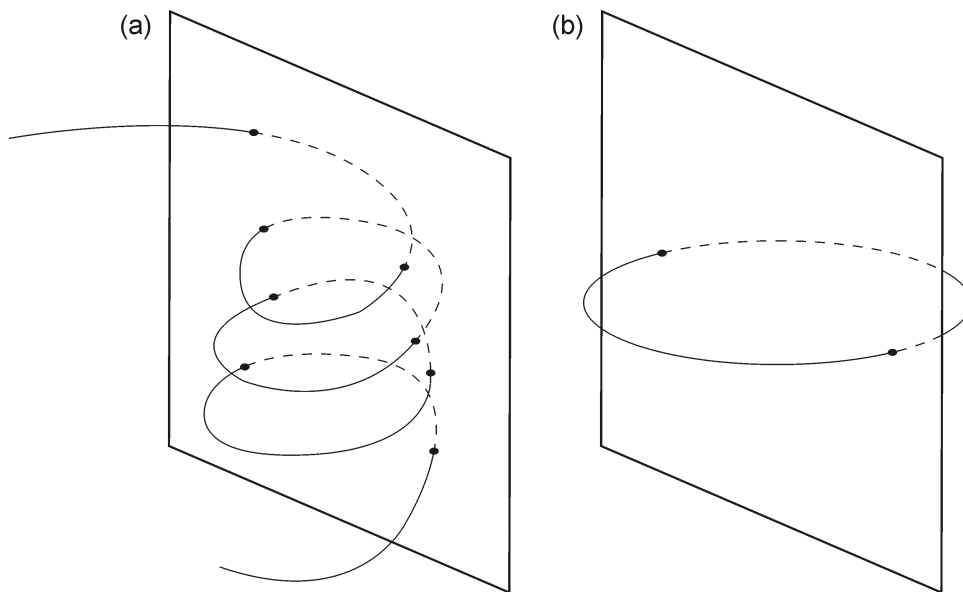


Figure 3.1: (a) an aperiodic path crossing a Poincaré section at numerous points, the path will never return to a point at which it has previously crossed the section. (b) a periodic path crossing and recrossing a Poincaré section at the same points.

If the system is dissipative, transient behaviour will be seen, with the points collapsing onto the attractor associated with a particular basin of attraction. In non-dissipative systems there will be no transient behaviour.

The second manner in which a Poincaré section may be constructed involves plotting a point on the section at equally spaced time intervals, this is termed a *stroboscopic Poincaré section*. The parameters on each axis of the two dimen-

sional section may correspond to any of the position or momentum coordinates, or combinations of these parameters.

In both cases, the choice of the plane in phase space/time interval and parameters on each axis, should be considered carefully. If the wrong Poincaré section is chosen then interesting behavior in phase space may be missed. The Poincaré section should be chosen in such a manner as to ensure that the path crosses the section at least once. This can be achieved by choosing the initial conditions for a path to lie on the Poincaré section itself.

In the systems being analysed in this work a point will be plotted on the section every time a ray turns from travelling from the left to the right. That is, a point is plotted each time the ray crosses the $p_x = 0$ plane if, and only if, p_x is increasing. The rays will also cross the $p_x = 0$ plane when the rays turn from travelling to the right to travelling the left, however, these points will be considered separately.

In chapter 2 it was mentioned that A holonomic constraints applied to the system will lead to the solution being confined to an $n = 2N - A$ dimensional surface in the $2N$ dimensional phase space, with $A = N$ for integrable systems. If the path is chaotic, instead of moving on a surface it will be confined to a volume of phase space. This will be shown by a spread of points on the Poincaré section and, given enough time, the ray should wander through the entire region of phase space that it is restricted to. The spread of points will then show the limit of the region in which the ray moves. If the ray is confined to a surface, the points plotted on the Poincaré section should follow a line corresponding to where the surface crosses the section.

Dynamic barriers

The areas of phase space that are of particular interest are those where two distinct chaotic regions are separated by a region in which the paths are stable.

The regions in which the paths become stable are termed *dynamic barriers*, stopping rays in one chaotic region from entering the other. The rays that follow stable paths in the dynamic barrier will be confined to move on a surface in phase space. This will result in the points on the Poincaré section lying on a curve given by the cross section of the surface the rays moves at the point that it crosses the two dimensional surface in phase space corresponding to the Poincaré section. This situation is show in figure (3.2). The curved surface

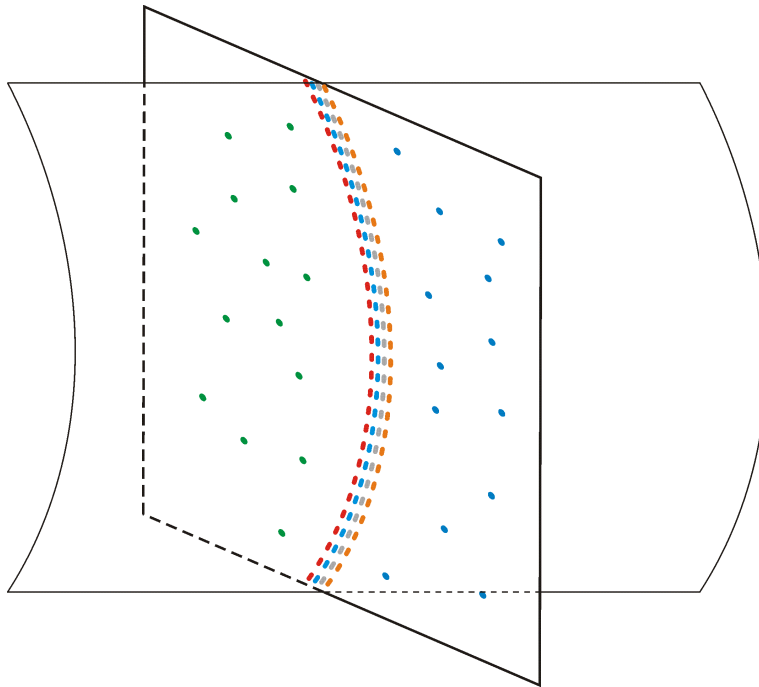


Figure 3.2: The curved surface is the surface a ray may move on. The second surface, the surface with points marked on it, is the Poincaré section. Each different colour represents points associated with a single path. The orange points correspond to a ray confined to the curved surface

represents the surface a ray is confined to, while the second surface, the surface with points marked on it, is the Poincaré section. The spread of green and blue points on either side of points following a curved line correspond to chaotic paths, while the points following the curves correspond to stable paths. It is

this feature that will be looked for in later chapters to help identify dynamic barriers in the system. It should be noted that great care must be taken when looking at Poincaré sections as, due to the greatly reduced number of dimensions shown, the points that are plotted on a surface may easily be misinterpreted as indicating behaviour that is not really there. They should be used as indicators of behaviour, rather than as a definitive test.

Chapter 4

One dimensional Photonic crystals

It has been shown in previous chapters that the bandstructure in a slowly varying photonic crystal of the type defined in chapter 1 is, locally, equivalent to that of an infinite crystal with a constant cell size equal to the local cell size. The variation of the bandstructure may mean that a Bloch wave travelling through the structure may encounter the top or bottom of the band that it is in. Upon doing so it will be Bragg reflected.

The following chapter will initially introduce the phenomenon of *Bloch oscillations* of electrons in semiconductors, whereby a uniform electric field applied to an electron in a periodic potential causes it to oscillate instead of accelerate uniformly [51]. An analogous situation involving Bloch waves in photonic crystals will then be considered, and calculations of the transmission profiles of, and electric fields that are inside, these structures will be made. These calculations will be compared to results gained from experiments carried out by the author in the microwave regime. Finally, some consideration of the relation between

structures with infinitesimally thin sheets, defined by $m = \epsilon_r d$ in chapter 1, and structures with finite width sheets will be made. This comparison will be of use in later work that involves the two dimensional photonic crystals considered in the later chapters.

4.1 Bloch oscillations

An electron in a periodic potential that has a constant electric field applied to it will undergo periodic oscillations unless scattering occurs. This rather counterintuitive fact occurs due to two processes, acceleration due to the field and Bragg reflection.

The *de Broglie* hypothesis states that any particle also has a wave like nature, with the wavelength associated with the particle being inversely proportional to its momentum [52]. As such, the de Broglie wavelength associated with an electron that is accelerated from rest by an electric field will decrease from an initially large value. Thus, while the periodicity of the potential remains constant, the wavelength associated with the particle will change. At some point the de Broglie wavelength will have shrunk to such an extent that the Bragg condition will be satisfied, scattering the electron back in the other direction. Having been reflected, the electron will then be decelerated by the field until it returns to its starting point and whereafter the process will repeat [53]. Thus, unless it scatters, the electron is confined between the point at which it is Bragg reflected and the point at which it is turned by the electric field, oscillating back and forth. The average time between scatterings for electrons in natural crystals is, however, sufficiently small that oscillations are rarely completed, and hence experimental observation of these oscillations has so far proved impossible.

Analogous Bloch oscillations may, however, be observed in photonic structures, with a variety of systems being used to model different aspects of the

electronic Bloch oscillations. Many of these use two dimensional structures, confining the photons by Bragg reflections, total internal reflection, or by variation in the lateral width of the crystal.

The structures used in this work will be of the form of the one dimensional photonic crystals that have been described in chapter 1. The cell length will vary slowly, shifting the bandstructure, and in doing so mimic the effect of the electric field on the electronic Bloch oscillations. As described above, the electric field causes a change in the de Broglie wavelength of an electron. However, the frequency of the electromagnetic wave is fixed. Thus, instead of the de Broglie wavelength of the electron changing in a fixed periodic potential, the frequency of the electromagnetic wave is held constant and the period of the potential is modulated spatially.

In this case, the electromagnetic wave is confined at both ends of the oscillation by a Bragg reflection, and it should be noted that this means that there are no Bloch oscillations in the lowest band. While the bandstructure will scale with changes of the local cell length, the lowest band always extends down to $\omega = 0$. This means that, while a Bloch wave in the lowest band may meet a point in the crystal where it is reflected off the top of the band, at no point will it be reflected off the bottom of the band.

4.2 Arrangement of the dielectric sheets

The lattice constant, l , at position x_a along the photonic crystal is defined using an exponential chirp [26] that is

$$l(x_a) = l_0 \exp[\eta(x_a - x_0)], \quad (4.1)$$

where l_0 is a predefined constant, the unit cell length, and η is a constant whose value will determine the rate of change of the cell length.

If x_0 is defined to be the left hand side of cell $n = 0$, then the left hand side of cell $n = 1$, $x = x_1$, is given by solving,

$$\int_{x_n}^{x_{n+1}} \exp(-\eta(x - x_0)) dx = l_0 \quad (4.2)$$

In the same way, once the position x_1 is known, equation (4.2) may be used to find the position of the left hand side of cell $n = 2$. As the start of cell $n = 1$ is also the end of cell $n = 0$ the length of each cell may be obtained. Repeating this process, with values of n from 0 to the desired value, a crystal with any number of cells may be obtained.

Alternatively, equation (4.2) may be used [26] to gain the approximate recursive relationship,

$$L_n \approx \frac{L_{n-1}}{1 - \eta L_{n-1}} \quad (4.3)$$

where n is the cell number, and L_n is the length of cell number n .

4.3 Transmission through, and electric fields inside, short photonic crystals

It was shown in chapter one that the left and right travelling components of electromagnetic waves may be related at any two points in, or either side of, a photonic crystal with the use of transmission matrices. The following will use this technique to examine the transmission of electromagnetic waves through photonic crystals made up of a small number of cells. Initially the cells will all have the same length, allowing the bandstructure to be seen. Following this, crystals whose cell length varies spatially, so that the frequency bandstructure

also varies, will be considered. These crystals will be constructed in such a way that a complete photonic Bloch oscillation will be possible in the structure. At one side of the crystal the frequency of the incident wave for which the Bloch oscillation will be seen will lie below the bottom of an allowed band while, due to the shift in bandstructure, at the far side it will lie above the top of the band. Consequently, the region of the crystal for which the frequency lies within the band is enclosed, with forbidden regions at either end. As these forbidden regions are narrow, the incident electromagnetic waves will tunnel [39] into the band with a relatively small loss of amplitude.

The exponential chirp used to determine the cell lengths in these crystals has the effect that, for each band, the top and the bottom of the bands are a constant spatial distance apart regardless of frequency. This leads to all Bloch oscillations in a single band to have the same spatial length, however, the spatial length of Bloch oscillations in other bands may be different.

The constant distance between the top and bottom of each band makes this situation analogous to a square potential well, with resonances being seen whenever the angular frequency of the electromagnetic wave allow the waves to interfere constructively. Due to the constant distance between the top and the bottom of the band, in the limit that the barriers Bragg reflect the waves perfectly at the band edge, these resonances will occur at equally spaced intervals in frequency. The ability of the waves to tunnel through the forbidden regions in these short crystals will mean that in the crystals considered here the resonances will not be perfectly equally spaced, though it should be possible to achieve a good approximation to this effect. This effect is analogous to a *Wannier-Stark ladder* that will be seen in semiconductors in the absence of scattering when an electric field is applied [54, 55, 56]. The discrete nature of the lattice that makes up the semiconductor will lead to Bragg reflections occurring at points

separated by one spatial period of the lattice. With this change in position comes a change in the potential due to the applied field, and hence a change in the energy associated with the Bloch oscillation. As the potential will change by a constant amount between each of the points at which Bragg reflections will occur, this will lead to a set of Bloch oscillations that are equally spaced in terms of energy, a Wannier-Stark ladder [57].

For these one dimensional photonic crystals, the electromagnetic waves will propagate perpendicular to the sheets and hence the polarisation of the electromagnetic waves will play no role, with the S and P polarisations being equivalent.

4.3.1 Constant cell length

It is useful to consider transmission through a short photonic crystal, which has a constant cell length, with the width of the dielectric sheet being a fixed fraction of the cell length. If the left hand side of the first cell is at $x = 0$, and the right hand side of the last cell is at $x = \alpha$, the left and right travelling components of the wave may be related by the use of a 2x2 transmission matrix as described in chapter 1 [see equation (1.27)],

$$\begin{bmatrix} E_{x=0}^+ \\ E_{x=0}^- \end{bmatrix} = \begin{bmatrix} Tr_{(1,1)} & Tr_{(1,2)} \\ Tr_{(2,1)} & Tr_{(2,2)} \end{bmatrix} \begin{bmatrix} E_{x=\alpha}^+ \\ E_{x=\alpha}^- \end{bmatrix} \quad (4.4)$$

Where $E_{x=0}^+$ and $E_{x=0}^-$ are the right and left travelling components of the electromagnetic wave at $x = 0$, $E_{x=\alpha}^+$ and $E_{x=\alpha}^-$ are the right and left travelling components of the electromagnetic wave at $x = \alpha$ and $Tr_{(1,2,1,2)}$ are the four elements of the transmission matrix.

If $E_{x=\alpha}^- = 0$, as is the case if the only electromagnetic wave incident upon the crystal is from the left hand side, then the relation between $E_{x=0}^+$ and $E_{x=\alpha}^+$

is given by,

$$E_{x=0}^+ = Tr_{(1,1)} E_{x=\alpha}^+ \quad (4.5)$$

Thus the field at the right hand side of the crystal is $1/Tr_{(1,1)}$ of that incident on the left, and the intensity is $1/Tr_{(1,1)}^2$.

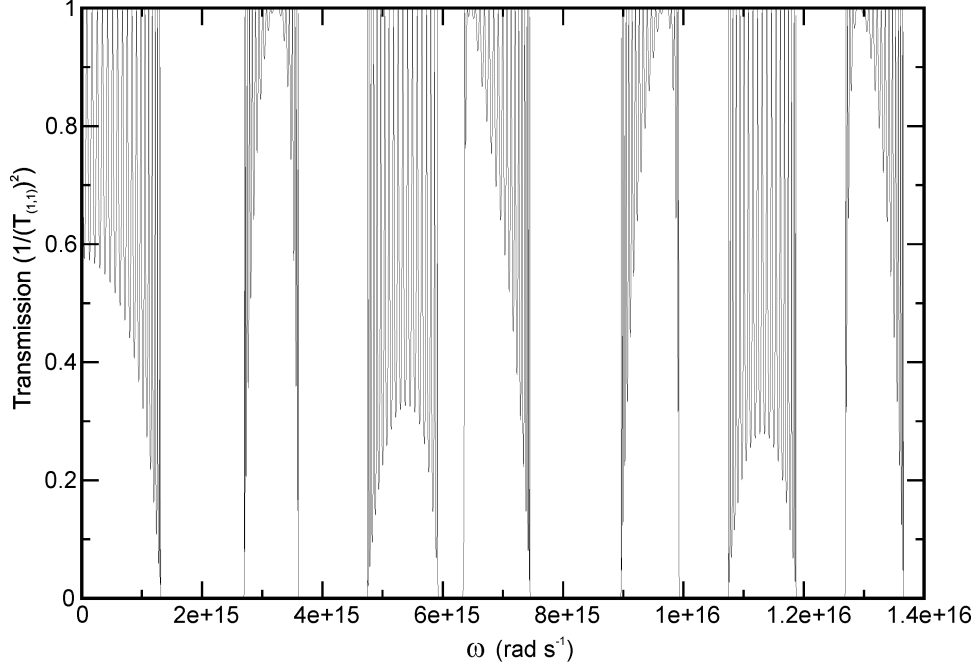


Figure 4.1: Transmission through a set of 20 sheets

Figure (4.1) shows the transmission through a set of 20 equally spaced dielectric sheets. The transmission is defined here as $1/Tr_{(1,1)}^2$ and, unless explicitly mentioned, this is the definition that will be used throughout the rest of this work. The cell length, the width of one dielectric sheet and one air gap, is constant with a value of $0.25\mu m$, and the sheet width is one third of the cell length. The refractive index of the dielectric sheets is $n_1 = 3.5$, while the air gaps have a refractive index of $n_0 = 1$.

As can be seen, the lowest band, which produces high transmissions, stretches

down to $\omega = 0$. The lack of a lower band edge is the reason for the absence of Bloch oscillations in the lowest band, as with no band edge there will be no Bragg reflection. It may also be seen that within each band there are a number of transmission peaks, both the nature of these, and the positioning of the bands will be discussed later in this chapter.

The bandstructure is clear, even for a relatively low number of sheets, due to the high refractive index that is used. This may be seen if the reflectance from a single interface between materials with different refractive indices is considered. The Fresnel equations show that the reflected amplitude from an interface is related to the difference between the refractive index of the two materials [58].

$$R = \left(\frac{n_1 - n_2}{n_1 + n_2} \right)^2 \quad (4.6)$$

where R is the reflected intensity, n_1 is the refractive index of the material the wave is in and n_2 it the refractive index of the material it is incident on. If this crystal is considered from the perspective of Bloch's theorem, as given in chapter 1, then the low number of sheets means that there are a low number of reciprocal lattice points from which reflections may be obtained. If there is only a small difference between the refractive index of each sheet then the reflectance from each sheet will be low, and hence the coefficient in each term of the fourier series, $V(\vec{G})$, in equation (4.7) [equation (1.16) from chapter 1] will be small, limiting the effect of each reflection.

$$\vec{u}_1 = \exp(i\vec{k} \cdot \vec{r}) \sum_{\vec{G}} V(\vec{G}) \exp(i\vec{G} \cdot \vec{r}) \quad (4.7)$$

A large difference in refractive index allows the contribution of each reflected wave to be greater, and thus fewer reflections are needed to image the potential of the crystal strongly. If each of the reflections is very weak, then in order to

mimic the periodicity of the crystal strongly and accurately, many more terms are needed in the summation in equation (4.7). That is, if the reflection from each reciprocal lattice point is low, then more reciprocal lattice points are needed to image the periodicity of the crystal strongly.

4.3.2 Varying cell length

The Bloch oscillation is created by introducing a slow variation in the length of the cell size, which will cause a shift in the positions of the band. As Maxwell's equations scale with length, the bands in a photonic crystal scale up or down, as opposed to shifting up or down as is the case with electrons in periodic potentials [26].

The exponential chirp that has been applied to the crystal causes the top and bottom of each band to shift in such a way that, in each band, the points at which a Bragg reflection occurs remain an equal distance apart. Thus all Bloch oscillations that occur in the second, or higher, band will have the same spatial amplitude regardless of the frequency they occur at. While all oscillations in a single band are of the same length, oscillations in different bands will have different lengths.

This situation may be seen in figure (4.2) which shows the positions of the bands in a photonic crystal w.r.t frequency as the local cell length changes. The grey regions are those for which there is no solution for a propagating Bloch wave at that frequency. The black regions mark the range of frequencies for which both limits of a band are within the crystal, the range of frequencies for which a complete Bloch oscillation may be found.

This is in some ways analogous to a potential well with resonances, the eigenmodes of the system, being seen when the frequency allows the Bloch wave to add constructively over the oscillation. If an infinite crystal is considered [26]

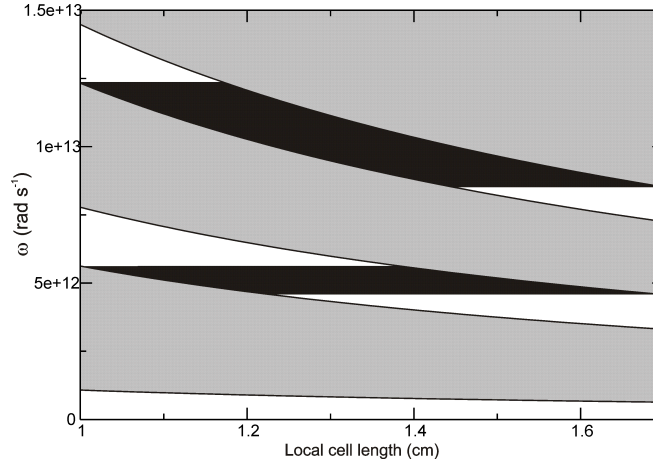


Figure 4.2: The varying band structure for a crystals whose cell length varies according to an exponential chirp. The grey regions are regions for which no real propagating Bloch waves may be found. The black regions show the range of frequencies for which both the top and bottom of the band may be found in the crystal.

the points at which these resonances occur are equally spaced in frequency and, due to the manner in which the band shifts, the oscillations take the same time to complete. The points of reflection become less perfect for crystals of a finite length, thus for a short crystal there is some spreading of the end positions.

Figure (4.3) shows the transmission calculated for a set of 45 sheets that, considering just the second band, encloses a single Bloch oscillation. The first cell, L_0 , has a length of $0.235\mu\text{m}$, and the length of subsequent cells being given by equation (4.3) with $\eta = 3.333 \times 10^4$. In each case the width of the dielectric sheet is $1/3$ of the length of the cell and has a refractive index of $n=3.5$, the air gap has a refractive index of 1.

The central transmission peak is at the frequency that corresponds to this eigenmode of the system, with the short forbidden regions at either end of the crystal causing only a small decay in the field. The peaks on either side correspond to Bloch oscillations that are shifted slightly spatially to the left and right of the central oscillation. Due to the fact that there is a greater distance

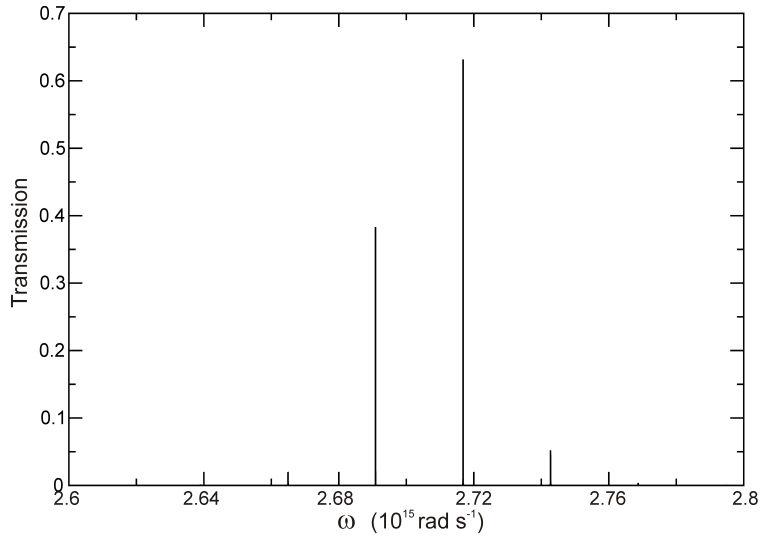


Figure 4.3: The transmission through a photonic crystal consisting of 45 dielectric sheets

of forbidden region that the field must pass in order to reach the eigenmode there is a greater decay of the field. As mentioned previously the spacing of the peaks is roughly equal.

Construction of the photonic crystal

If an infinite crystal was being considered, the bandstructure at any point would be equivalent to that of the local cell size. This becomes slightly more approximate for the use of non-infinite crystals, however it still has some validity. As such, the use of bandstructures for photonic crystals with a constant cell size may still be of use when constructing and analysing non-infinite crystals.

To find a structure that may contain a complete Bloch oscillation, a cell size, l_1 , is selected, and the bandstructure for a crystal with this as its constant cell size is made. A frequency, f_1 , is then selected that lies below the bottom of the band of interest, and the cell size is then changed until it reaches a value l_2 for which this frequency lies above the top of the band. As the bandstructure

should be roughly equivalent to that of the local cell size, if the range of cell sizes in the crystal spans both l_1 and l_2 , both the top and the bottom of the band should be found in the crystal at the frequency selected. This is true regardless of chirp rate, with a crystal with a slower chirp merely containing more cells and a longer Bloch oscillation. While there will be a frequency for which the top and the bottom of the band are contained in the crystal, if this frequency does not correspond to an eigenstate, there will be no complete Bloch oscillation contained.

To increase the chance that an eigenstate is contained within a photonic crystal, and that the length of the forbidden region at either end of the crystal is sufficiently long to lead to a strong reflection of the Bloch wave from the top or bottom of the band, the cells corresponding to the lengths l_1 and l_2 will not be the first and last cells in the crystal. Instead if more cells are included at both ends of the crystal, leading to a larger forbidden region in the crystal, the top and the bottom of the band will be within the crystal for a range of frequencies, not just for the frequency f_1 .

It should be noted that regardless of whether a Bloch oscillation is completely contained or not, the transmission graph will take the same form. This is because even if only one end of the Bloch oscillation is present in the system, a transmission peak will still be seen.

The electric fields inside the crystals

The transmission matrix method may be used to gain more information about the system than just the transmission through, and reflectance from, the entire structure. If $x = \alpha$ is a point at the right hand edge of the photonic crystal and $E_{x=\alpha}^- = 0$, equation (4.8) may once again be used to calculate the relation between $E_{x=\alpha}^+$, $E_{x=0}^-$, and the incident wave $E_{x=0}^+$. Having set the values of $E_{x=0}^+$ and $E_{x=0}^-$ by the calculation involving the entire crystal, a new

transmission matrix may then be constructed between $x = 0$ and $x = \alpha$, where α is now any point in the crystal.

$$\begin{bmatrix} E_{x=0}^+ \\ E_{x=0}^- \end{bmatrix} = \begin{bmatrix} A_{0 \rightarrow \alpha} & B_{0 \rightarrow \alpha} \\ C_{0 \rightarrow \alpha} & D_{0 \rightarrow \alpha} \end{bmatrix} \begin{bmatrix} E_{x=\alpha}^+ \\ E_{x=\alpha}^- \end{bmatrix} \quad (4.8)$$

Where $A_{0 \rightarrow \alpha}, B_{0 \rightarrow \alpha}, C_{0 \rightarrow \alpha}$ and $D_{0 \rightarrow \alpha}$ are the four elements of the transmission matrix relating the electric fields at $x = 0$ and $x = \alpha$. This equation may then be solved for $E_{x=\alpha}^+$ and $E_{x=\alpha}^-$, the sum of which is the electric field at $x = \alpha$.

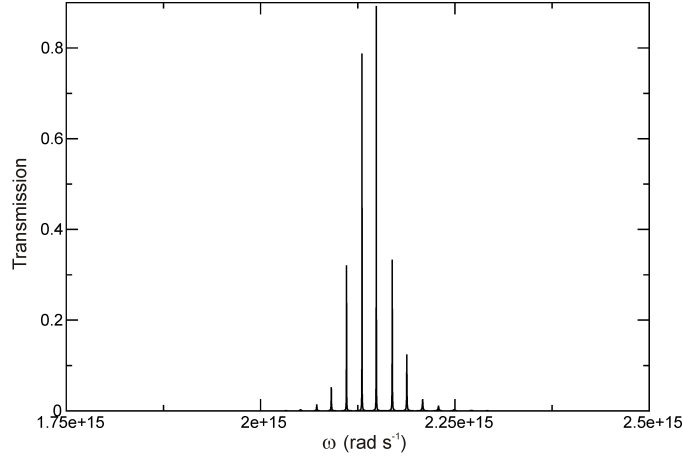


Figure 4.4: Transmission through a photonic crystal consisting of 41 dielectric sheets

Figure (4.4) shows the transmission through a photonic crystal that is made of 41 dielectric sheets, refractive index 3.5, separated by air gaps, refractive index 1. The first cell has a length of 375nm, with subsequent cells again being given by equation (4.3) with $\eta = 3.333 \times 10^4$. In each cell the dielectric sheet is 2/9 of the cell length.

Selecting the frequency at which the largest transmission peak occurs, and calculating the value of the field at many points through the crystal, gives a field of the form shown in figure (4.5).

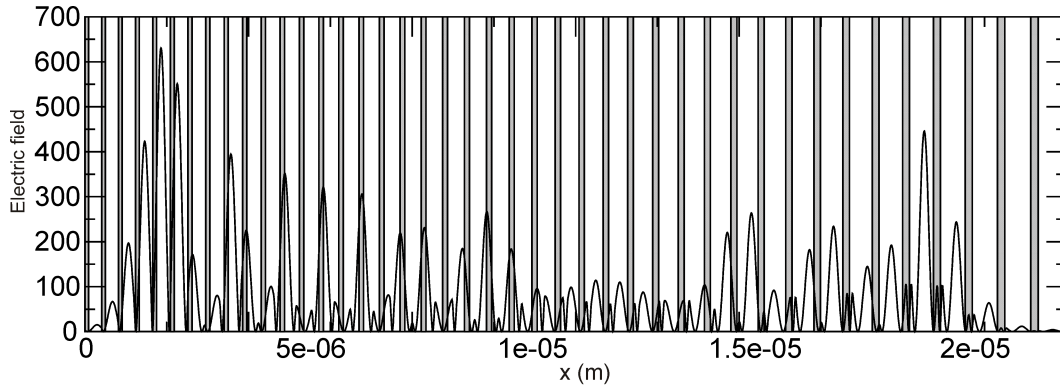


Figure 4.5: The electric field of an allowed eigenmode superimposed onto the photonic crystal, the grey bars are the dielectric sheets.

While it might be expected that the field profile would be symmetrical, with maxima at the turning points of the corresponding Bloch oscillation, the variation in the spacing and widths of the sheets introduces the asymmetry seen.

4.4 The form of the Bandstructure

Due to the multiple reflections that occur in photonic crystals, the bandstructure may become highly complex and difficult to interpret. As such it is useful to consider the transmission through a small number of sheets, and the relation of this to the transmission through a single sheet.

Figure (4.6) shows the transmission through, (a) a single dielectric sheet of refractive index 13 and width 83nm, (b) two dielectric sheets of refractive index 13 and width 83nm that are separated by an air gap of width 167nm, (c) two dielectric sheets of refractive index 13 and width 83nm separated by an air gap of width 334nm.

The dashed lines mark the ω values at which there are transmission peaks for the single sheet. When a second dielectric sheet is included, figure (4.6) part (b), each transmission peak may be seen to split in two. As such, it is

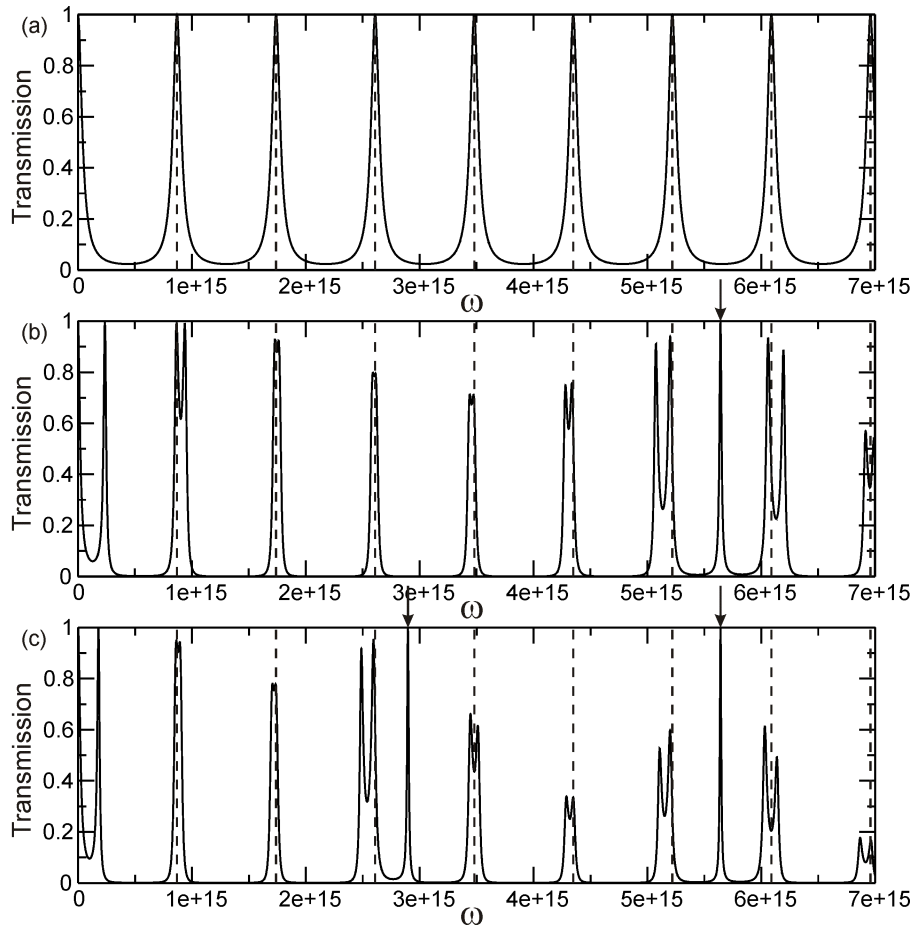


Figure 4.6: Transmission through, (a) a single dielectric sheet, (b) two dielectric sheets, (c) two dielectric sheets separated by an air gap of twice the size of that in (b).

quite common to have the same number of peaks in each band as there are sheets in the crystal. However other transmission peaks due to the interference of reflections from other pairs of surfaces may be seen. The single transmission peak marked by an arrow arises from the introduction of the air gap, as it is not only reflections from the front and back of each sheet, but also from the interfaces at the front and back of the air gap that will give rise to transmission peaks. If there are several air gaps in the crystal then the transmission peaks due to the air gap will group together in the same manner as the transmission

peaks due to the sheets.

The relation of the single peak to the air gap is shown by figure (4.6), part (c). This figure shows the transmission through the structure when the separation of the sheets is doubled. While the amplitude of the pairs of transmission peaks may change, their position does not change dramatically. However the doubling of the width of the air gap introduces a new single transmission peak at half of the frequency of the old peak, as would be expected to accompany the doubling of the optical path length of the cavity.

This may be further confirmed by considering the transmission through a single cavity in a uniform material of refractive index 13. If the cavity has the same optical path length as the single sheet considered previously, an identical transmission profile to that shown in figure (4.6), part (a), is gained.

The appearance of the bandstructure may be greatly simplified if the optical path length of both the dielectric sheets and the air gaps is equivalent. Figure (4.7) shows the transmission through a set of 20 dielectric sheets of refractive index 15. Each sheet has a width of 83nm and is separated by an air gap of width $1.25\mu\text{m}$. In this case, instead of the bands having the same number of peaks as the number of dielectric sheets, they contain the same number of peaks as the number of sheets and air gaps combined. In addition, each band is centered on the frequency for which a peak is seen for a single dielectric sheet. This results in the set of bands that are shown being equally spaced.

The definition of the slowly varying crystals that have been considered in the work so far only limits them to having the cell lengths given by equation (4.3), and by the fact that the dielectric sheet must remain a constant ratio of the cell length. As such the optical path lengths of the sheets and the air gaps may be equal. The variation of the lowest three bands across a slowly varying photonic crystal is shown in figure (4.8). It should be noted that the position

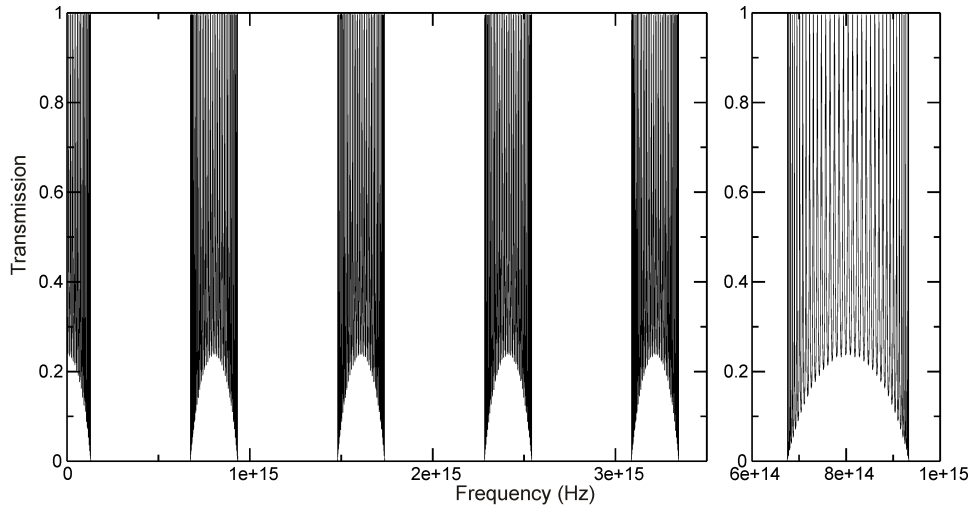


Figure 4.7: Transmission through a set of twenty dielectric sheets. In this case the optical path length of a sheet and an air gap are the same. Each band is virtually identical and contains the same number of transmission peaks, the number of sheets and air gaps combined. The figure on the right shows an enlarged view of a single band.

of the fourth band has not been calculated, and as such it may lie in what is currently labelled the forbidden region above band three.

4.5 Experimental measurements in the microwave regime

As Maxwell's equations scale with length, an effect that may be seen in a photonic crystal may be recreated on a much larger scale using electromagnetic waves with a longer wavelength. The following work involves the use of microwaves to measure experimentally the transmission and electric field profiles associated with structures that may be defined by equation (4.3). This allows the dielectric material, in this case teflon, to have dimensions of the order of centimeters. This is advantageous in several ways, from the ease of construction and reduced cost to simple advantage of being able to see the device with the

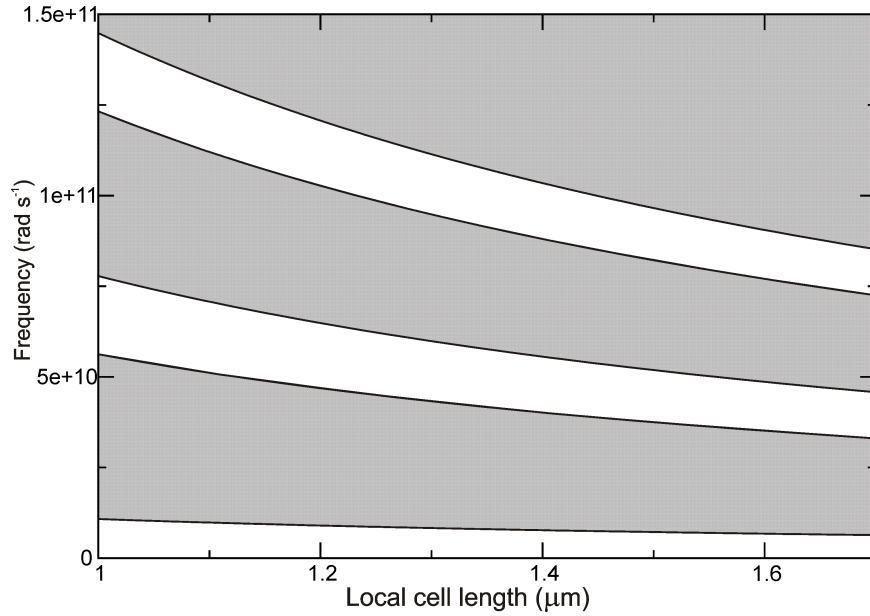


Figure 4.8: The change of the bandstructure as the local cell size changes. In this example the optical path length in the dielectric sheet is the same as the optical path length in the air gap. The white areas are the bands, while the grey regions are the bandgaps.

naked eye.

The experiment was carried out on a circular waveguide, whose curvature was sufficiently small that it plays no significant role, with the device being created in such a way as to mimic a linear waveguide with open ends [59, 60, 61, 62, 63]. A ‘Wiltron 360B’ vector network analyser was used in conjunction with the waveguide to measure the scattering matrix [64], a similar concept to the transmission matrix that has been introduced earlier.

4.5.1 The experimental setup

Figure (4.9) shows a schematic diagram of the equipment used. It consists of a brass ring with a channel, 1cm by 2cm, cut out of it. The channel was enclosed with a brass lid that was mounted in such a way as to allow it to be rotated.

Two carbon absorbers were placed back to back in the channel, thus defining a start and end point. The inclusion of the absorbers allow the waveguide to be considered equivalent of an open ended waveguide.

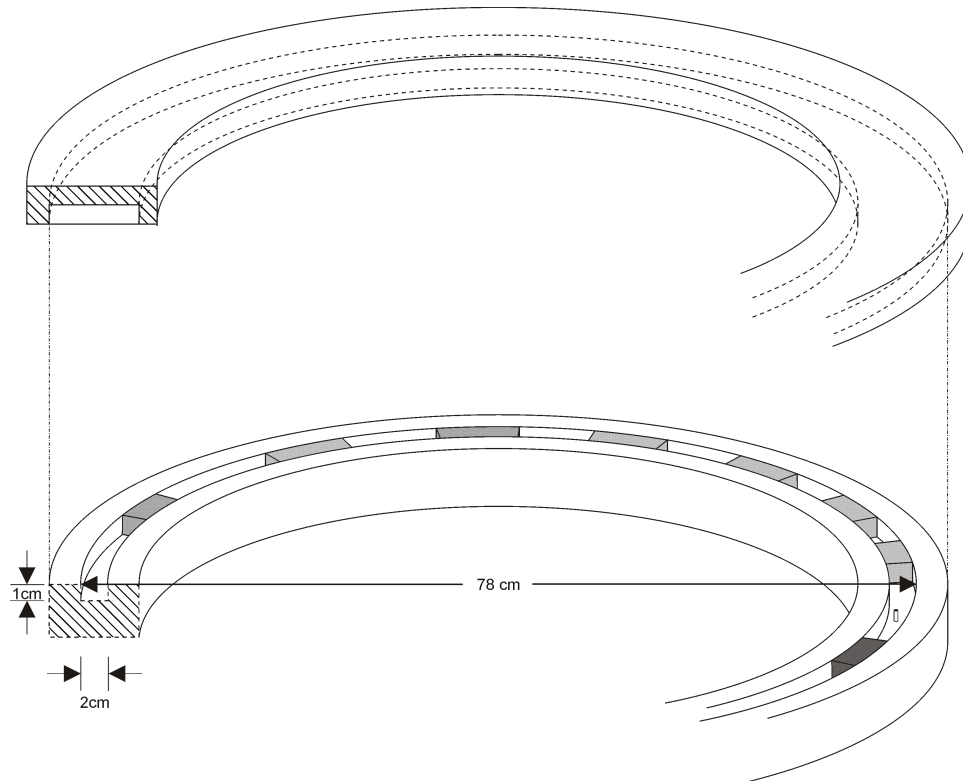


Figure 4.9: Schematic of the equipment used in Germany. This consisted of a brass ring with a channel into which the teflon blocks were placed. The lid was attached in such a way as to allow it to rotate. As one antenna entered through the lid and one through the base this allowed the distance between the two antennae to be changed. The black block in the channel represents the carbon absorbers and the grey blocks represent the teflon.

The teflon blocks have the same cross section as the waveguide, however a slight complication arises in determining their length. As the inner and outer radius of the waveguide are of different lengths, the block must be considered to have a length equivalent to that which lies on a particular radius somewhere between these two limits. This radius has been determined using comparisons between experiments and theory. The transmission through an identical set of

teflon blocks with equal spacing was measured experimentally and compared to transmission matrix calculations. A further complication arises from the fact that the carbon absorbing blocks are not perfectly absorbing, leading to further deviations from the theoretical results.

The nature of the waveguide is such that a wave travelling around the waveguide must, in order to be a solution of the Helmholtz equation [65, 66], have the form of a standing wave across the waveguide. The lowest frequency that may be accepted by the guide is therefore that of a standing wave of the form of half a sine wave across the longest dimension of the cross section, a frequency of 7.5Ghz. It is however the component of the wavevector around the waveguide that needs to be considered. The relationship between the component of the wavevector around the waveguide, k_g , the component forming the standing wave across the waveguide k_s , and the total wavevector, k , is,

$$k^2 = k_s^2 + k_g^2 \quad (4.9)$$

or, equivalently, that the relation between k and k_g is,

$$k_g = \sqrt{k^2 - k_s^2} = \sqrt{k^2 - \left(\frac{2\pi(7.5 \times 10^9)}{c}\right)^2} \quad (4.10)$$

For a comparison to be made between photonic crystals in the waveguide, and those in free space with an electromagnetic wave incident perpendicular to the dielectric sheets, the values of ω given earlier will be equivalent to $\omega = ck_g$ in the waveguide.

If the frequency is increased sufficiently then other modes will be possible; At a frequency of 15Ghz the standing wave across the waveguide may alternatively take the form of a full period sine wave, or may form a half sine standing wave across the smaller dimension of the cross-section of the waveguide. To avoid

exciting such higher modes, the range of frequencies that will be considered will only cover the range 7.5GHz to 15GHz.

Analysis of the experiment involved obtaining values for the *scattering matrix*, shown in equation (4.11), a concept similar to the transfer matrix defined previously. Here a_1 and b_1 are respectively the amplitudes of the right and left travelling components of the wave at antenna 1, while a_2 and b_2 are the right and left travelling components of the wave at antenna 2.

The S parameters are used most often when considering transmission and reflection in experiments carried out at microwave frequencies and relate the incident and reflected waves at each antenna. The values of the elements of the scattering matrix are obtained through the use of a *vector network analyser* and relate the power of the signal produced and received by each antenna. The matrix element $S_{(1,1)}$ represents the power of the signal that is received at antenna 1 due to the signal emitted by antenna 1, i.e. the reflection of the signal by the system. Similarly, $S_{(2,1)}$ is the relation of the power of the signal received by antenna 2 to that emitted by antenna 1. Both the amplitude and phase of the signal may be found.

$$\begin{bmatrix} a_2 \\ b_1 \end{bmatrix} = \begin{bmatrix} S_{(1,1)} & S_{(1,2)} \\ S_{(2,1)} & S_{(2,2)} \end{bmatrix} \begin{bmatrix} a_1 \\ b_2 \end{bmatrix} \quad (4.11)$$

The initial experiment involved measuring the transmission through the entire structure. This was achieved by inserting the antenna into the waveguide, one at either end of the structure. In this case the antenna extended across the entire height of the cavity. The network analyser was then used to obtain the S matrix values across the range of frequencies desired.

4.5.2 Transmission experiments

The photonic crystal consisted of a set of 19 teflon blocks, each of which has a refractive index of $n = 1.44$. The initial cell, cell 0, had a length of 8cm with the teflon block being half the length of the cell. The subsequent cells were obtained [26] from a more accurate form of the recursion relation given in equation (4.12).

$$L_j = -\frac{1}{\eta} \ln \left(1 - \frac{\eta l_0}{1 - j\eta l_0} \right) \quad (4.12)$$

where j is the cell number, $\eta = 0.11$, and l_0 is the length of cell 0. The teflon block in each case being half the cell length.

To convert this linear setup into a set of blocks to be used in the waveguide, the teflon blocks used in the waveguide must have a length equivalent to those in the linear setup at a radius of 36.12 cm.

Figure (4.10) shows both calculations and the experimental measurements of the transmission through this structure verses the frequency of the incident microwaves. It may be seen that the first two bands have been suppressed in the experiment, and each of the three higher bands shown are at slightly higher frequencies in the experiment than predicted from the transmission matrix calculations. The amplitude of the signal is greatly reduced due to imperfections in the equipment, with a large reduction in the signal after transmission through an empty waveguide also being seen.

The shift in the bands is probably because the radius at which the actual structure and 1D model become equivalent is slightly larger than the value assumed in the calculations shown in figure (4.10). The suppression of the right hand side of the first band that is seen experimentally is mimicked in the third band seen experimentally, with this region in the third band occurring at twice the frequency as the region in the first band. Consequently it is likely to arise from an error in the construction of the crystal, leading to the introduction of

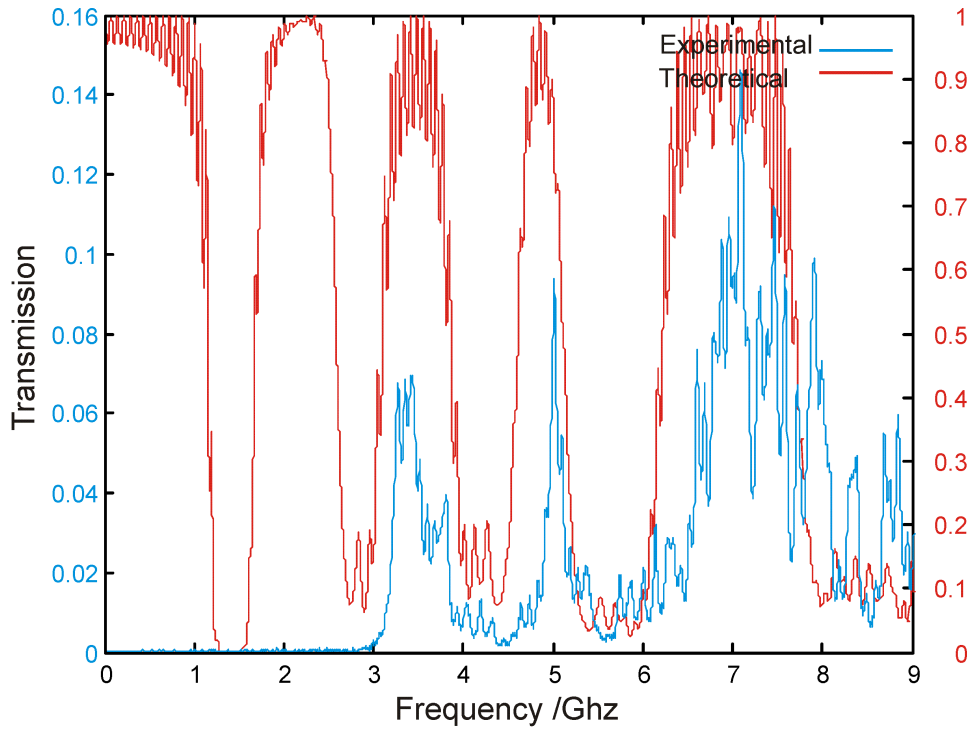


Figure 4.10: The transmission through the 19 blocks of teflon. The red line shows the calculated values, while the blue line shows the experimental results.

an unexpected resonance, rather than an error in the measurement.

Figure (4.11) is an enlarged view of the frequency range 2.5 to 4.5 GHz. The two graphs have been scaled to allow a comparison between the peaks to be made more easily. This scaling reveals that the experimental peaks are spaced slightly further apart than those predicted from the theoretical model. It is because the crystal is fairly short that the transmission peaks are so broad, however they are still virtually equally spaced.

As the data was sampled at equally spaced values of k , in order to use a *Fast Fourier Transform*, it must be converted into a set of data that is sampled at equally spaced values of k_g . To achieve this, a set of k_g values is defined and the transmission at these points is gained by interpolation. In this case

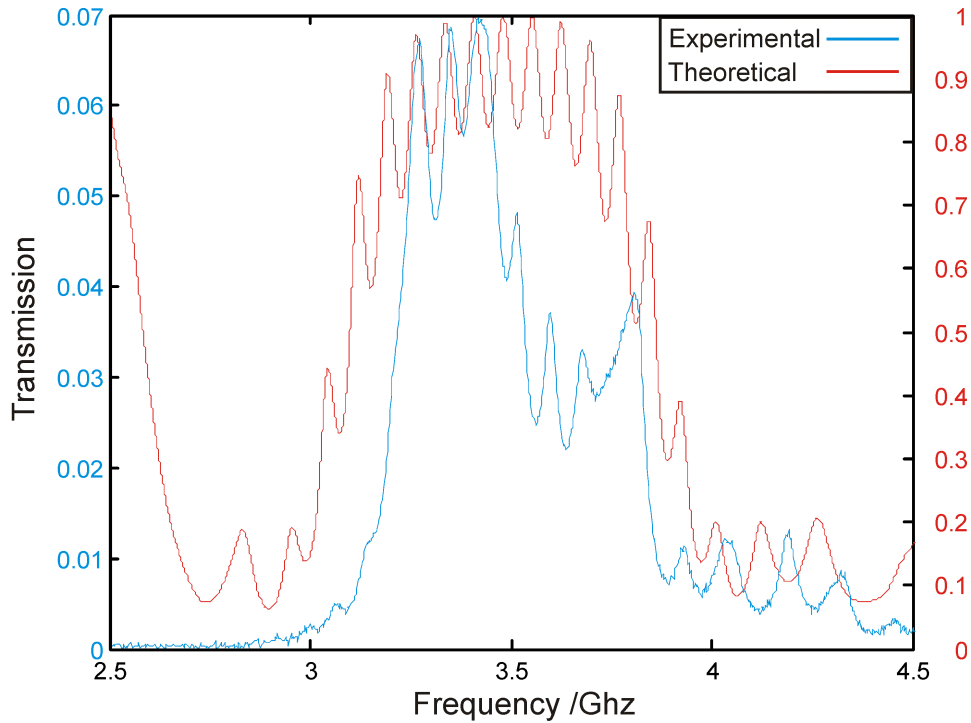


Figure 4.11: A clearer comparison of the results over the frequency range in which the first band is seen experimentally.

the values are interpolated through the use of the IDL function ‘SPL_INTERP’ which calculates the values through the use of a spline [45].

If a Fast Fourier Transform of the data in the range 3.0 - 4.6 GHz is made (not shown here) a small grouping of peaks is shown, indicating several frequencies are important to accurately represent the function by a fourier series.

Figure (4.12) shows the transmission over this range overlaid by a sine wave with the frequency corresponding to that of the highest peak in the fourier transform. As this peak is far higher than its neighbors it will play a dominant role in determining the shape of the function and the spacing of the peaks. It should be noted that as the fast fourier transform involves transforming only a small set of points, and as the transform itself is represented by the same

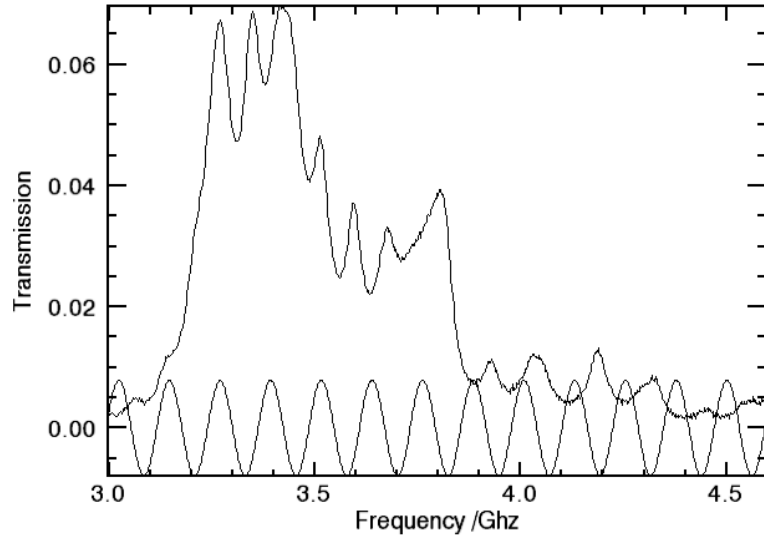


Figure 4.12: The lowest band that is seen experimentally, overlaid by a sine wave with the frequency corresponding to that of the highest peak in its fourier transform.

number of points, the discrete nature of the transform may mean that the frequency given by a single peak is unlikely to ever match the periodicity of the original function perfectly. That is to say, the set of points returned by the fast fourier transform correspond to discrete frequencies, unless one of these frequencies exactly matches the original function then several frequencies will need to be used in order to give the best approximation of it.

4.5.3 Fields inside the crystal

The waveguide is constructed so that, while one of the antenna enters the system through the lid, the other enters through the base. This allows the distance between the antennae to be varied by rotating the top of the waveguide. Numerous measurements may then be taken at a set of points throughout the crystal, allowing a spatial map of the field throughout the crystal, at a particular

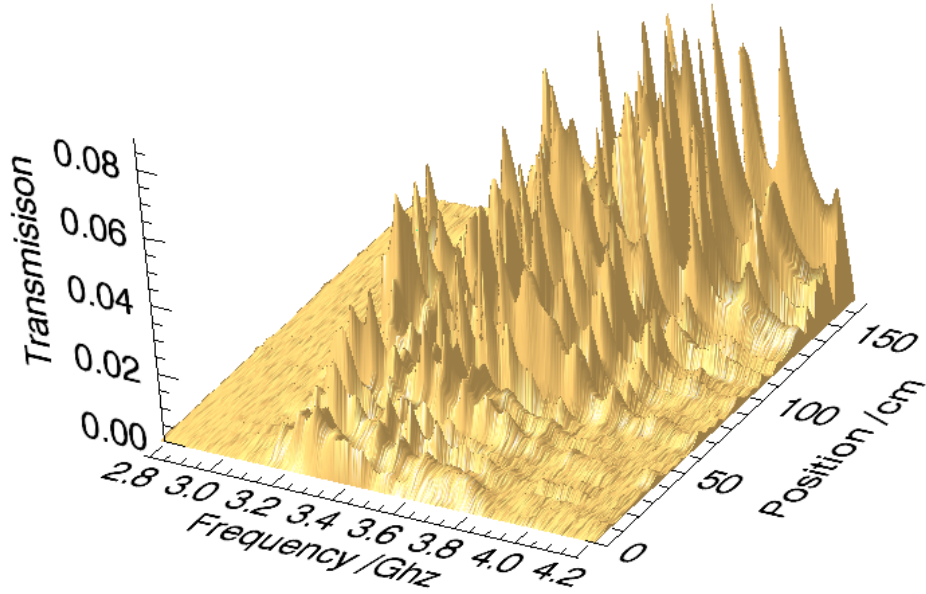


Figure 4.13: The electric field measured at a range of positions, and for a range of frequencies, throughout the 1D photonic crystal

frequency, to be obtained.

In order to allow the top to be rotated to points where dielectric blocks lie, the movable antenna needs to be changed from one that extends through the full height of the cavity to one that is flush with the bottom of the lid. It should be noted that the antenna may couple to the radiation field differently when above an air gap and above a dielectric block. In addition, the antenna may act as perturbation on the system, distorting the results from those that would be gained from the same crystal subjected to different measurement techniques. This problem is exacerbated by the fact that the antenna takes numerous positions in the crystal throughout the experiment.

Figures (4.13) and (4.14) show the values of $S_{(2,1)}$ for the 1D photonic crystal that has been described previously, over the range of frequencies for which the

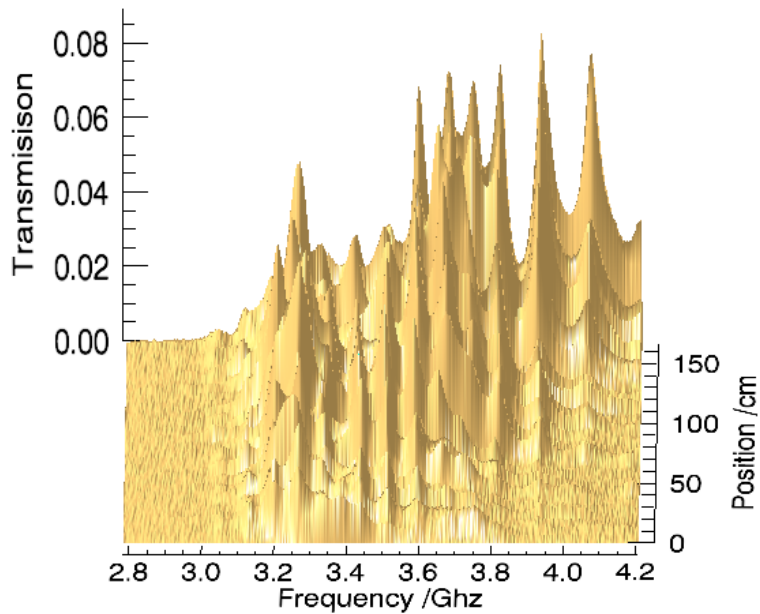


Figure 4.14: The same results as in figure (4.13), shown at a different rotation.

first band is seen. The data on each graph is identical, and is just shown at different rotations.

The previous section showed that the crystal measured experimentally does not correspond exactly to the structure that was modelled theoretically, with the bands and peaks being positioned slightly incorrectly. Consequently no similarity beyond general shape can be identified in the theoretical and experimental $S_{(2,1)}$ surfaces shown in figures (4.13) and (4.14). A better comparison between the real waveguide and 1D linear model may lead to predicted peaks being matched to those seen experimentally, at which point the fields in the crystal may be meaningfully compared.

Figure (4.15) shows the field through the crystal at a frequency of 3.52 GHz, corresponding to a peak in figure (4.14). The value of the field has been taken at 55 equally spaced points through the crystal. The high peak at a

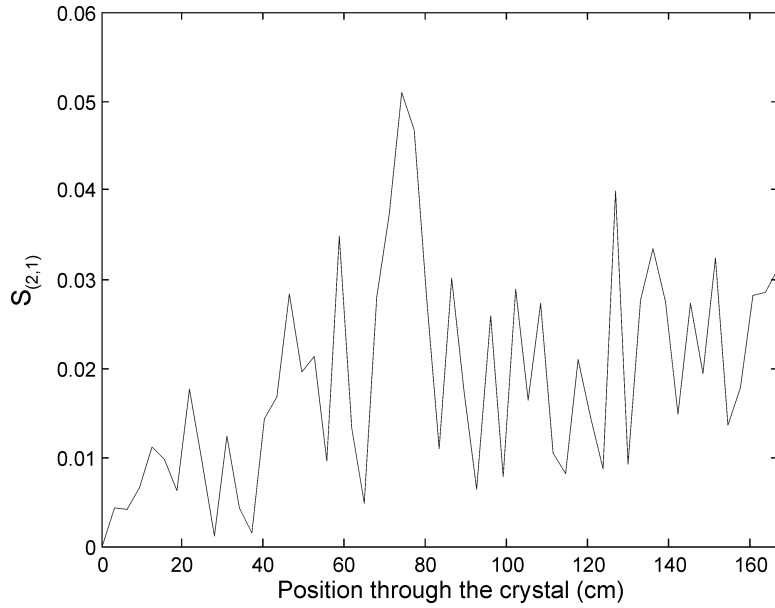


Figure 4.15: The electric field measured at numerous points throughout the photonic crystal. The incident microwaves are at a frequency of 3.52 GHz

distance of about 70cm through the crystal corresponds to the edge of an allowed eigenmode, with the field tailing off for positions below this value in the same manner as shown in theory, see figure (4.5). The mode is not entirely contained by the crystal and hence only its right-hand end is seen. It should be noted that the number of points at which the field has been sampled are not sufficient to give a detailed view of the field.

The comparison between the theoretical and experimental results would be greatly improved if these experiments were repeated with the prior knowledge that the first two bands are suppressed, and with the comparison between the 1D linear model and in the actual waveguide being improved.

4.6 Varying the sheet width

The two dimensional crystals that are considered in the next chapter are considered in the limit of infinitesimally thin sheets. These sheets are defined by the function $m = \epsilon_r d$ where ϵ_r is the *relative permittivity* of the sheets, and d their width. While looking at this in the limit of infinitesimally thin sheets simplifies the maths greatly, it does however describe a crystal that cannot be made.

The definition $m = \epsilon_r d$ does not uniquely define a sheet, only giving the relation between the relative permittivity and the widths of the sheets. In the following work a photonic crystal with a slowly varying cell size, as given by the recursive relation (4.3), will be compared to other photonic crystals created from a set of sheets with the same values of m , but with different values of ϵ_r and d . Both the situation in which the set of cell lengths is kept constant, and the situation in which the optical path length of each cell is kept constant, will be considered.

It should be noted that, as the maximum reflection from each sheet is related to the difference in refractive index between the sheet and the air gap, there must be some change in the transmission through, and fields within, these short structures as the refractive index of the sheet changes.

Figure (4.16) shows transmissions through 40 dielectric sheets. The initial photonic crystal, the transmission through which is shown in black in both part (a) and (b), is constructed according to a set of cell lengths given by equation (4.3), where $l_0 = 2.5 \times 10^{-7}$ and $\eta = 3.333 \times 10^4$. The refractive index of the dielectric sheets is 3.5, with the air gaps having a refractive index of 1. The width of the dielectric sheet in each cell is 1/3 of the cell length.

The red peaks in part (a) show the transmission through a structure in which the width of each dielectric sheet has been increased to 190% of the

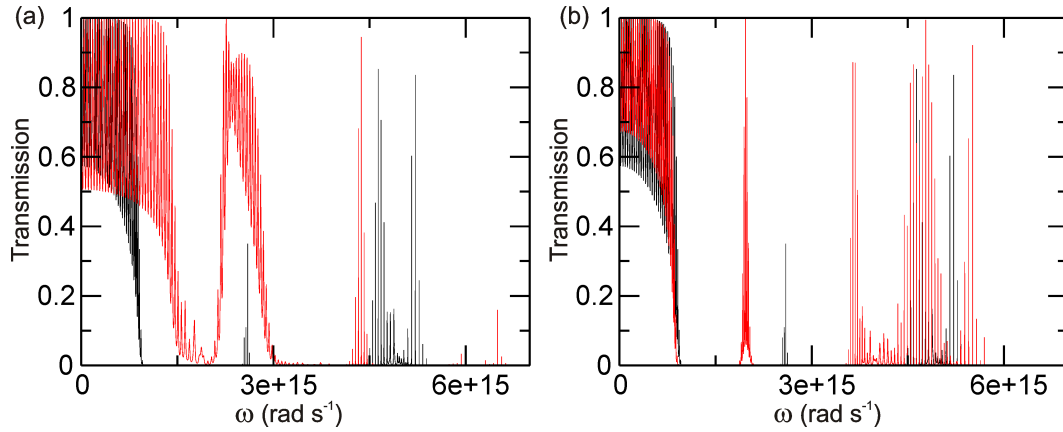


Figure 4.16: The two graphs show two different sets of sheets, the second of which, shown in red, is 90% longer than the first set, shown in black. In part (a) the red peaks are the transmission through a crystal that maintains the cell length used in the original crystal. The red peaks in part (b) are for a crystal that maintains the length of air gap next to each sheet, thus varying the cell length.

initial set. This is done while maintaining the same set of cell lengths as used in the original crystal, hence reducing the width of each air gap. It can be seen that as the sheet width increases, and hence the refractive index decreases, the overall reflectance of the structure drops, leading to the general transmittance through the structure being increased.

As the refractive index of the sheets increases, the height of the transmission peaks do not all drop. While some of the peaks do decrease in height other peaks will increase, illustrating again the complex manner in which the multiple reflections in the crystal combine.

It can be seen that for the second band, as the widths of the dielectric sheets change, the form of the band is maintained better when the width of the air gaps are kept the same while the sheet width is varied. However, changing the crystal in this manner appears to alter the form of the higher bands more significantly. While in the initial crystal there are two bands between $\omega = 4 \times 10^{15} \text{ rad s}^{-1}$ and $\omega = 6 \times 10^{15} \text{ rad s}^{-1}$, after the change in sheet widths the higher of these two bands appears to be suppressed. This effect is less pronounced when the

cell length is kept constant while the sheet width varies.

It is very easy to show that the reflection from, and the change of phase that is caused by, one sheet cannot be held constant for two different width sheets that have the same value of m . While a change in the refractive index will always lead to a change in the maximum reflectance from a sheet, the optical path length of the sheet is kept constant then the change in phase across a sheet will also be constant.

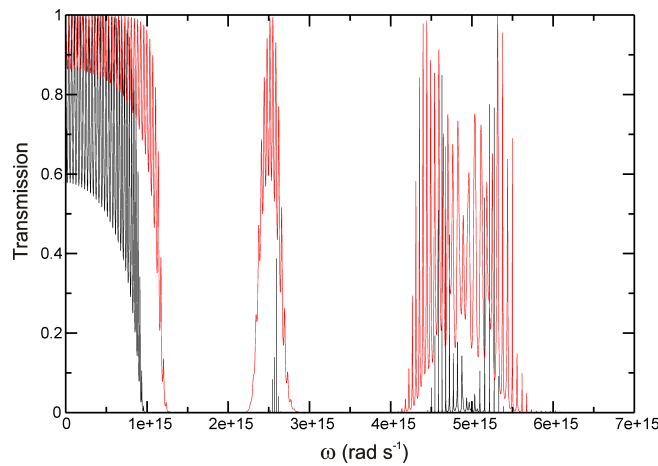


Figure 4.17: constant value of optical path length across the sheet, instead of ϵ_r being changed the sheets are defined by $m_1 = nd$, where n is the refractive index of the sheet and d is the width of it.

Figure (4.17) shows the transmission through the original set of 40 dielectric sheets, shown again in black, along with a second set of dielectric sheets that are again 190% of the width of the original sheets, however this time the optical path lengths of the second set of sheets are the same as the first. The air gaps between the sheets are the same for both sets of sheets. As can be seen, there is less shift in the frequencies that the bands appear at than in the previous cases.

In the second set of sheets, the set with a lower refractive index, the maximum reflectance of each sheet is lower than the first. This leads to a greater transmittance through the structure and as such an expansion of the bands to

a larger range of frequencies.

The dispersion relation of a one dimensional photonic crystal, gained in a similar manner to that shown in appendix A, is given by equation (4.13),

$$\cos(\mu(a + b)) = \cos(k_1 a) \cos(k_2 b) - \frac{1}{2} \left(\frac{n_1}{n_2} + \frac{n_2}{n_1} \right) \sin(k_1 a) \sin(k_2 b) \quad (4.13)$$

here a is the width of the dielectric sheet which has a refractive index of n_1 , b is the width of the air gap with a refractive index of n_2 , μ is the Bloch wavevector and k_1 and k_2 are the wavevectors in the dielectric sheet and air gap respectively.

From this equation it can be seen that, if the optical path length of the sheet and the air gap is the same, the only term that changes is that which involves only the refractive indices. This changes the magnitude of the second term but does not change its form.

It may be noted that the peaks are slightly further apart for the sheets of lower refractive index. Some of the differences may be removed by using more sheets as, as the reflectance of each sheet is lower, the Bloch oscillations are not confined to the allowed regions as strongly. However, the change in the bandstructure that arises from changing the magnitude of the second term will also change the frequency the eigenstates are found at. This may also lead to a change in the length of, and time to complete, the associated Bloch oscillation.

While it is not a perfect solution, the use of the optical path lengths to define the crystal would appear to be far superior to a definition in terms of m , giving more consistent results for different crystals that take the same values for these defined quantities.

Chapter 5

Two dimensional photonic crystals

In chapter 1 and 2 techniques by which the bandstructure of a two dimensional photonic crystal may be obtained and then used to calculate ray paths in the structure have been detailed. In this chapter this methodology will be applied to a slowly varying two dimensional photonic crystal, being used to determine both the limits of the regions in which the rays may travel, and the nature of the ray paths within these regions. The photonic crystals considered here will be shown to support both stable and chaotic paths. It is possible to find regions of phase space in which the ray paths are unstable which are separated by areas of stable motion; These boundaries separating distinct regions of unstable motion are called *dynamic barriers* [42].

In addition to unstable paths occurring in separate regions of phase space, it is possible to find regions of the crystal where this phase space separation translates into a spatial separation too. This spatial separation is advantageous when considering real devices, as rays in one chaotic region will not enter the second

chaotic region unless scattering off imperfections induces such a transition. In addition, if the chaotic regions overlap, and rays enter the system at a range of angles, then the rays will access both regions of phase space. If the rays enter a single chaotic region with no spatial or phase space separation connections to a separate sea of chaos, then all of the rays will move in this region.

5.1 Defining the crystal

The photonic crystals in this chapter are defined in the limit of infinitesimally thin sheets. A crystal with constant cell size may therefore be defined by its relative permittivity profile,

$$\epsilon(\vec{r}) = 1 + m \left(\sum_{n_x=-\infty}^{\infty} \delta(x - n_x l_x) + \sum_{n_y=-\infty}^{\infty} \delta(y - n_y l_y) \right) \quad (5.1)$$

where $m = \epsilon_r d$, n_x and n_y are integers, l_x and l_y are the cell lengths in the x and y directions respectively, and δ is a delta function which is non-zero only when $(x - n_x l_x = 0)$ or $(y - n_y l_y = 0)$ and has a spatial integral equal to unity. As such, the dielectric sheets have a relative permittivity of $(1 + m)$ except at points where the sheets cross, where the permittivity is $(1 + 2m)$. All other points in space have a relative permittivity of 1.

The bandstructure of a slowly varying photonic crystal is, at any point, equivalent to that of an infinite crystal with constant cell size equal to the local cell size. For S polarisation, as shown in chapter 1, this bandstructure is given by equations,

$$\cos(\mu_x l_x) = \cos(k_x l_x) - \frac{mk^2}{2k_x} \sin(k_x l_x) \quad (5.2a)$$

$$\cos(\mu_y l_y) = \cos(k_y l_y) - \frac{mk^2}{2k_y} \sin(k_y l_y) \quad (5.2b)$$

where, if they are less than zero, k_x or k_y may be replaced by iq_x or iq_y respectively.

It can be seen from these equations that the physical properties of the photonic crystal that need to be defined are the cell length in the x direction, l_x , the cell length in the y direction, l_y , and the value of m at each point in the crystal. All the other quantities relate to the electromagnetic wave. While the value of l_y will remain constant throughout the crystal, the values of l_x and m will both vary. The cell length in the x direction is given by the exponential function,

$$l_x = l_0 \exp^{-\eta x} \quad (5.3)$$

where l_x is the (continuously varying) cell length defined at any point in the crystal and η and l_0 are constants. While this is a continuous function, defining a different cell length at every point, a set of cells that correspond to this chirp may be found in the manner shown in the last chapter. As noted in that chapter, the value of m is given at any point by,

$$m = m_0(1 - \rho y'^2) \quad (5.4)$$

where ρ is a constant and y' is an axis, paired with x' , that are related to the axes x and y through a rotation of an angle θ about the origin.

A physically realistic crystal is limited to regions where m is positive. Outside such regions either the refractive index or the width of the sheet would need to be negative. As with the one dimensional crystal described in chapter 4, considerations of solutions in the lowest band will be avoided as the band always extends down to $\omega = 0$.

It may be seen that, for the lowest bands, the Bloch waves have a locally evanescent character in one direction and a locally propagating character in the

second [13]. These two dimensional photonic crystals contain a far more complicated bandstructure than the one dimensional crystals, with bands overlapping, making it difficult to label any particular band as the first band etc. In the band of interest here, each of the rays will take starting conditions that are given by approximate solutions to the dispersion relation. This is an approximate solution that, in the air gap between dielectric sheets, gives a wave with a real propagating local character in the x direction and an evanescent character in the y direction. In the tight binding regime, $q_{x,y}l_{x,y} \gg 1$, equation (5.2b) allows the following approximations to the components of the wavevector may be made [13],

$$k_x = \frac{\omega}{c} \left(\frac{m^2 \omega^2}{4c^2} + 1 \right)^{1/2} \approx \frac{m\omega^2}{2c^2} + \frac{1}{m} \quad (5.5)$$

and

$$q_y = \frac{m\omega^2}{2c^2} \quad (5.6)$$

These may then be substituted into equation (5.2a) allowing the following relation to be gained,

$$\omega^2 = \frac{2c^2}{ml_x} \left((2n - 1/4)\pi - \frac{l_x}{m} \pm \cos^{-1} \left(\frac{\cos(\mu_x l_x)}{\sqrt{2}} \right) \right) \quad (5.7)$$

where $\omega^2 = (k_x^2 - q_y^2)c^2$, μ_x is the Bloch wavevector in the x direction, and n is an integer. This band will be specified by the combination of n and the initial constraint that the evanescent character of the wave is in the y direction.

Initially the crystal will be defined with the following properties, $l_y = 0.5\mu\text{m}$, $l_0 = 0.5\mu\text{m}$, $\theta = 21^\circ$, $\eta = 1 \times 10^4 \text{m}^{-1}$, $m_0 = 2\mu\text{m}$, $\rho = 1 \times 10^{10} \text{m}$ and the angular frequency of the electromagnetic wave, ω , will have a value of $6 \times 10^{14} \text{rad s}^{-1}$. The approximation of ω for the band under consideration will then be given by equation (5.7) when $n = 2$, with the evanescent component of the wave being in the y direction.

5.2 The square-celled crystal

The dispersion surface that is shown in chapter one [figure (1.8)] is that for a wave of the form described above, at the point in the crystal $x = 0, y = 0$. At this point the cell lengths in the x and y direction are equal. It may be seen in figure (5.1) that the band is not symmetric through a rotation of 90° . However, as the crystal itself is symmetric through this rotation there must exist a second dispersion surface, one that is identical to this one under a rotation of 90° . This turns out to be the band for which the real propagating component of the wavevector is in the y direction and evanescent component in the x direction. Figure (5.1) shows these two bands plotted across the full first Brillouin zone.

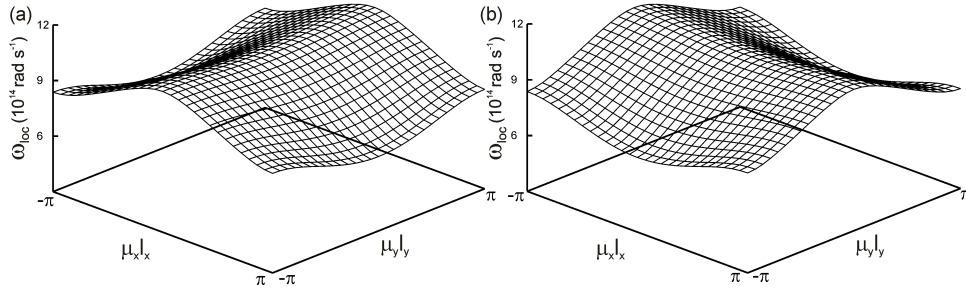


Figure 5.1: (a) shows the band through which ray motion will be considered here, calculated at the point $x = 0, y = 0$. The real propagating component is in the x direction and an evanescent component in the y , (b) shows its companion, a band in which the propagation component is in the y direction and the evanescent component is in the x direction. These regions are obtained by plotting the points in the crystal where the highest and lowest frequency points on the band are equal to the frequency of the E.M. waves.

It may be seen from figure (5.1) that for some values of $\mu_x l_x$ and $\mu_y l_y$, the bands *cross*. However, as the electromagnetic waves are not identical at these points, one with an evanescent character in the x direction and the other with it in the y direction, the wave is constrained to the band it starts in and will not cross into the other band. Consequently, when the ray path is calculated it is only solutions in a single band that are taken into account.

As the cell length varies in the x direction, at other points in the crystal the rotational symmetry will be broken. This shifts the bands causing them to cover different ranges of ω . Eventually a point will be reached where the bands shift sufficiently that there are no values of ω common to both bands, a situation that will be considered later in this chapter.

This shifting of the bands throughout the crystal means that while there may be a propagating solution for a particular frequency at one point in the crystal, there may exist other points in the crystal where no propagating solution exists. Figure (5.2) shows the limit to the region for which any solution may be found for the rays and crystal described above, part (a) and (b) showing the limits for rays moving in the bands corresponding to 5.1(a) and 5.1(b) respectively. The grey regions are those for which there is no propagating solution in the respective band.

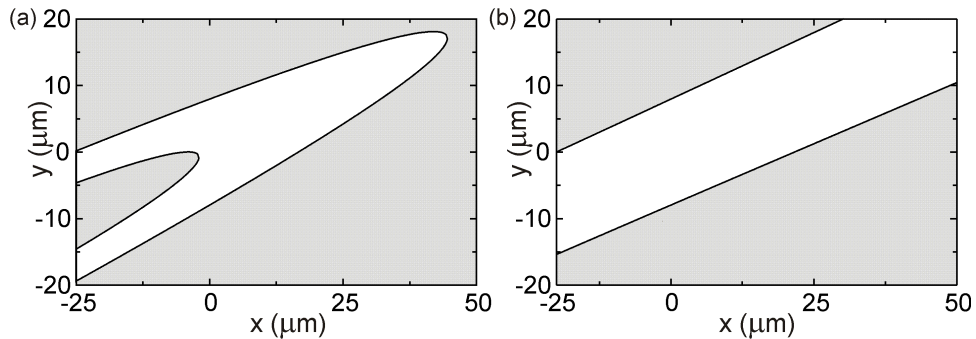


Figure 5.2: Shows the regions in this crystal for which ray paths may be found (white) and those for which there are no solutions (grey), $\omega = 6.248 \times 10^{14} \text{ rad s}^{-1}$. (a) real propagating component is in the x direction and an evanescent component in the y , (b) shows its companion, a band in which the propagation component is in the y direction and the evanescent component is in the x

While the limit shown in the left figure is that for the band of interest here, some note of the second band should be made. While in this model the rays will not cross from one band to the other, in a real crystal imperfections may cause the rays to scatter into the second band. In addition, the electromagnetic waves

may tunnel from one band to the other [67]. Transmission from the allowed region in figure 5.2(a) to that in figure 5.2(b) may change a ray path that is bounded along x ($x \leq 40\mu m$) to one that is free, thus altering the transmission characteristics of the crystal. This process will be suppressed if there are no band states for the wave to scatter/tunnel to. In addition, if solutions exist for a wave a small spatial distance away the electromagnetic wave may tunnel across the forbidden region, changing the results seen from those obtained here. While the shape and position of the second band will be considered here, this is the limit of the considerations of it that will be made in this work. No attempt will be made to quantify the effect of the scattering, and the effects of tunnelling will be left to be revealed by a solution of Maxwells equations for these structures at some point in the future.

Ray tracing in the second band reveals numerous paths which will travel across the whole length of the region of interest in the first band; Several of these rays are shown in figure (5.3). The rays shown are not complete, rather cut off after the relevant pair of Hamilton's equations [equations (2.30)] have been advanced by a number of steps, using the previously described fourth order Runge-Kutta method. As noted above, any ray that scatters onto this second band from the other band will be able to traverse the crystal unimpeded.

5.3 The band of interest

For the band with the evanescent component in the y direction, as can be seen in figure 5.1(a), the dispersion sheet will have its lowest frequency solution at the point where $\mu_x l_x = \pi$ and $\mu_y l_y = 0$, and the highest frequency solution at the point where $\mu_x l_x = 0$ and $\mu_y l_y = \pi$. The limits of the region in which the ray may move are given by the loci of points in the crystal where the frequency of the electromagnetic waves coincides with one of the local band extrema. However it

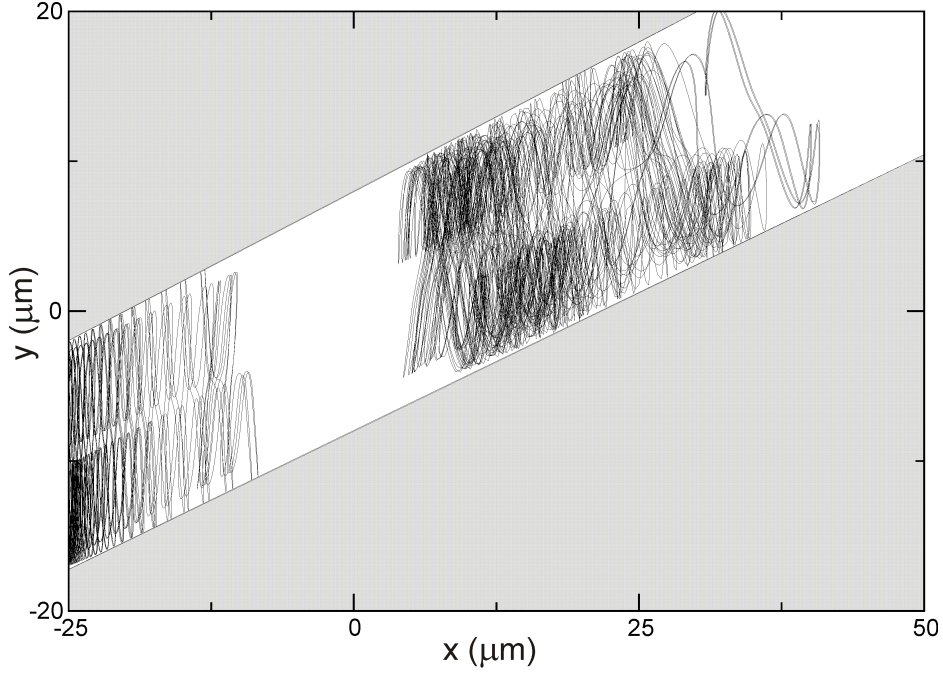


Figure 5.3: Two ray paths in the second band

is not just these two loci that determine the shape of the rays, but the 4 corners of the reduced Brillouin Zone. These four points lie where $(\mu_x l_x, \mu_y l_y) = (0, 0)$, $(\mu_x l_x, \mu_y l_y) = (\pi, 0)$, $(\mu_x l_x, \mu_y l_y) = (0, \pi)$ and $(\mu_x l_x, \mu_y l_y) = (\pi, \pi)$. The four lines on figure (5.4) are the locations at which these four points on the band are equal to the frequency of the ray.

The (forbidden) grey area is that for which the value of m would be less than zero, and hence the crystal is not defined. The outermost (black) line shows the locus of points at which the dispersion relation for the band of interest at $(\mu_x l_x, \mu_y l_y) = (\pi, 0)$ equals ω , while the innermost (red curve) gives the point for which $(\mu_x l_x, \mu_y l_y) = (0, \pi)$ equals ω . The blue [green] curves give the loci of points at which $(\mu_x l_x, \mu_y l_y) = (\pi, \pi)$ [$(\mu_x l_x, \mu_y l_y) = (0, 0)$] equals ω . The black and red lines represent the limits to the region in which an allowed propagating solution may be found. However, this does not mean that a ray may travel in

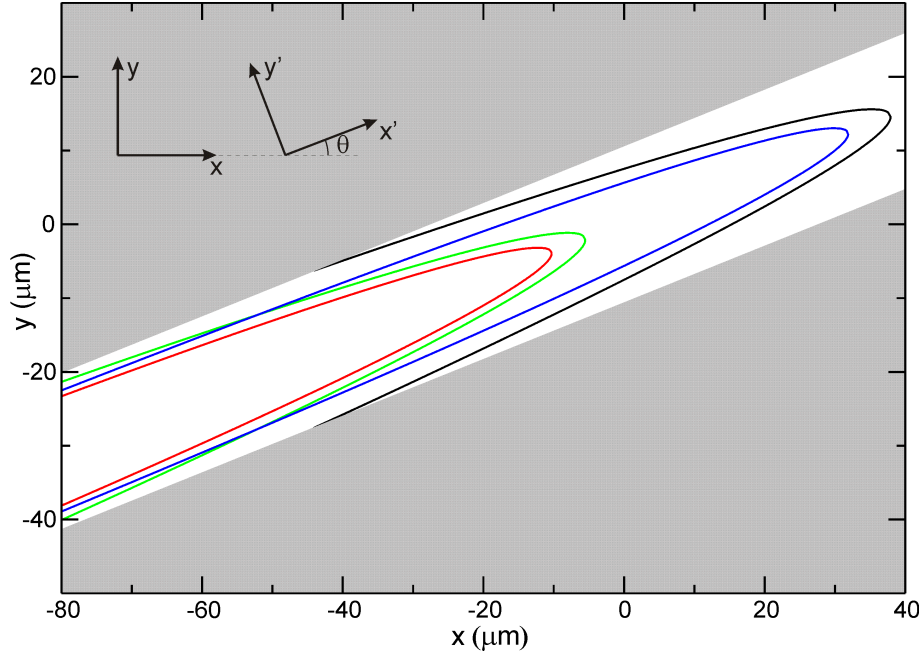


Figure 5.4: The four loci of points corresponding to the four corners of the reduced Brillouin Zone, $(\mu_x l_x, \mu_y l_y) = (\pi, 0)$ in black, $(\mu_x l_x, \mu_y l_y) = (0, \pi)$ in red, $(\mu_x l_x, \mu_y l_y) = (\pi, \pi)$ in blue, and $(\mu_x l_x, \mu_y l_y) = (0, 0)$ in green. The white region shows the area for which $m \geq 0$, the region in which the crystal is defined, while the grey region is that for which $m < 0$.

any direction when it lies inside this allowed region.

For the dispersion surfaces considered here, if the frequency lies between the band position at $(\mu_x l_x, \mu_y l_y) = (\pi, 0)$, and $(\mu_x l_x, \mu_y l_y) = (\pi, \pi)$, then the ray may travel in any direction. However, if the frequency is greater than that given at the point at $(\mu_x l_x, \mu_y l_y) = (\pi, \pi)$, then no solution for a Bloch wave travelling parallel to the x axis may be found. This may be seen in figure (5.5), a figure showing two constant frequency contours, $\omega = 6 \times 10^{14} \text{ rad s}^{-1}$ and $\omega = 6.9 \times 10^{14} \text{ rad s}^{-1}$, on the dispersion surface that is given for the point in the crystal where $l_x = 0.75 \mu\text{m}$, $l_y = 0.5 \mu\text{m}$ and $m = 2 \mu\text{m}$.

The ray in each case will correspond to a point on the respective contour, and will propagate in a direction that is perpendicular to it. As such, the contour corresponding to $\omega = 6 \times 10^{14} \text{ rad s}^{-1}$ allows propagation in any direction. At

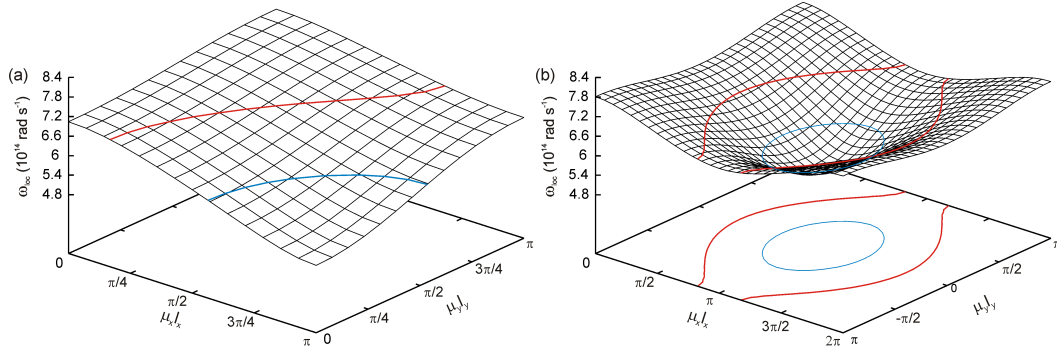


Figure 5.5: Constant frequency contours, (a) shows the reduced Brillouin zone, (b) shows the full Brillouin zone. The blue contour lies at a value of $\omega = 6 \times 10^{14}$ rad s $^{-1}$ and $\omega = 6.9 \times 10^{14}$ rad s $^{-1}$. (a) shows contours on the surface, while part (b) shows the same contours on the surface along with a projection of these contours onto the base of the figure

the point at which the contour reaches the edge of the Brillouin zone, Bragg reflection occurs meaning that the ray path is restricted to a limited range of directions. While it may be seen in figure (5.4) that the solution at $(\mu_x l_x, \mu_y l_y) = (0, 0)$, is at a lower frequency than that at $(\mu_x l_x, \mu_y l_y) = (\pi, \pi)$ for values of x less than about $-50 \mu\text{m}$, the rays of interest in this work are those constrained by the limit given by $(\mu_x l_x, \mu_y l_y) = (\pi, 0)$, i.e. the black line, which will not constrain the rays at this point. As such it may be stated generally that the rays considered here will be able to travel in any direction between the red and green lines.

If devices are made using these structures then it may be best to have rays entering the device from some point along the red line rather than along the black. This is because with a Bloch wave travelling over a greater range of angles will be accepted by the device, if the wave is to be entered at a point in the crystal corresponding to the black line then the angle it enters at will be far more restricted. If there is no solution for a wave travelling through the crystal at that angle, then instead of entering the device the wave will be

reflected. Alternatively, this need for the wave to be incident upon the device in the correct manner is a property that could be exploited by a device to filter out the correct waves. Figure (5.6) shows several points of interest in the crystal.

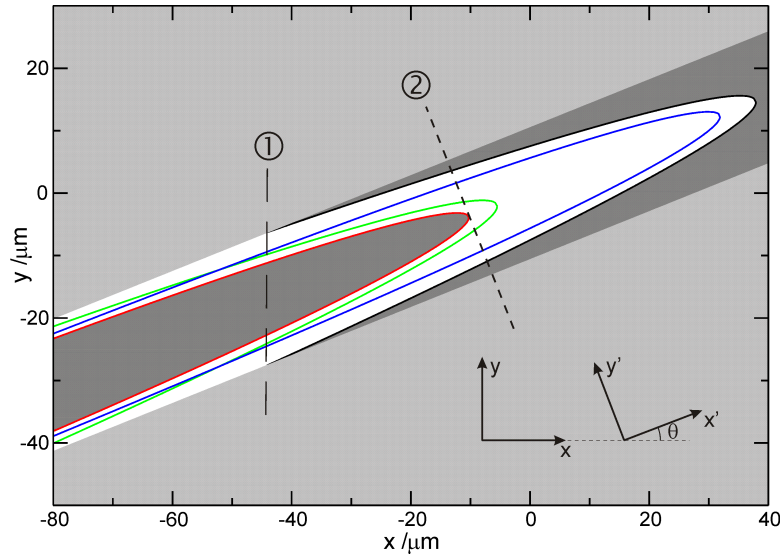


Figure 5.6: The same loci of points shown in figure (5.4). The light grey region is that for which the crystal is not defined. While the dark grey is the region for which it is defined, but for which there is no solution at this frequency.

The light grey region is that for which the crystal is not defined, while the light grey region covers the points where the crystals structure is defined but where no real propagating solution exists at this frequency. For values of x less than the point marked by line 1, x less than about $-45\mu\text{m}$, the solutions for Bragg waves extend to the edge of the crystal. In addition just above this value of x the forbidden region that surrounds the path is very narrow: When $x = 0$ the distance between the region in which the rays move within the crystal, and the region outside the crystal is only of the order of a couple of micrometers. As the cell length in the y direction is $0.5\mu\text{m}$ this is only a few cell lengths, and hence a relatively low number of sheets. The cell lengths are longer in the x direction, meaning that there will be even fewer sheets in an equivalent distance. So long

as the model is considered in the limit of infinitesimally thin sheets, with the refractive index $\rightarrow \infty$, and with continuous functions relating to its properties being considered rather than the exact structure of a crystal, this does not cause a problem. However, in real crystals the confinement of the rays at this point is unlikely to be very strong. To confine the rays, the outer edges of the crystal will therefore need to be reflection coated. Cladding the device in a reflective material will most likely lead to unexpected interferences. It may therefore be best to leave both the value of m , and the cell length, constant outside of the region in which the rays will travel. If the values of m and the cell length are left at a value corresponding to a point just inside the forbidden region then this should strengthen the Bragg reflection confining the rays. Alternatively, if the value of ρ is lowered, the point at which $m = 0$ will occur at a higher value of y' . This will leave a higher number of sheets both in the region in which the rays move and in the forbidden regions.

For values of x' less than the point marked by line 2 in figure (5.6) it may be seen that the allowed region divides into two branches. Figure (5.7) shows several rays following stable paths in the region below this division.

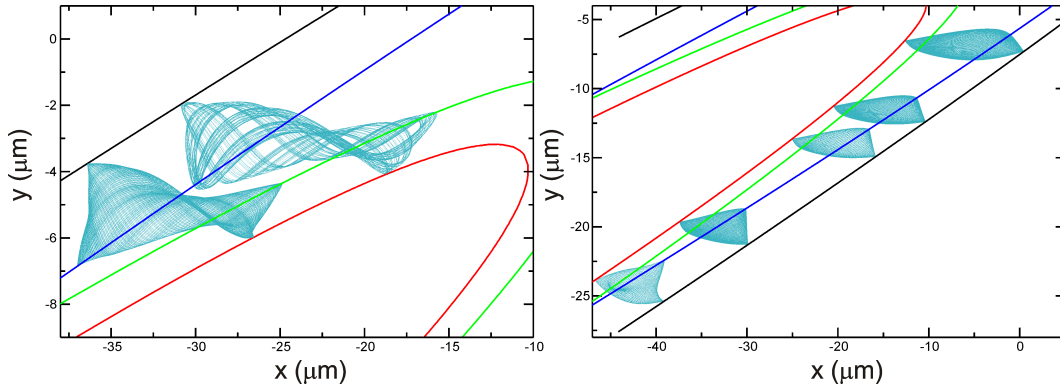


Figure 5.7: Several ray paths in the crystal.

It may be seen that the blue and green lines mark turning points for the rays,

at these points they may be *Bragg reflected*, though in some instances the shape of the band may cause the ray to change direction before a Bragg reflection is reached.

5.4 Dynamic Barriers

Figure (5.8) shows three ray paths in the photonic crystal, two of which are chaotic with a stable path dividing them spatially. The grey regions in the figure are forbidden regions for the rays, regions for which there is either no solution at that frequency or for which $m < 0$.

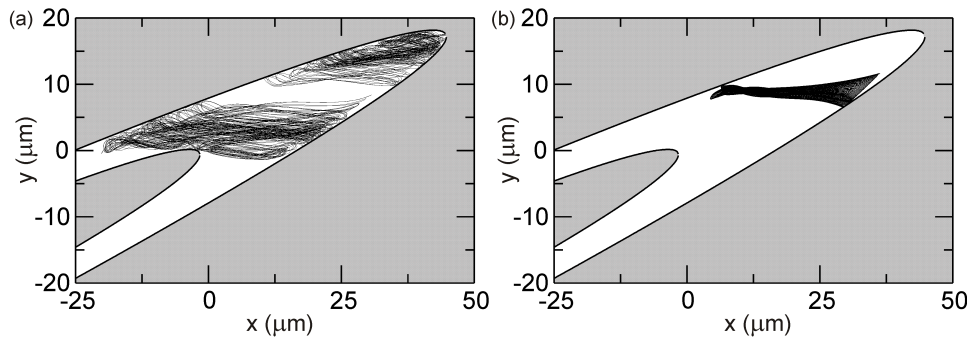


Figure 5.8: The two paths in (a) are moving in two separate chaotic regions in phase space. These two chaotic regions are separated by a region in which stable paths propagate, an example of which is shown in (b). $\omega = 6.12 \times 10^{14}$ rad s^{-1}

Figure (5.9) shows the Poincaré section gained after calculating numerous paths in this crystal. A point is plotted on the Poincaré section every time the ray turns from travelling to the right to travelling to the left, with each point on the Poincaré section being unique to a single path.

The points that correspond to the three paths shown in figure (5.8) are coloured, while the black points correspond to other paths and are shown in order to give a more complete picture of the Poincaré section. The green points correspond to the stable path forming the dynamical barrier, that shown in

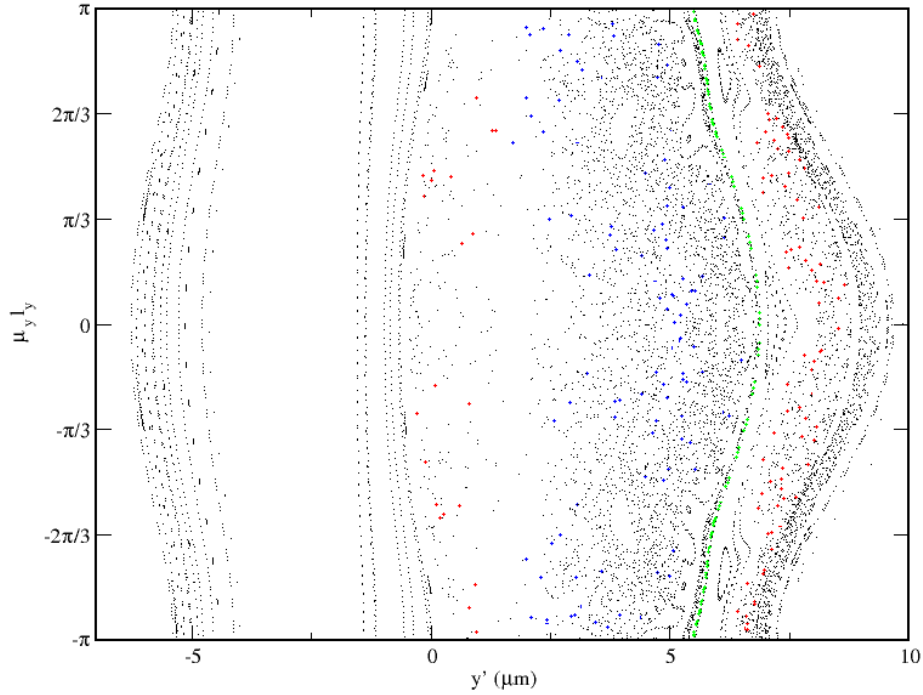


Figure 5.9: A Poincaré section showing the points due to the three ray paths shown in figure (5.8) along with points due to numerous other ray paths in that crystal. $\omega = 6.12 \times 10^{14} \text{ rad s}^{-1}$

figure 5.8(b), while the red points are those for the path below the dynamic barrier, the lower path in figure 5.8(a), and the blue points for the path above it, the upper path in figure 5.8(a). The spread of both the blue and red points indicates the chaotic nature of the paths, while the stable nature of the third path means the points lie on a continuous curve in phase space, corresponding to the surface the ray is constrained to move upon.

While this Poincaré section is useful for indicating whether the path is stable or chaotic, it also shows the problems that may arise in interpreting the nature of phase space with a single slice through it. The red points that lie to the left of the green curve, and hence on the same side of it as the blue points, may give

the impression that the paths occupy the same region of phase space. However, these points on the left of the green line are the turning points due to the inner limit, the red line in figure (5.4), which explains why they occur at low values of y' . As the paths travel in regions of space that are spatially separated, they must move in separate regions of phase space. Different Poincaré sections may both reveal, and miss, different features in phase space. In addition, regions of phase space that may appear separate in one Poincaré section may be joined in a different section of phase space.

One of the main problems with the use of these structures is that, due to chaotic nature of the paths, any distortion through damage or expansion through heat etc, may dramatically change the paths which the rays take through the structure.

5.5 Switching

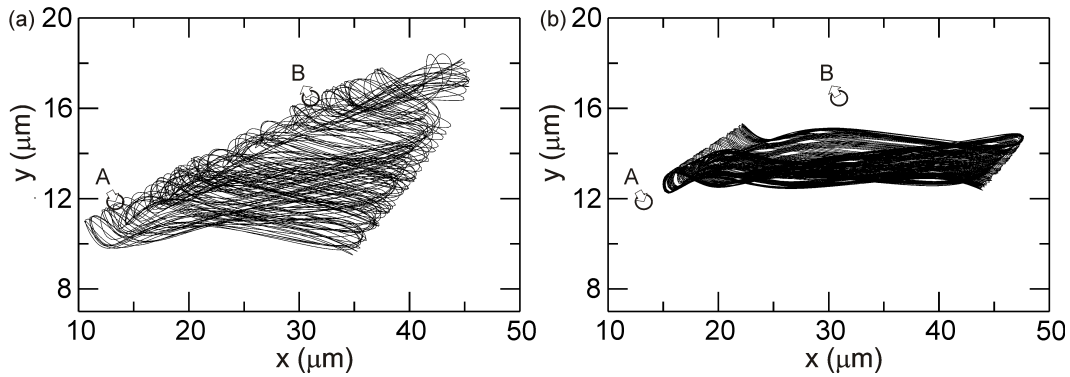


Figure 5.10: Ray paths when (a) $m = 2.1\mu m$ and (b) $m = 2.5\mu m$. In each case $\omega = 6 \times 10^{14}$. (a) Rays entering at point A may be detected at point B , (b) Rays entering at point A are not detected at point B as a dynamic barrier lies between these two points

If these photonic crystals are created out of a non-linear optical material [68], a material whose refractive index may be changed by electric or magnetic fields [69, 70, 71, 72, 73], then the construction of a device such as a switch is

possible. However, care must be taken as the use of non-linear optical materials may lead to the introduction of many unwanted effects. An example of this would be birefringence, whereby the refractive index of the material is different for different polarisations. However, as the electromagnetic waves are all S polarised this will have no effect on the rays considered here.

If the crystal is constructed out of appropriate material and has metal contacts attached to the top and bottom of it, with the crystal being thick enough for the rays to not reach the contacts, then the application of an electric field may be used to alter the refractive index of the material. An alternative to creating the crystal out of a non-linear optical material would be to fill what are currently air gaps with a non-linear optical material. The advantage of this method would be that the non-linear material would not need to be a solid. Figure (5.10) shows two rays travelling in a photonic crystal with an identical structure, i.e. that described previously, except that in (a) $m = 2.1$ and in (b) $m = 2.5$. In both cases $\omega = 6 \times 10^{14}$ rad s⁻¹. If a Bloch wave enters the crystal at point A then, in case (a), a high transmission will be seen at point B . However, if the refractive index is changed in such a way as to satisfy the profile for $m = 2.5$ then chaotic region into which the Bloch wave is injected no longer extends to the point at B .

While it would appear that the only region of the crystal in which the refractive index needs to be changed is that in which the dynamic barrier lies, allowing the lower region of chaos to extend up until it reaches the upper region, it should be noted that simply because two regions that contain chaotic paths may meet in space it does not mean that a ray may cross from one to the other; The conditions of the ray in the first chaotic region may prohibit it moving into the second chaotic region. The regions in phase space may still be completely separate.

If the value of m is varied across the region in which the dynamic barrier is found, increasing linearly from a value of 2.0 in the chaotic regions either side to a value of about 2.5 between them, then the occasional path may be found that crosses from one region to the second, however these rays would appear to be rare. Considering the rarity of these rays, it is very possible that they arise simply out of errors in the program, allowing a ray to cross from one region to the other.

It may be seen from figure (5.5) that, as the directions in which the rays may travel are restricted, it is the rays that predominantly travel in the y direction that are forbidden first. This is the reason that the ray paths are far more extended in the x direction than in the y . If the refractive index is changed in such a way that the electromagnetic wave lies close to the bottom of the band the ray will have more freedom to travel in the y direction.

Care needs to be taken when considering such rapid changes of m . The condition mentioned earlier, that the cells need to vary slowly in order to use the approximation that the bandstructure is at any point equal to a corresponding infinite crystal, does not only apply to the cell length; All properties of the crystal must vary slowly in order to use this bandstructure approximation.

If the voltage applied to the plate is not uniform, perhaps by the use of several plates attached to the top and the bottom of the crystal each of which may be set to a different voltage, than the refractive index across the crystal may be changed in a far more subtle manner.

While this is the most simple manner in which a switch may be created, shifting the region in which chaotic paths are found so that it covers both the points at which rays are injected into and detected, if the variation in refractive index is changed carefully it is possible to breach the dynamic barrier, constructing a chaotic path from one separate region of chaos to the next. That is,

after the change in refractive index in regions of the crystal, the phase space is changed from one in which there are two distinct regions of chaos separated by a separated by a dynamical barrier, to one in which this is changed to a single chaotic region.

5.6 Separate values of m

The photonic crystal has, up to this point, been described by the relative permittivity profile,

$$\epsilon(\vec{r}) = 1 + m \left(\sum_{n_x=-\infty}^{\infty} \delta(x - n_x l_x) + \sum_{n_y=-\infty}^{\infty} \delta(y - n_y l_y) \right) \quad (5.8)$$

However, as the dispersion relations for S polarisation separate in the x and y directions, it is not difficult to calculate the bandstructure for a crystal with a different value of m in each direction. The relative permittivity profile of this new crystal is thus,

$$\epsilon(\vec{r}) = 1 + \left(m_x \sum_{n_{\vec{x}}=-\infty}^{\infty} \delta(\vec{x} - n_{\vec{x}} \vec{a}) + m_y \sum_{n_{\vec{y}}=-\infty}^{\infty} \delta(\vec{y} - n_{\vec{y}} \vec{a}) \right) \quad (5.9)$$

where m_x is the value of m for the sheets perpendicular to the x direction and m_y is the value of m for the sheets perpendicular to the y direction.

Calculating the dispersion relations in the same manner as previously, with the electromagnetic wave once again having a locally evanescent character in the y direction and a locally propagating character in the x direction, leads to

the following relations,

$$\cos(\mu_x l_x) = \cos(k_x l_x) - \frac{m_x k^2}{2k_x} \sin(k_x l_x) \quad (5.10a)$$

$$\cos(\mu_y l_y) = \cosh(q_y l_y) - \frac{m_y \omega^2}{2c^2 q_y} \sinh(q_y l_y) \quad (5.10b)$$

The second of these two equations has, in the tight binding regime where $q_y l_y \gg 1$, the approximate solution,

$$q_y = \frac{m_y \omega^2}{2c^2} \quad (5.11)$$

irrespective of the value of μ_y . This may be substituted into the relation between the total wavevector and its components in the x and y directions,

$$-q_y^2 + k_x^2 = \frac{\omega^2}{c^2} \quad (5.12)$$

to obtain an approximation to the x component of the wavevector,

$$k_x = \frac{\omega}{c} \left(\frac{m_y^2 \omega^2}{4c^2} + 1 \right) \approx \frac{m_y \omega^2}{2c^2} + \frac{1}{m_y} \quad (5.13)$$

The values of k_x and q_y obtained from equations (5.11) and (5.13) may be substituted into equation (5.10a) to give the following equation that may be solved numerically for any fixed value of ω ,

$$\cos(\mu_x l_x) \approx \cos\left(\frac{m_y \omega^2}{2c^2} l_x + \frac{l_x}{m_y}\right) - \left(\frac{m_x}{m_y^2 \omega / 4c + c / \omega}\right) \sin\left(\frac{m_y \omega^2}{2c^2} l_x + \frac{l_x}{m_y}\right) \quad (5.14)$$

These approximations may then be used with with the numerical solver *hybrd1*, in the way described in previous chapters, to gain a solution that satisfies equations (5.10a) and (5.10b).

The ability to vary the value of m in each direction separately brings in

an additional way in which the symmetry of the crystal may be broken. As the wave has an evanescent character in one direction, and a real propagating character in the second, changing the crystal in a single direction will affect different bands in different manners. As such, for the two bands considered so far, it may be possible to shift the second band so that it covers a different set of frequencies than the first band.

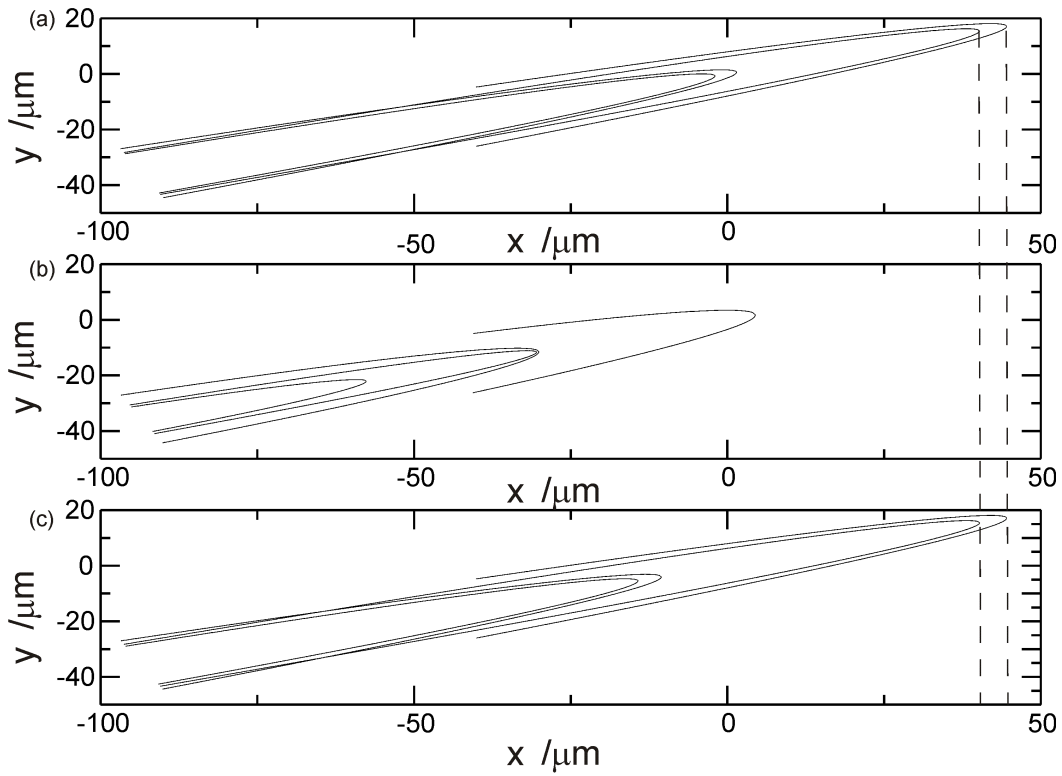


Figure 5.11: Effect of changing m_x and m_y on the spatial regions in which propagating rays exist, (a) $m_y = 2$, $m_x = 2$, (b) $m_y = 1$, $m_x = 2$, (c) $m_y = 2$, $m_x = 1$, in all cases $\omega = 1.25 \times 10^{15}$. The dashed lines across all three section are the limit of bands in (a)

Figure (5.11) shows the region in which the rays may move for a square celled crystal, where $l_x = 1.0\mu m$ and $l_y = 1.0\mu m$. It may be seen that changing m in the direction that the wave takes an evanescent character has far more

effect than varying m in the other direction. The dashed line across all three parts of figure (5.11) marks the limit of the region in which rays may move for part (a). While the limit in part (c) appears to be at the same location, there is a slight shift to a lower value of x . This point is further illustrated by figure (5.12), the dispersion surfaces at the point $x = 0, y = 0$. Part (a) shows the dispersion surface when $m_x = 2, m_y = 2$ (blue), and $m_x = 1, m_y = 2$ (green). While the band retains its overall shape as m_x changes from 2 to 1, there is a significant shift in the range of frequencies over which it occurs. Part (b) again shows the dispersion surface in blue for which $m_x = 2, m_y = 2$, with the second (red) dispersion surface being for $m_x = 2, m_y = 1$. While it is not apparent

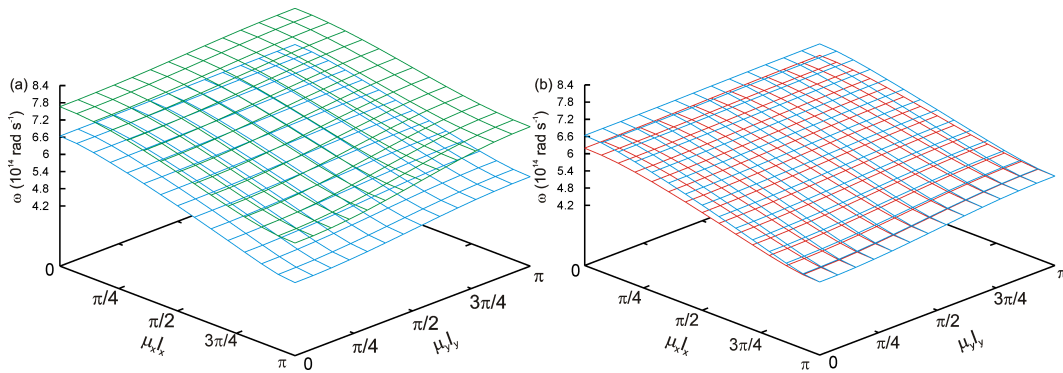


Figure 5.12: In both diagrams the blue surface is for $m_x = 2.0, m_y = 2.0$. For the green band in (a) the value of m_x is reduced to one. For the red band in (b) m_y is reduced to one.

from the diagram, there is a slight change in the band position at $\mu_x l_x = \pi$. While changing the shape of the band will change the ray dynamics to some extent, the crystal still supports both stable paths and chaotic paths.

While it is useful to know how these bands change with m , it is the relative position of the band for electromagnetic waves with an evanescent component in the second direction that needs to be considered. As variation of the value of m_x (as opposed to m_y) has less effect on the shape and position, the region in

which the rays may move, it is this that will be considered. Figure (5.13) shows the bands at the position $x = 0, y = 0$, for the structure with $m_x = 1, m_y = 2$, again for a value of $\omega = 6 \times 10^{14} \text{ rad s}^{-1}$

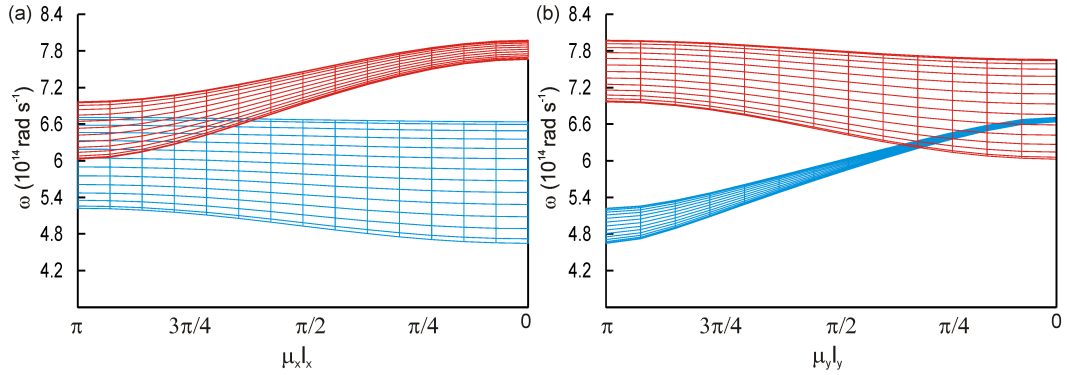


Figure 5.13: The bands when $m_x = 1, m_y = 2$. The band that is of interest to us is only changed slightly, however the second band shifts quite dramatically. The same dispersion surface is shown in (a) and (b), however (b) is (a) after a rotation of 90°

While the overlap of the bands is considerably reduced, it is not until m_x is reduced to a value of about 0.6 that the bands are completely separate. The dispersion surfaces for this case are shown in figure (5.14).

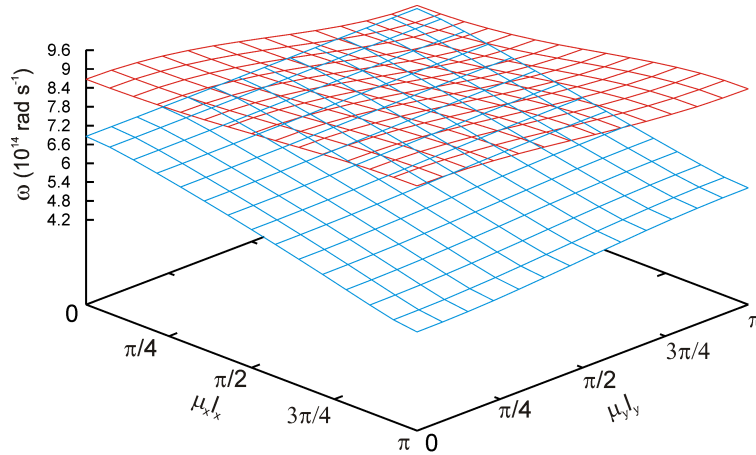


Figure 5.14: The bands when $m_x = 0.6, m_y = 2$

5.7 Shifting the region of interest

While the previous section has introduced a manner in which the symmetry of the crystal may be broken, it is only because the region that the rays are restricted to travel in lies around the point $x = 0, y = 0$, that such symmetry reduction is actually needed to remove band degeneracy. In other regions of the crystal, away from the point at which $l_x \approx l_y$, the crystal will not be symmetric through a rotation of 90° . Figure (5.15) shows the regions in which the rays

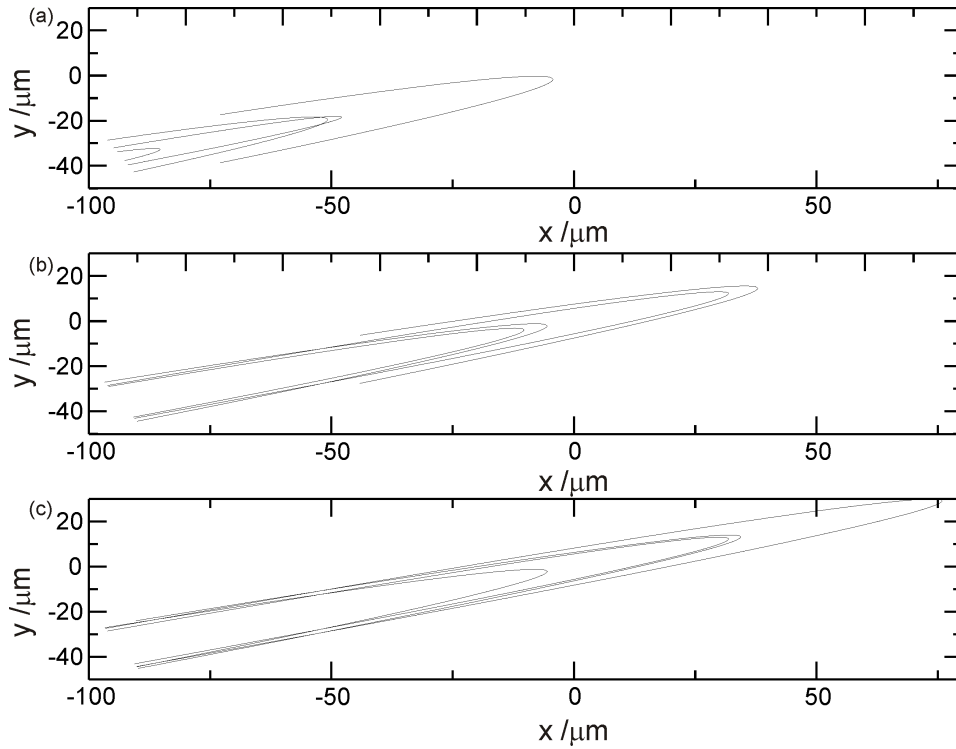


Figure 5.15: regions in which the band may move, $m = 2.0$ in both directions, (a) $\omega = 4.5 \times 10^{14} \text{ rad s}^{-1}$, (b) $\omega = 6 \times 10^{14} \text{ rad s}^{-1}$, (c) $\omega = 7.5 \times 10^{14} \text{ rad s}^{-1}$

may move for the crystal with $m = 2$, the rest of the structure being the same as previously defined. While the region around $x = 0, y = 0$ may be avoided for lower frequencies, far fewer ray paths are completely contained by the limits of

the region the ray may move in, instead most ray paths will leave the crystal. This can be seen in figure 5.15(a), here the outermost line showing the region in which the rays moves reaches the edge of the crystal at about $x = -70\mu\text{m}$. For values of x less than this, the allowed region extends to the edge of the crystal and rays will not be contained. It may be seen that at higher frequencies more of the paths are periodic. While extending the width of the allowed region in the x direction, and with it extending the ray paths in this direction, each ray only has a small difference between the maximum and minimum position they take on the y axis, a far smaller variation than at lower frequencies.

Chapter 6

Two dimensional photonic crystals, finite width sheets

While the previous chapter focused on photonic crystals in the limit of infinitesimally thin sheets, this chapter will focus on crystals constructed from dielectric sheets with an appreciable width. This is of course a necessary step to take before a real photonic device may be constructed, as useful features that show up in the limit of infinitesimally thin sheets may not appear away from this limit.

As has been mentioned previously, due to the crystals being defined using the function m , the crystals considered so far have not been uniquely defined; Sheets that have different widths may be defined by the same value of m if their refractive index is selected appropriately. A problem with this definition is that, as the change in phase for a wave travelling between interfaces is different for each sheet, not only will the magnitude of the reflections from each sheet change, but also the frequencies at which transmission peaks occur. A far better way to define the sheets is by their optical path length. Although, once again,

the magnitude of the reflection at the interfaces between the sheets and the air will be different due to the different refractive indices, if the optical path length is the same then the change in phase of a wave travelling across the sheet will be constant. Hence, while the strength of the reflection may change, the transmission peaks will still occur at the same frequencies. While this chapter is not as complete a consideration of these crystals as that presented in chapters 4 and 5, use of the work here should lead to more detailed work being carried out by others in the future.

Appendix A contains details of how the expressions for the dispersion relations of these photonic crystals are obtained, along with other approximations that are needed for the ray tracing process described in chapter 2. While the dispersion relations are again obtained analytically, the program calculates the solution to these relations numerically. The non-linear solver *hybrd1* uses an approximate solution to k_x and k_y as a starting point and, in the case of infinitesimally thin sheets, approximate values of k_x and k_y may be gained analytically. However, away from this limit the approximate values for k_x and k_y must be obtained numerically.

6.1 Finite width sheets

While the introduction of finite width sheets will clearly change the band-structure, if thin sheets with a high refractive index are used then some approximation to the previous model may be possible. While the value of the refractive index of the sheet may be high, it will still be far lower than in the previous model in which $\epsilon_r \rightarrow \infty$. This reduction of the refractive index of each sheet, and hence the maximum reflectance from each, may mean that the confinement of the electromagnetic waves in the crystal is reduced and that useful features may be lost. However, these effects may be missed by the ray tracing

method used here, and it is not until a more complete consideration of a solution for electromagnetic waves in a real structure using Maxwell's equations is made that this will be seen. The calculations here make no consideration of the actual structure of a single crystal, and only involve its cell length, refractive index, etc, expressed as continuous functions of x and y .

The problems created by reducing the maximum reflectance of each sheet may be countered by the used of more dielectric sheets in the crystal. This is achieved by reducing the value of ρ , the strength of the parabolic variation in the equation $m = m_0(1 - \rho y'^2)$, and the chirp applied to the crystal, η . If ρ is reduced then $m = 0$ will occur at a larger value of y' , and as the cell length has not been changed, this will mean that more sheets are included. In a similar manner, if η is reduced then there will be a slower variation in cell size in the x direction. As the points in the crystal at which the Bloch waves are Bragg reflected depend on the local cell size, for a smaller value of η , the points at which the Bragg reflection occur will be further apart.

The inclusion of a greater number of sheets increases the number of points in reciprocal lattice associated with the crystal. Consequently, even though the coefficient of each term in the Bloch wave, as given by the plane wave expansion, may be small, the greater number of terms may mean that the cumulative effect of all terms is still strong.

As the width of the dielectric sheets increases, at some point the sheet width will become comparable to the cell length. As such, electromagnetic waves in these structures behave like electromagnetic waves in the photonic crystals described in Chapter 5 in the case of thin sheets, or like electromagnetic waves in a gradient index fibre [74, 75] with refractive index profile $m = m_0(1 - \rho y'^2)$ in the case of dielectric sheets whose width equals the cell length.

In these two limits, the rays either behave in the same manner as the pho-

tonic crystal described in the previous chapter, or, as the sheets width becomes comparable to the cell length, the rays will behave in the same manner as those in a gradient index fibre, with the refractive index profile given by m .

In the following section, we will consider electromagnetic waves in a two dimensional photonic crystal. As before, for S polarisation the solution in each direction may be considered completely separately. The electromagnetic waves are confined to move in the x, y plane. With the electric field in the air gap being given as,

$$\vec{E}(x, y) = \hat{z}(E_{x,n}^+ \exp^{ik_x x} + E_{x,n}^- \exp^{-ik_x x})(E_{y,n}^+ \exp^{ik_y y} + E_{y,n}^- \exp^{-ik_y y}) \quad (6.1)$$

If the width of the dielectric sheet in the x or y direction is $a_{x,y}$, and the width of the air gap is $b_{x,y}$, then the new dispersion relations for a wave with a real propagating character in each direction is,

$$\cos(\mu_x(a_x + b_x)) = \cos(k_{a_x} a_x) \cos(k_{b_x} b_x) - \left(\frac{k_{a_x}^2 + k_{b_x}^2}{2k_{a_x} k_{b_x}} \right) \sin(k_{a_x} a_x) \sin(k_{b_x} b_x) \quad (6.2a)$$

$$\cos(\mu_y(a_y + b_y)) = \cos(k_{a_y} b_y) \cos(k_{b_y} b_y) - \left(\frac{k_{a_y}^2 + k_{b_y}^2}{2k_{a_y} k_{b_y}} \right) \sin(k_{a_y} a_y) \sin(k_{b_y} b_y) \quad (6.2b)$$

Where k_{a_x, a_y} is the component of the wavevector in the x, y direction within the dielectric sheet, and k_{b_x, b_y} is the component of the wavevector in the x, y direction in the air gap. Once again the situation whereby, in the air gap, the wave takes an evanescent character in one direction and a propagating character in the second will be considered. In this case the wave will have an evanescent character in the x direction. As such the substitution $k_{b_x} = iq_{b_x}$ will be made.

Substituting this into equation (6.2a) changes the pair of equations to

$$\cos(\mu_x(a_x + a_x)) = \cos(k_{a_x} a_x) \cosh(q_{b_x} b_x) + \left(\frac{q_{b_x}^2 - k_{a_x}^2}{2k_{a_x} q_{b_x}} \right) \sin(k_{a_x} a_x) \sinh(q_{b_x} b_x) \quad (6.3a)$$

$$\cos(\mu_y(a_y + b_y)) = \cos(k_{a_y} a_y) \cos(k_{b_y} b_y) - \left(\frac{k_{a_y}^2 + k_{b_y}^2}{2k_{a_y} k_{b_y}} \right) \sin(k_{a_y} a_y) \sin(k_{b_y} b_y) \quad (6.3b)$$

Within the sheets, the waves will have a real propagating character in both directions. In the tight binding regime, where $q_{b_x} b \gg 1$, the approximation $\cosh(q_{b_y} b) \approx \sinh(q_{b_y} b) \gg 1$ may be used with equation (6.3a) to give the approximate relation,

$$\left(\frac{k_{a_y}^2 - q_{b_y}^2}{2k_{a_y} q_{b_y}} \right) \tan(k_{a_y} a) = 1 \quad (6.4)$$

The relation between the components of the electromagnetic wave in the x and y directions in the sheet and the air gap are given by,

$$k_x^2 + k_y^2 = \frac{\epsilon_r \omega^2}{c^2} \quad \text{and} \quad -q_x^2 + k_y^2 = \frac{\omega^2}{c^2} \quad (6.5)$$

As k_y , being parallel to the interface being considered, is common in both regions it is useful to use equations (6.5) to eliminate k_{a_y} and q_{b_y} from equation (6.4) to give,

$$\left(\frac{(\epsilon_r + 1) \frac{\omega^2}{c^2} - 2k_y^2}{2\sqrt{\frac{\epsilon_r \omega^2}{c^2} - k_y^4 - \frac{\omega^2}{c^2}}} \right) \tan \left(\sqrt{\left(\epsilon_r \frac{\omega^2}{c^2} - k_y^2 \right) a} \right) = 1 \quad (6.6)$$

This equation may then be solved numerically for a value of k_y that is independent of the value of μ_x . This may then be substituted into equation (6.3b) and, for a given value of μ_y , a value of k_x may be obtained. These values of k_y and

k_x are only approximations to the true solutions of equations (6.3a) and (6.3b), and as such are merely used as an initial guess as a solution to these equations for input into the solver *hybrd1*. The use of *hybrd1* removes the independence of the solution from μ_x , giving a more accurate solution of the dispersion relation.

When this is carried out in the limit of infinitesimally thin sheets, the value of k_y may be gained analytically, and is given by

$$k_y = \left(\frac{m^2 \omega^4}{4c^4} - \frac{\omega^2}{c^2} \right)^{1/2} \quad (6.7)$$

This is a single valued function for k_y , which is clearly not the case for the solution of k_y with finite width sheets.

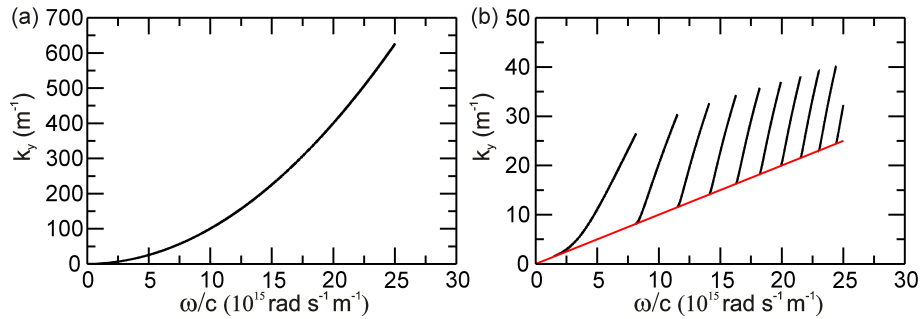


Figure 6.1: Plots of k_y versus ω for (a) infinitesimally thin and (b) finite width sheets. The red line in (b) is the solution for $k_y = \omega/c$, the free space dispersion curve.

Figure (6.1) shows both the analytical solution for infinitesimally thin sheets as used in Chapter 5, and the numerical approximation that is used in the program for finite width sheets. As equation (6.6) is a function involving *tan* it is possible to find more than one solution of ω for each value of k_y , hence the numerous branches that may be seen in figure 6.1(b). Figure 6.1(a), the solution when considering the limit of infinitesimally thin sheets, gives only the solution with the lowest value of omega, hence only one branch being seen. Each of the branches in (b), and the solution in (a), may be solved for higher values of ω ,

however these solutions have not been calculated at this point.

It can be shown that equation (6.6) has no real solution for $k_y < \omega/c$, which should be expected as ω/c is the free space dispersion relation. If $k_y < \omega/c$ then k_x will take a real value, as may be seen from the condition $k_x^2 + k_y^2 = \omega/c$, and the wave will have a locally propagating character in both directions.

This process is slightly less accurate than the method used in the previous work, that concerning the solution for infinitesimally thin sheets, whereby the solution of k_y may be used to gain the following solution,

$$\omega = \frac{2c^2}{m_x l_x} \left((2n - 1/4)\pi - \frac{l_x}{m_x} \pm \cos^{-1} \left(\cos \left(\frac{\mu_y l_y}{\sqrt{2}} \right) \right) \right), \quad (6.8)$$

which is used to calculate the approximations to k_x and k_y . These are again used with *hybrd1* to obtain a solution to the dispersion relations to gain a more accurate solution.

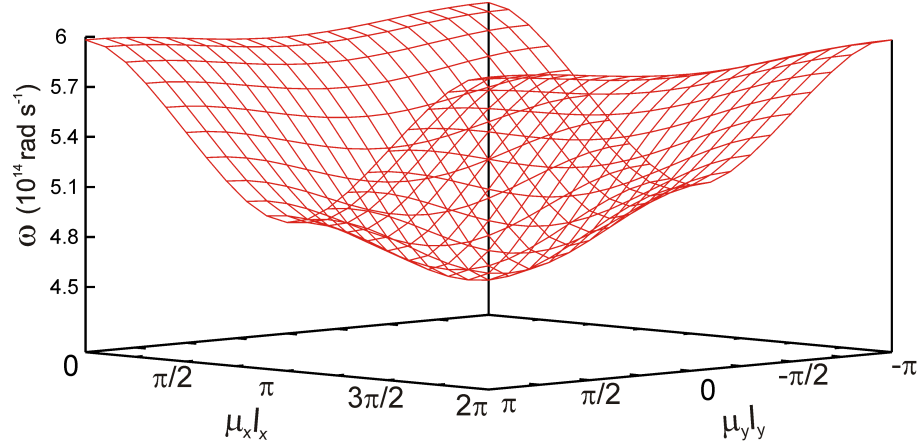


Figure 6.2: A dispersion curve for a crystal with finite width sheets

Figures (6.2) and (6.3) show the dispersion surface for a square-celled photonic crystal with sheets of a finite width, with figure (6.2) showing the entire first Brillouin zone and figure (6.3) showing the reduced Brillouin zone. The

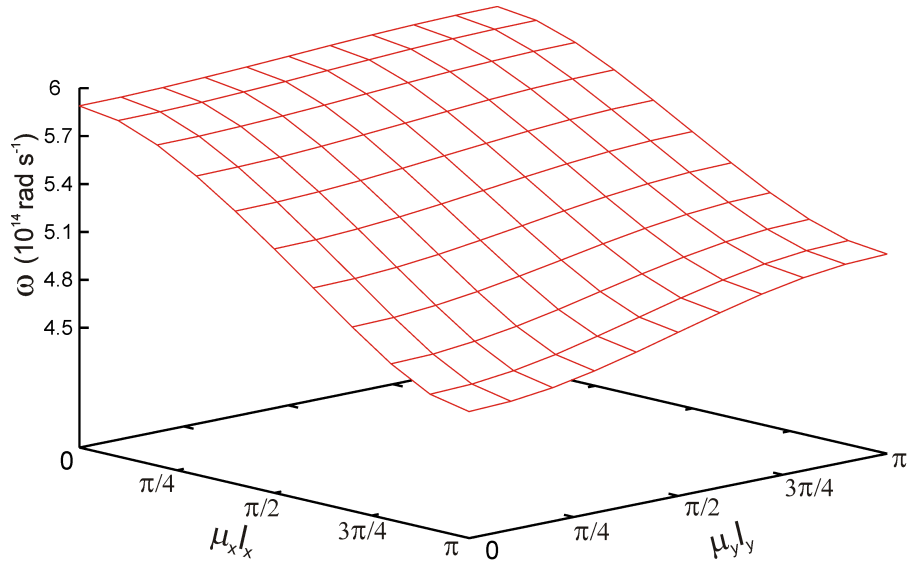


Figure 6.3: A dispersion curve for a crystal with finite width sheets, shown for the reduced Brillouin zone

cell length in each direction is $0.5\mu m$ with the dielectric sheet taking up $1/30$ of the cell length. The relative permittivity of the sheets is $\epsilon_r = 300$.

It is clear from the diagrams that the dispersion surface still takes a form that is very similar to that given by the photonic crystals in their limit. As such, it may be possible to create crystals for which the ray patterns are similar to those taken in the limit. It should be noted, though, that as the materials considered in this example have a refractive index $n > 17$ for a single sheet, and $n > 35$ for the points at which the sheet cross, it would be hard to find real materials that match this criteria. As such other designs may need to be considered for a practical device.

Figure (6.4) is the dispersion surface for a crystal in the limit of infinitesimally thin sheets and with a cell length of $0.4833\mu m$ in each direction. In order to make a comparison with the dispersion surface for the crystal with finite width sheets, the value of m is set to 5. While there are some differences

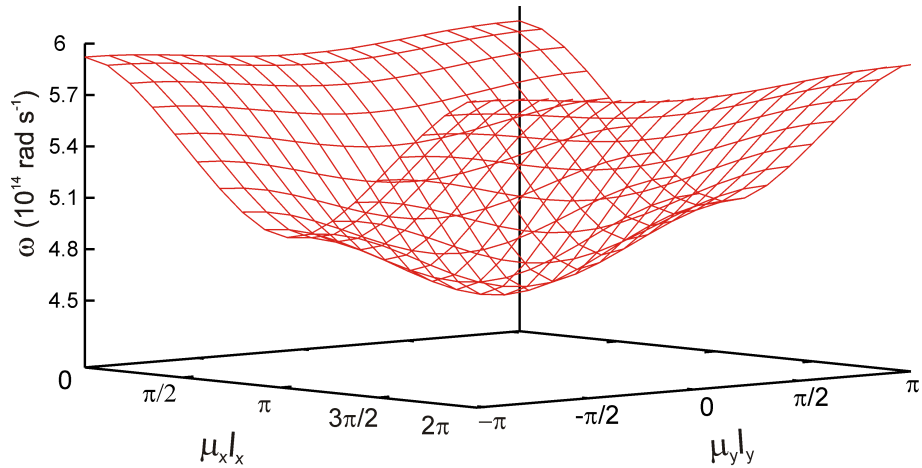


Figure 6.4: dispersion curve for crystal with infinitely thin sheets

in the dispersion surface, the top of the surface being lower in the limit of infinitesimally thin sheets for example, the shape of the surface remains largely unchanged. It is therefore possible that using the same ray tracing model for crystals with finite width sheets will reveal paths of a similar nature to those in the limit of infinitesimal sheet width.

Unfortunately, at present the program used to calculate the dispersion surfaces for these crystals is not stable enough to make a much more detailed consideration of these structures. In many cases, the solver *hybrd1* returns an error message indicating that it is not making good progress in finding a solution to the dispersion relations. The program could be changed for a more reliable method, or care could be taken in selecting problems in such a way as to ensure a solution is found.

In addition to the program having problems in finding a dispersion surface for all cases, due to the extra numerical steps that are taken in this method, the current programs are far too slow to carry out ray tracing in these crystals. The methods used in these calculations have not been optimised, so it is possible

that rewriting the programs carefully may yield the improvements in speed to allow ray tracing in these crystals.

Conclusions and suggestions for further work

6.2 One dimensional photonic crystals

The use of transmission matrices for the calculation of the fields and transmission profile of structures such as these is a tried and tested method, and so good agreement between theory and experiment is only to be expected. The fact that only part of a Bloch oscillation was seen when the fields in the photonic crystal were measured is due mainly to two reasons. The first reason is the suppression of the first two bands in the experimental measurements. As this was not expected the crystal was not designed in order to see a full oscillation in the first band that was seen experimentally. The second reason is that the dielectric blocks were initially cut incorrectly. As there was no more material available, and limited time in which to use the equipment, a new set of shorter block lengths had to be calculated. The incorrectly cut set of blocks were then cut down to these new set of lengths. The new set of block lengths were calculated to minimise the adjustment to the blocks, while keeping the correct exponential chirp. While the adjustment was minimised, this still introduced an unwanted change to the bandstructure.

The failure to enclose both ends of the band within the crystal is likely to be the reason that the peaks are not as equally spaced as would be expected. However, the peaks seen in a single band do still have roughly equal spacing, with the spacing changing from band to band as would be expected.

If this experiment was carried out again with the knowledge of which bands would be seen experimentally, and with the correct set of blocks, the results should be far clearer. However, if the experiment is to be repeated, it should be done on a linear waveguide rather than on the ring resonator used in the experiment. There are no benefits to be gained in this experiment from the use of a circular waveguide, and numerous drawbacks. The microwave absorbers that are used in order to make this equivalent to an open waveguide are not perfectly absorbing, and so introduce a unnecessary source of error. In addition, the curve of the waveguide, and the need to convert the teflon blocks into curved blocks, is another source of errors. If such equipment is to be used again, then a greater analysis of the comparison between a linear setup and this circular setup needs to be made.

As can be seen from the work at the end of chapter 4, the definition of $m = \epsilon_r d$ is not enough to uniquely define a crystal. The crystals should instead be defined by the optical path lengths of both the sheets and the gaps between the sheets.

6.3 Two dimensional photonic crystals

While useful in showing features that should be seen in photonic crystals such as these, Hamiltonian ray tracing has several weaknesses that should be considered before real structures are made. One of the most notable is the absence of tunnelling in this model. In a real crystal, if an allowed solution lies at the far side of a dynamical barrier, some of the Bloch wave may tunnel

through exciting a Bloch wave in what was previously an inaccessible region. Careful design of the crystal may be needed to ensure that tunnelling is reduced to a minimum.

The bandstructure is gained using the assumption that the crystal is infinite in extent, and rays are unaffected by the structure beyond its allowed region. However, in the structures that are considered here the crystal may end close to the edge of an allowed region. This has no effect on the ray tracing in this model, however in reality the waves will penetrate into this region and be affected by the structure beyond the edge of the allowed region.

The approach used here will not show any transient behaviour. It has been shown that the Bloch wave is a superposition of plane waves that are gained from scattering from the crystal. The locations at which the waves scatter from are at a variety of spatial distances away from any point, and as such it will take different amount of time for scattered waves to arrive at that point. Such behaviour will be missed by this model.

Finally, it should be noted that any attempt to calculate a chaotic ray path is doomed to failure. Each step of the ray path will be slightly away from the true path that the ray follows. As the second step makes no reference to the initial step it may be considered as the start of a new path a slight distance away from the point that should have been calculated for the original path. It has already been mentioned in chapter 3 that, in a chaotic region, paths that start off an infinitesimal distance apart will diverge exponentially. As such the second step will rapidly diverge from the original path. As each step may be taken in isolation, the ray path that is calculated may be seen as an approximation to a different ray path in the chaotic region, each of which is diverging rapidly from the path given in the previous step.

While the ray paths will not be accurate, they will still travel throughout

the chaotic region of phase space it is confined to. So while not accurately representing any single path, it should give the region in which chaotic paths will move.

From these points it can be seen that, while a useful tool for investigating these structures, another method needs to be used to help complete the picture of what will be seen. The best manner in which to continue this work is to find a solution of Maxwells equations. A possible method to achieve this is through finite difference methods, though the complexity of the structure means care must be taken in order to leave a program that runs in a reasonable amount of time. This has been attempted by the author, using a square grid, however the run time of the program was too long to be practical. With multi-gridded or variable mesh grids the sufficient gains in speed may be found, however this will not be looked at in this thesis.

Chapter 7

Appendix A

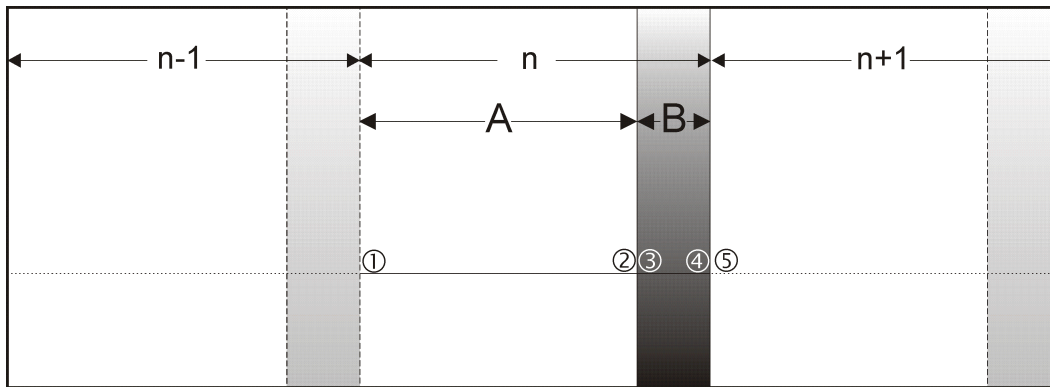


Figure 1: A cross section of three cells of a one-dimensional crystal. Transmission is calculated across the cell that is shown darker than its neighbors. The width of the air gap is A , and the sheet B .

In order to gain the dispersion relation for an infinite one dimensional crystal, three sheets of which is shown in figure (1), the first step that needs to be made is to relate the left and right travelling components of the wave at a point in one cell to the identical point in the next cell. For convenience, the point in each cell will be chosen to be that on the air side of the interface between the dielectric material and the air at the left hand side of the cell. While not changing the

result in any way, choosing this point simplifies the maths. This is because the propagation of the waves across both the air gap and dielectric sheet is dealt with by two 2x2 matrices, combined with matrices relating the fields at either side of each interface. If a point away from an interface is chosen then, while there will still only be 2 matrices dealing with the waves at interfaces, there will need to be three matrices dealing with the propagation of the waves; Propagation of the wave up to the sheet, propagation across the sheet, and then a third matrix dealing with the propagation from the sheet to the correct point on the far side of the interface.

As the results are separable in each direction the following will consider only the component of the waves propagating in the x direction. If the results for a two dimensional photonic crystal are wanted, in order to gain the dispersion relation in the y direction, exactly the same process will be used considering the y component of the wave and the sheets perpendicular to the y direction.

As shown in chapter 1, the transmission across a cell is given by the following,

$$\begin{bmatrix} \left(\frac{1}{2} + \frac{\vec{k}_{x,b}}{2\vec{k}_{x,a}}\right) & \left(\frac{1}{2} - \frac{\vec{k}_{x,b}}{2\vec{k}_{x,a}}\right) \\ \left(\frac{1}{2} - \frac{\vec{k}_{x,b}}{2\vec{k}_{x,a}}\right) & \left(\frac{1}{2} + \frac{\vec{k}_{x,b}}{2\vec{k}_{x,a}}\right) \end{bmatrix} \begin{bmatrix} e^{-i\vec{k}_{x,b}B} & 0 \\ 0 & e^{i\vec{k}_{x,b}B} \end{bmatrix} \begin{bmatrix} \left(\frac{1}{2} + \frac{\vec{k}_{x,a}}{2\vec{k}_{x,b}}\right) & \left(\frac{1}{2} - \frac{\vec{k}_{x,a}}{2\vec{k}_{x,b}}\right) \\ \left(\frac{1}{2} - \frac{\vec{k}_{x,a}}{2\vec{k}_{x,b}}\right) & \left(\frac{1}{2} + \frac{\vec{k}_{x,a}}{2\vec{k}_{x,b}}\right) \end{bmatrix} \\ \times \begin{bmatrix} e^{-i\vec{k}_{x,a}A} & 0 \\ 0 & e^{i\vec{k}_{x,a}A} \end{bmatrix} \begin{bmatrix} E_1^+ \\ E_1^- \end{bmatrix} = \begin{bmatrix} E_5^+ \\ E_5^- \end{bmatrix}$$

This may be rearranged as,

$$\begin{aligned}
& \begin{bmatrix} \left(\frac{1}{2} + \frac{\vec{k}_{x,b}}{2\vec{k}_{x,a}}\right) & \left(\frac{1}{2} - \frac{\vec{k}_{x,b}}{2\vec{k}_{x,a}}\right) \\ \left(\frac{1}{2} - \frac{\vec{k}_{x,b}}{2\vec{k}_{x,a}}\right) & \left(\frac{1}{2} + \frac{\vec{k}_{x,b}}{2\vec{k}_{x,a}}\right) \end{bmatrix} \begin{bmatrix} e^{-i\vec{k}_{x,b}B} & 0 \\ 0 & e^{i\vec{k}_{x,b}B} \end{bmatrix} \begin{bmatrix} \left(\frac{1}{2} + \frac{\vec{k}_{x,a}}{2\vec{k}_{x,b}}\right) & \left(\frac{1}{2} - \frac{\vec{k}_{x,a}}{2\vec{k}_{x,b}}\right) \\ \left(\frac{1}{2} - \frac{\vec{k}_{x,a}}{2\vec{k}_{x,b}}\right) & \left(\frac{1}{2} + \frac{\vec{k}_{x,a}}{2\vec{k}_{x,b}}\right) \end{bmatrix} \\
& \quad \times \begin{bmatrix} e^{-i\vec{k}_{x,a}A} & 0 \\ 0 & e^{i\vec{k}_{x,a}A} \end{bmatrix} \begin{bmatrix} E_1^+ \\ E_1^- \end{bmatrix} = \\
& \begin{bmatrix} \left(\frac{1}{2} + \frac{\vec{k}_{x,b}}{2\vec{k}_{x,a}}\right) e^{-i\vec{k}_{x,b}B} & \left(\frac{1}{2} - \frac{\vec{k}_{x,b}}{2\vec{k}_{x,a}}\right) e^{i\vec{k}_{x,b}B} \\ \left(\frac{1}{2} - \frac{\vec{k}_{x,b}}{2\vec{k}_{x,a}}\right) e^{-i\vec{k}_{x,b}B} & \left(\frac{1}{2} + \frac{\vec{k}_{x,b}}{2\vec{k}_{x,a}}\right) e^{i\vec{k}_{x,b}B} \end{bmatrix} \begin{bmatrix} \left(\frac{1}{2} + \frac{\vec{k}_{x,a}}{2\vec{k}_{x,b}}\right) e^{-i\vec{k}_{x,a}A} & \left(\frac{1}{2} - \frac{\vec{k}_{x,a}}{2\vec{k}_{x,b}}\right) e^{i\vec{k}_{x,a}A} \\ \left(\frac{1}{2} - \frac{\vec{k}_{x,a}}{2\vec{k}_{x,b}}\right) e^{-i\vec{k}_{x,a}A} & \left(\frac{1}{2} + \frac{\vec{k}_{x,a}}{2\vec{k}_{x,b}}\right) e^{i\vec{k}_{x,a}A} \end{bmatrix} \\
& \quad \times \begin{bmatrix} E_1^+ \\ E_1^- \end{bmatrix} = \begin{bmatrix} W & X \\ Y & Z \end{bmatrix} \begin{bmatrix} S & T \\ U & V \end{bmatrix} \begin{bmatrix} E_1^+ \\ E_1^- \end{bmatrix} = \begin{bmatrix} E_5^+ \\ E_5^- \end{bmatrix}
\end{aligned}$$

Where $\vec{k}_{x,a}$ and $\vec{k}_{x,b}$ are the x component of the wavevector in the air gap and dielectric sheet respectively, E_1^+ and E_1^- are respectively the right and left travelling components of the wave at point one on figure (1), and E_1^+ and E_1^- the right and left travelling components at point 5.

E_1 and E_5 may be identified as identical points in cells n and $n+1$, relabelling them E_n and E_{n+1} gives,

$$\begin{bmatrix} W & X \\ Y & Z \end{bmatrix} \begin{bmatrix} S & T \\ U & V \end{bmatrix} \begin{bmatrix} E_n^+ \\ E_n^- \end{bmatrix} = \begin{bmatrix} E_{n+1}^+ \\ E_{n+1}^- \end{bmatrix}$$

Then multiplying out the first two matrices on the right hand side

$$\begin{bmatrix} W & X \\ Y & Z \end{bmatrix} \begin{bmatrix} S & T \\ U & V \end{bmatrix} = \begin{bmatrix} WS + XU & WT + XV \\ YS + ZU & YT + ZV \end{bmatrix} = \begin{bmatrix} \theta & v \\ \phi & \xi \end{bmatrix}$$

$$\begin{bmatrix} \theta & v \\ \phi & \xi \end{bmatrix} \begin{bmatrix} E_n^+ \\ E_n^- \end{bmatrix} = \begin{bmatrix} E_{n+1}^+ \\ E_{n+1}^- \end{bmatrix} \quad (1)$$

Alternatively, using Bloch's theorem, the fields at equivalent points in cell n and cell $n + 1$ may be related as

$$\begin{bmatrix} E_n^+ \\ E_n^- \end{bmatrix} = \exp^{-i\mu_x(A+B)} \begin{bmatrix} E_{n+1}^+ \\ E_{n+1}^- \end{bmatrix} \quad (2)$$

Rearranging equation (2), and substituting it into equation (1) to eliminate the E_{n+1}^+ and E_{n+1}^- terms, leaves the following equation which contains terms only relating to the field in the first cell,

$$\begin{bmatrix} \theta & v \\ \phi & \xi \end{bmatrix} \begin{bmatrix} E_n^+ \\ E_n^- \end{bmatrix} = \exp^{i\mu_x(A+B)} \begin{bmatrix} E_n^+ \\ E_n^- \end{bmatrix}$$

This may be separated into two simultaneous equations,

$$\left(\frac{\theta - \exp^{i\mu_x(A+B)}}{v} \right) E_n^+ = E_n^- \quad (3)$$

$$\left(\frac{\xi - \exp^{i\mu_x(A+B)}}{\phi} \right) E_n^- = E_n^+ \quad (4)$$

After rearranging and substituting to eliminate either E_n^+ or E_n^- , it can be seen that the following relation must be true

$$\exp^{i(2\mu_x(A+B))} - (\xi + \theta) \exp^{i\mu_x(A+B)} + (\xi\theta - v\phi) = 0 \quad (5)$$

substituting in from earlier,

$$\begin{aligned} & \overbrace{\exp^{i(2\mu_x(A+B))}}^{T_1} - \overbrace{((YT + ZV) + (WS + XU)) \exp^{i\mu_x(A+B)}}^{T_2} + \\ & \overbrace{((YT + ZV)(WS + XU) - (WT + XV)(YS + ZU))}^{T_3} = 0 \end{aligned} \quad (6)$$

This will be considered in three parts T_1 , T_2 and T_3 .

$$\begin{aligned} T_2 &= (YT + ZV) + (WS + XU) = \frac{k_{x,a} - k_{x,b}}{2k_{x,a}} \exp^{-ik_{x,b}B} \frac{k_{x,b} - k_{x,a}}{2k_{x,b}} \exp^{ik_{x,a}A} \\ & \quad + \frac{k_{x,a} + k_{x,b}}{2k_{x,a}} \exp^{-ik_{x,b}B} \frac{k_{x,b} + k_{x,a}}{2k_{x,b}} \exp^{-ik_{x,a}A} + (WS + XU) \\ &= -\frac{(k_{x,a} - k_{x,b})^2}{4k_{x,a}k_{x,b}} \exp^{i(k_{x,a}A - k_{x,b}B)} + \frac{(k_{x,a} - k_{x,b})^2}{4k_{x,a}k_{x,b}} \exp^{-i(k_{x,a}A + k_{x,b}B)} + (WS + XU) \end{aligned}$$

substituting in, and multiplying out $(WS + XU)$ in the same manner leads to

$$\begin{aligned} T_2 &= -\frac{(k_{x,a} - k_{x,b})^2}{4k_{x,a}k_{x,b}} \exp^{i(k_{x,a}A - k_{x,b}B)} + \frac{(k_{x,a} - k_{x,b})^2}{4k_{x,a}k_{x,b}} \exp^{-i(k_{x,a}A + k_{x,b}B)} \\ & \quad + \frac{k_{x,a} + k_{x,b}}{2k_{x,a}} \exp^{ik_{x,b}B} \frac{k_{x,b} + k_{x,a}}{2k_{x,b}} \exp^{ik_{x,a}A} \\ & \quad + \frac{k_{x,a} - k_{x,b}}{2k_{x,a}} \exp^{ik_{x,b}B} \frac{k_{x,b} - k_{x,a}}{2k_{x,b}} \exp^{-ik_{x,a}A} \\ &= -\frac{(k_{x,a} - k_{x,b})^2}{4k_{x,a}k_{x,b}} \exp^{i(k_{x,a}A - k_{x,b}B)} + \frac{(k_{x,a} - k_{x,b})^2}{4k_{x,a}k_{x,b}} \exp^{-i(k_{x,a}A + k_{x,b}B)} \\ & \quad + \frac{(k_{x,a} + k_{x,b})^2}{4k_{x,a}k_{x,b}} \exp^{i(k_{x,a}A + k_{x,b}B)} \\ & \quad - \frac{(k_{x,a} - k_{x,b})^2}{4k_{x,a}k_{x,b}} \exp^{-i(k_{x,a}A - k_{x,b}B)} \end{aligned}$$

rearranging gives,

$$\begin{aligned}
T_2 &= \frac{(k_{x,a} + k_{x,b})^2}{4k_{x,a}k_{x,b}} (\exp^{i(k_{x,a}A + k_{x,b}B)} + \exp^{-i(k_{x,a}A + k_{x,b}B)}) \\
&\quad - \frac{(k_{x,a} - k_{x,b})^2}{4k_{x,a}k_{x,b}} (\exp^{i(k_{x,a}A - k_{x,b}B)} + \exp^{-i(k_{x,a}A - k_{x,b}B)}) \\
&= \frac{(k_{x,a} + k_{x,b})^2}{4k_{x,a}k_{x,b}} (2\cos(k_{x,a}A + k_{x,b}B)) - \frac{(k_{x,a} - k_{x,b})^2}{4k_{x,a}k_{x,b}} (2\cos(k_{x,a}A - k_{x,b}B))
\end{aligned}$$

$$T_3 = \overbrace{(YT + ZV)(WS + XU)}^{\Gamma} - \overbrace{(WT + XV)(YS + ZU)}^{\Pi}$$

again considering this in two sections labelled Γ and Π ,

$$\begin{aligned}
\Gamma &= \left(\frac{k_{x,a} - k_{x,b}}{2k_{x,a}} \exp(-ik_{x,b}B) \frac{k_{x,b} - k_{x,a}}{2k_{x,b}} \exp(ik_{x,a}A) + \frac{k_{x,a} + k_{x,b}}{2k_{x,a}} \exp^{-ik_{x,b}B} \frac{k_{x,a} + k_{x,b}}{2k_{x,b}} \exp^{-ik_{x,a}A} \right) \\
&\quad \times \left(\frac{k_{x,a} + k_{x,b}}{2k_{x,a}} \exp(ik_{x,b}B) \frac{k_{x,b} + k_{x,a}}{2k_{x,b}} \exp(ik_{x,a}A) + \frac{k_{x,a} - k_{x,b}}{2k_{x,a}} \exp^{ik_{x,b}B} \frac{k_{x,b} - k_{x,a}}{2k_{x,b}} \exp^{-ik_{x,a}A} \right) \\
&= \left(-\frac{(k_{x,a} - k_{x,b})^2}{4k_{x,a}k_{x,b}} \exp^{i(k_{x,a}A - k_{x,b}B)} + \frac{(k_{x,a} + k_{x,b})^2}{4k_{x,a}k_{x,b}} \exp^{-i(k_{x,a}A + k_{x,b}B)} \right) \\
&\quad \times \left(\frac{(k_{x,a} + k_{x,b})^2}{4k_{x,a}k_{x,b}} \exp^{i(k_{x,a}A + k_{x,b}B)} - \frac{(k_{x,a} - k_{x,b})^2}{4k_{x,a}k_{x,b}} \exp^{-i(k_{x,a}A - k_{x,b}B)} \right) \\
&= -\frac{(k_{x,a} + k_{x,b})^2(k_{x,a} - k_{x,b})^2}{16k_{x,a}^2k_{x,b}^2} \exp^{i2k_{x,a}A} + \frac{(k_{x,a} - k_{x,b})^4}{16k_{x,a}^2k_{x,b}^2} + \frac{(k_{x,a} + k_{x,b})^4}{16k_{x,a}^2k_{x,b}^2} \\
&\quad - \frac{(k_{x,a} - k_{x,b})^2(k_{x,a} + k_{x,b})^2}{16k_{x,a}^2k_{x,b}^2} \exp^{-i(2k_{x,a}A)} \\
&= \left(-\frac{(k_{x,a} + k_{x,b})^2(k_{x,a} - k_{x,b})^2}{16k_{x,a}^2k_{x,b}^2} \right) (2\cos(2k_{x,a}A)) + \frac{(k_{x,a} - k_{x,b})^4}{16k_{x,a}^2k_{x,b}^2} + \frac{(k_{x,a} + k_{x,b})^4}{16k_{x,a}^2k_{x,b}^2}
\end{aligned}$$

$$\begin{aligned}
\Pi &= \left(\frac{k_{x,a} + k_{x,b}}{2k_{x,a}} \exp(ik_{x,b}B) \frac{k_{x,b} - k_{x,a}}{2k_{x,b}} \exp(ik_{x,a}A) + \frac{k_{x,a} - k_{x,b}}{2k_{x,a}} \exp^{ik_{x,b}B} \frac{k_{x,a} + k_{x,b}}{2k_{x,b}} \exp^{-ik_{x,b}A} \right) \\
&\times \left(\frac{k_{x,a} - k_{x,b}}{2k_{x,a}} \exp(-ik_{x,b}B) \frac{k_{x,b} + k_{x,a}}{2k_{x,b}} \exp(ik_{x,a}A) + \frac{k_{x,a} + k_{x,b}}{2k_{x,a}} \exp^{-ik_{x,b}B} \frac{k_{x,b} - k_{x,a}}{2k_{x,b}} \exp^{-ik_{x,a}A} \right) \\
&= \left(\frac{(k_{x,b}^2 - k_{x,a}^2)}{4k_{x,a}k_{x,b}} \exp^{i(k_{x,a}A + k_{x,b}B)} + \frac{(k_{x,a}^2 - k_{x,b}^2)}{4k_{x,a}k_{x,b}} \exp^{i(k_{x,b}B - k_{x,a}A)} \right) \\
&\times \left(\frac{(k_{x,a}^2 - k_{x,b}^2)}{4k_{x,a}k_{x,b}} \exp^{i(k_{x,a}A - k_{x,b}B)} + \frac{(k_{x,b}^2 - k_{x,a}^2)}{4k_{x,a}k_{x,b}} \exp^{-i(k_{x,a}A + k_{x,b}B)} \right) \\
&= -\frac{(k_{x,a}^2 - k_{x,b}^2)^2}{16k_{x,a}^2k_{x,b}^2} \exp^{i2k_{x,a}A} + \frac{(k_{x,b}^2 - k_{x,a}^2)^2}{16k_{x,a}^2k_{x,b}^2} + \frac{(k_{x,a}^2 - k_{x,b}^2)^2}{16k_{x,a}^2k_{x,b}^2} - \frac{(k_{x,a}^2 - k_{x,b}^2)^2}{16k_{x,a}^2k_{x,b}^2} \exp^{-i(2k_{x,a}A)} \\
&= -\frac{(k_{x,a}^2 - k_{x,b}^2)^2}{16k_{x,a}^2k_{x,b}^2} (2 \cos(2k_{x,a}A)) + \frac{(k_{x,b}^2 - k_{x,a}^2)^2}{16k_{x,a}^2k_{x,b}^2} + \frac{(k_{x,a}^2 - k_{x,b}^2)^2}{16k_{x,a}^2k_{x,b}^2}
\end{aligned}$$

$$\begin{aligned}
\Gamma - \Pi &= -\frac{(k_{x,a} + k_{x,b})^2(k_{x,a} - k_{x,b})^2}{16k_{x,a}^2k_{x,b}^2} (2 \cos(2k_{x,a}A)) + \frac{(k_{x,a} - k_{x,b})^4}{16k_{x,a}^2k_{x,b}^2} + \frac{(k_{x,a} + k_{x,b})^4}{16k_{x,a}^2k_{x,b}^2} \\
&+ \frac{(k_{x,a}^2 - k_{x,b}^2)^2}{16k_{x,a}^2k_{x,b}^2} (2 \cos(2k_{x,a}A)) - \frac{(k_{x,b}^2 - k_{x,a}^2)^2}{16k_{x,a}^2k_{x,b}^2} - \frac{(k_{x,a}^2 - k_{x,b}^2)^2}{16k_{x,a}^2k_{x,b}^2} \\
&= \underbrace{\left(\frac{(k_{x,a}^2 - k_{x,b}^2)^2}{16k_{x,a}^2k_{x,b}^2} - \frac{(k_{x,a} + k_{x,b})^2(k_{x,a} - k_{x,b})^2}{16k_{x,a}^2k_{x,b}^2} \right)}_{=0} 2 \cos(2k_{x,a}A) + 1
\end{aligned}$$

$$\begin{aligned}
T_1 - T_2 + T_3 &= \exp^{i2\mu_x(A+B)} + \\
&\left(\frac{(k_{x,a} - k_{x,b})^2}{2k_{x,a}k_{x,b}} \cos(k_{x,a}A - k_{x,b}B) - \frac{(k_{x,a} + k_{x,b})^2}{2k_{x,a}k_{x,b}} \cos(k_{x,a}A + k_{x,b}B) \right) \exp^{i\mu_x(A+B)} \\
&+ 1 \\
&= 0
\end{aligned}$$

dividing by $\exp^{i2\mu_x(A+B)}$

$$\exp^{i\mu_x(A+B)} + \left(\frac{(k_{x,a} - k_{x,b})^2}{2k_{x,a}k_{x,b}} \cos(k_{x,a}A - k_{x,b}B) - \frac{(k_{x,a} + k_{x,b})^2}{2k_{x,a}k_{x,b}} \cos(k_{x,a}A + k_{x,b}B) \right) + \exp^{-i\mu_x(A+B)} = 0$$

rearranged to,

$$\overbrace{\left(\frac{(k_{x,a} - k_{x,b})^2}{2k_{x,a}k_{x,b}} \cos(k_{x,a}A - k_{x,b}B) - \frac{(k_{x,a} + k_{x,b})^2}{2k_{x,a}k_{x,b}} \cos(k_{x,a}A + k_{x,b}B) \right)}^{\Theta} + 2 \cos(\mu_x(A+B)) = 0 \quad (7)$$

$$\begin{aligned} \Theta &= \frac{(k_{x,a} - k_{x,b})^2}{2k_{x,a}k_{x,b}} \cos(k_{x,a}A - k_{x,b}B) - \frac{(k_{x,a} + k_{x,b})^2}{2k_{x,a}k_{x,b}} \cos(k_{x,a}A + k_{x,b}B) \\ &= \frac{(k_{x,a} - k_{x,b})^2}{2k_{x,a}k_{x,b}} (\cos(k_{x,a}A) \cos(k_{x,b}B) + \sin(k_{x,a}A) \sin(k_{x,b}B)) \\ &\quad - \frac{(k_{x,a} + k_{x,b})^2}{2k_{x,a}k_{x,b}} (\cos(k_{x,a}A) \cos(k_{x,b}B) - \sin(k_{x,a}A) \sin(k_{x,b}B)) \\ &= \overbrace{\left(\frac{(k_{x,a} - k_{x,b})^2}{2k_{x,a}k_{x,b}} - \frac{(k_{x,a} + k_{x,b})^2}{2k_{x,a}k_{x,b}} \right)}^{\Psi} \cos(k_{x,a}A) \cos(k_{x,b}B) \\ &\quad + \underbrace{\left(\frac{(k_{x,a} - k_{x,b})^2}{2k_{x,a}k_{x,b}} + \frac{(k_{x,a} + k_{x,b})^2}{2k_{x,a}k_{x,b}} \right)}_{\Xi} \sin(k_{x,a}A) \sin(k_{x,b}B) \end{aligned}$$

$$\Psi = \left(\frac{(k_{x,a}^2 - 2k_{x,a}k_{x,b} + k_{x,b}^2)}{2k_{x,a}k_{x,b}} - \frac{(k_{x,a}^2 + 2k_{x,a}k_{x,b} + k_{x,b}^2)}{2k_{x,a}k_{x,b}} \right) = -\frac{4k_{x,a}k_{x,b}}{2k_{x,a}k_{x,b}} = -2$$

$$\Xi = \left(\frac{(k_{x,a}^2 - 2k_{x,a}k_{x,b} + k_{x,b}^2)}{2k_{x,a}k_{x,b}} + \frac{(k_{x,a}^2 + 2k_{x,a}k_{x,b} + k_{x,b}^2)}{2k_{x,a}k_{x,b}} \right) = 2 \frac{(k_{x,a}^2 + k_{x,b}^2)}{2k_{x,a}k_{x,b}} = \frac{k_{x,a}^2 + k_{x,b}^2}{k_{x,a}k_{x,b}}$$

substituting back in gives,

$$\Theta = -2 \cos(k_{x,a}A) \cos(k_{x,b}B) + \frac{k_{x,a}^2 + k_{x,b}^2}{k_{x,a}k_{x,b}} \sin(k_{x,a}A) \sin(k_{x,b}B)$$

substituting this into equation (7),

$$2 \cos(\mu_x(A+B)) - 2 \cos(k_{x,a}A) \cos(k_{x,b}B) + \frac{k_{x,a}^2 + k_{x,b}^2}{k_{x,a}k_{x,b}} \sin(k_{x,a}A) \sin(k_{x,b}B) = 0$$

dividing by 2,

$$\cos(\mu_x(A+B)) = \cos(k_{x,a}A) \cos(k_{x,b}B) - \frac{k_{x,a}^2 + k_{x,b}^2}{2k_{x,a}k_{x,b}} \sin(k_{x,a}A) \sin(k_{x,b}B)$$

This is the dispersion relation if the wave takes a locally propagating character in the air gap. If the solution in the air gap is for an evanescent wave, then the substitution $k_{x,a} = iq_{x,a}$ needs to be made, and using the fact that $\sin(iq_{x,a}) = -\sinh(q_{x,a})/i$ and $\cos(iq_{x,a}) = \cosh(q_{x,a})$ this changes to,

$$\begin{aligned} \cos(\mu_x(A+B)) &= \cos(k_{x,b}B) \cosh(q_{x,a}A) - \left(\frac{k_{x,b}^2 - q_{x,a}^2}{i2k_{x,b}q_{x,a}} \right) \sin(k_{x,b}B) (-\sinh(q_{x,a}A)/i) \\ &= \cos(k_{x,b}B) \cosh(q_{x,a}A) - \left(\frac{k_{x,b}^2 - q_{x,a}^2}{2k_{x,b}q_{x,a}} \right) \sin(k_{x,b}B) \sinh(q_{x,a}A) \end{aligned}$$

$$\cos(\mu_x(A+B)) = \cos(k_{x,b}B) \cosh(q_{x,a}A) + \left(\frac{q_{x,a}^2 - k_{x,b}^2}{2k_{x,b}q_{x,a}} \right) \sin(k_{x,b}B) \sinh(q_{x,a}A) \quad (8)$$

In the tight binding regime, where $q_{x,a}A \gg 1$, then $\cosh(q_{x,a}A) \approx \sinh(q_{x,a}A) \gg$

1

$$0 = \cos(k_{x,b}B) + \left(\frac{q_{x,a}^2 - k_{x,b}^2}{2k_{x,b}q_{x,a}} \right) \sin(k_{x,b}B)$$

rearranging,

$$0 = 1 + \left(\frac{q_{x,a}^2 - k_{x,b}^2}{2k_{x,b}q_{x,a}} \right) \tan(k_{x,b}B)$$

$$1 = \left(\frac{k_{x,b}^2 - q_{x,a}^2}{2k_{x,b}q_{x,a}} \right) \tan(k_{x,b}B) \quad (9)$$

The relation between the component of the wavevector in the x and y directions in the air gap is given by,

$$-q_{x,a}^2 + k_y^2 = \frac{\omega^2}{c^2} \quad (10)$$

$$q_{x,a}^2 = k_y^2 - \frac{\omega^2}{c^2} \quad (11)$$

Inside the sheet the wave will take a propagating character in the x direction, with the relation between the two components of the wave being given by,

$$k_{x,b}^2 + k_y^2 = \frac{\epsilon_r \omega^2}{c^2} \quad (12)$$

$$k_{x,b}^2 = \frac{\epsilon_r \omega^2}{c^2} - k_y^2 \quad (13)$$

substituting this into equation (9)

$$\begin{aligned} 1 &= \left(\frac{k_{x,b}^2 - q_{x,a}^2}{2k_{x,b}q_{x,a}} \right) \tan(k_{x,b}B) = \left(\frac{\left(\frac{\epsilon_r \omega^2}{c^2} - k_y^2 \right) - \left(k_y^2 - \frac{\omega^2}{c^2} \right)}{2\sqrt{\frac{\epsilon_r \omega^2}{c^2} - k_y^2} \sqrt{k_y^2 - \frac{\omega^2}{c^2}}} \right) \tan \left(B \sqrt{\frac{\epsilon_r \omega^2}{c^2} - k_y^2} \right) \\ &= \left(\frac{\left(\frac{(\epsilon_r + 1)\omega^2}{c^2} - 2k_y^2 \right)}{2\sqrt{\frac{\epsilon_r \omega^2}{c^2} - k_y^2} \sqrt{k_y^2 - \frac{\omega^2}{c^2}}} \right) \tan \left(B \sqrt{\frac{\epsilon_r \omega^2}{c^2} - k_y^2} \right) \end{aligned} \quad (14)$$

which, once a value of ω and ϵ_r is set, may be solved numerically for a value of k_y

Bibliography

- [1] J.-M. Lourtioz et al. *Photonic Crystals, Towards Nanoscale Photonic Devices*. Springer, 2005.
- [2] C. M. Soukoulis et al. *Photonic Band Gap Materials*. Springer, 1996.
- [3] S.G. Johnson and J.D. Joannopoulos. *Photonic Crystals, The Road from Theory to Practice*. Kluwer Academic Publishers, 2002.
- [4] J.D. Joannopoulos, R.D. Meade, and J.N. Winn. *Photonic Crystals, Moulding the Flow of Light*. Princeton University Press, 1995.
- [5] P.A. Tipler. *Physics for scientists and engineers*. W.H. Freeman and Company, 1999.
- [6] L.E. Reichl. *A Modern Course in Statistical Physics*. John Wiley & sons, Inc, 1998.
- [7] L.D. Landau and E.M. Lifshitz. *Statistical Physics*. Pergamon Press, 1980.
- [8] edited by W.E. Brittin et al. *Lectures in Theoretical Physics: volume V*. Interscience Publishers, 1963.
- [9] S. Borowitz and A. Beiser. *Essentials of Physics*. Addison Wesley, 1966.
- [10] E. Yablonovitch and T.J. Gmitter. Photonic band structure: The face-centred-cubic case. *Physical Review Letters*, 63, 1989.
- [11] E. Yablonovitch. Photonic band-gap structures. *Opt. Soc. Am. B*, 10, 1993.
- [12] K.M. Ho, C.T. Chan, and C.M. Soukoulis. Existence of a photonic gap in periodic dielectric structures. *Physical Review Letters*, 65:3152–3155, 1990.
- [13] T.J. Shepherd, P.J. Roberts, and R. Loudon. Soluble two-dimensional photonic-crystal model. *Physical Review E*, 55:6024–6038, 1997.
- [14] C. Kittel et al. *Introduction to Solid State Physics eighth edition*. John Wiley & Sons, 2005.
- [15] M.A. Omar. *Elementary Solid State Physics*. Addison-Wesley, 1975.

- [16] D. Park. *Introduction to quantum theory*. McGraw-Hill, 2005.
- [17] P.St.J. Russell. Photonic band gaps. *Physics World*, pages 37–42, 1992.
- [18] P.St.J. Russell. *Designing Photonic Crystals, a chapter in ‘Proceedings of the International School of Physics ‘Enrico Fermi’: Electron and Photon Confinement in Semiconductor Nanostructures’*. IOS Press Ohmsha, 2003.
- [19] P.St.J. Russell and T.A. Birks. Hamiltonian optics of nonuniform photonic crystals. *Journal of Lightwave Technology*, 17:1982–1988, 1999.
- [20] J.D. Patterson and B.C. Bailey. *Solid-State Physics: Introduction to the Theory*. Springer, 2007.
- [21] F.G. Smith and T.A. King. *Optics and Photonics*. John Wiley & Sons, 2000.
- [22] J. Callaway. *Energy Band Theory*. Academic Press, 1964.
- [23] W. Jones and N.H. March. *Theoretical Solid State Physics: Vol 2*. John Wiley & Sons, 1973.
- [24] J.R. Hook and H.E. Hall. *Solid State Physics, second edition*. John Wiley & Sons, 1991.
- [25] N.W. Ashcroft and N.D. Mermin. *Solid State Physics*. Holt, Rinehart and Winston, 1976.
- [26] P.B. Wilkinson. Photonic bloch oscillations and wannier-stark ladders in exponentially chirped bragg gratings. *Physical Review E*, 65, 2002.
- [27] P. Yeh. *Optical Waves in Layered Media*. John Wiley & sons, 2005.
- [28] S.J. Orfanidis. *Electromagnetic Waves & Antennas*. 2004.
- [29] G. Malpuech et al. Theory of photonic bloch oscillations in photonic crystals. *Physical Review B*, 63, 2001.
- [30] R. Sapienza et al. Optical analogue of electronic bloch oscillations. *Physical Review letters*, 91, 2003.
- [31] A. Kavokin et al. Photonic bloch oscillations in laterally confined bragg mirrors. *Physical Review B*, 61, 2000.
- [32] H. Goldstein. *Classical mechanics, second edition*. Addison-Wesley publishing company, 1980.
- [33] M.A. Alonso and G.W. Forbes. Generalization of hamilton’s formalism for geometrical optics. *J. Opt.Soc.Am.*, 12, 1995.
- [34] Born and Wolf. *Principle of Optics*. Pergamon Press, 1980.

- [35] D. Marcuse. *Light Transmission Optics*. Van Nostrand Reinhold Company, 1972.
- [36] E. Ott. *Chaos in Dynamical Systems*. Cambridge University press, 1993.
- [37] L.E. Reichl. *The Transition to Chaos*. Springer-Verlag New York, 2004.
- [38] G.M. Zaslavsky. *Chaos in Dynamic Systems*. Harwood academic publishers, 1985.
- [39] M. Kline and I. Kay. *Electromagnetic Theory and Geometrical Optics*. Interscience Publishers, 1965.
- [40] A.K. Ghatak and E.G. Sauter. The harmonic oscillator problem and the parabolic index optical waveguide: 1. classical and ray optic analysis. *Eur.J.Phys*, 10, 1989.
- [41] J.A. Arnaud. *Beam and Fiber Optics*. Academic Press, Inc, 1976.
- [42] P. Wilkinson and M. Fromhold. Chaotic ray dynamics in slowly varying two-dimensional photonic crystals. *Optics Letters*, 1034:1034–1036, 2003.
- [43] K.F. Riley, M.P. Hobson, and S.J. Bence. *Mathematical Methods for Physics and Engineering*. Cambridge University Press, 1998.
- [44] D.S. Jones. *Methods in Electromagnetic wave propagation*. Oxford University Press, 1979.
- [45] W.H. Press et al. *Numerical Recipes in C, The Art of Scientific Computing*. Cambridge University Press, 2002.
- [46] I. Stewart. *Does God Play Dice*. Penguin Books, 1989.
- [47] R.C. Hilborn. *Chaos and Nonlinear Dynamics*. Oxford University Press, 1994.
- [48] R.Z. Sagdeev, D.A. Usikov, and G.M. Zaslavsky. *Nonlinear Physics: From the Pendulum to Turbulence and Chaos*. Harwood Academic Publishers, 1988.
- [49] G.M. Zaslavsky. *Hamiltonian Chaos and Fractional Dynamics*. Oxford University Press, 2005.
- [50] G.M. Zaslavsky. *Weak Chaos and Quasi-Regular Patterns*. Cambridge University Press, 1991.
- [51] M.J. Kelly. *Low-Dimensional Semiconductors*. Oxford University Press, 1995.
- [52] S. Datta. *Electronic Transport in Mesoscopic Systems*. Cambridge University Press, 1995.

- [53] G.H. Wannier. Wave functions and effective hamiltonian for bloch electrons in an electric field. *Physical Review*, 117, 1960.
- [54] C.M. de Sterke et al. Observation of an optical wannier-stark ladder. *Physical Review E*, 57, 1998.
- [55] J. Leo and A. MacKinnon. Stark-wannier states and stark ladders in semiconductor superlattices. *J.Phys.:Condens. Matter*, 1, 1989.
- [56] G. Monsivais et al. Stark-ladder resonances in the propagation of electromagnetic waves. *Physical Review letters*, 64, 1990.
- [57] G.H. Wannier. Dynamics of band electrons in electric and magnetic fields. *Reviews of modern physics*, 34, 1962.
- [58] J.D. Jackson. *Classical Electrodynamics*. John Wiley & sons,Inc, 1962.
- [59] U. Kuhl and H-J. Stöckmann. Microwave realization of the hofstadter butterfly. *Physical review letters*, 80, 1998.
- [60] H.-J. Stöckmann. *Quantum Chaos: an introduction*. Cambridge University Press, 1999.
- [61] U. Kuhl et al. Experimental observation of the mobility edge in a waveguide with correlated disorder. *Applied Physics Letters*, 77:633–635, 2000.
- [62] A. Krokhin et al. Random 1d structures as filters for electrical and optical signals. *Physica E*, 13:695–698, 2002.
- [63] U. Kuhl and H.-J. Stöckmann. Microwave transmission spectra in regular and irregular one-dimensional scattering arrangements. *Physica E*, 9:384–388, 2001.
- [64] edited by K. Bursh et al. *Photonic Crystals: Advances in Design, Fabrication and Characterisation*. John Wiley & sons,Inc, 2004.
- [65] Jin Au Kong. *Electromagnetic Wave Theory*. John Wiley & Sons, 1990.
- [66] E. Hecht. *Optics*. Addison Wesley, 2002.
- [67] edited by E. Burstein and S. Lundqvist. *Tunneling Phenomena in Solids*. Plenum Press, 1969.
- [68] R.W. Boyd. *Nonlinear Optics*. Elsevier, 2003.
- [69] edited. P. Günter. *Nonlinear Optical Effects and Materials*. Springer, 2000.
- [70] P. Chakraborty. Metal nanoclusters in glasses as non-linear photonic materials. *Journal of materials science*, 33, 1998.
- [71] S. Visnovsky, K. Postava, and T. Yamaguchi. Magneto-optic polar kerr and faraday effects in periodic multilayers. *Optics Express*, 9, 2001.

- [72] G.B. Whitham. *Linear and Nonlinear Waves*. John Wiley & Sons, 1974.
- [73] J.M. Stone. *Radiation and Optics*. McGraw-Hill, 1963.
- [74] P.B. Wilkinson et al. Electromagnetic wave chaos in gradient refractive index optical cavities. *Phys. Rev. Lett.*, 86, 2001.
- [75] P.B. Wilkinson et al. Chaotic ray dynamics and fast optical switching in micro-cavities with a graded refractive index. *Physica B*, 272, 1999.